May 2014

# Experimental and Analytical Characterization of Regenerated/nano Cellulose Composites

Issam I A Qamhia
*University of Wisconsin-Milwaukee*

# EXPERIMENTAL AND ANALYTICAL CHARACTERIZATION OF REGENERATED/NANO CELLULOSE COMPOSITES

by

Issam I. A. Qamhia

A Thesis Submitted in

Partial Fulfillment of the

Requirements for the Degree of

Master of Science

in Engineering

at

The University of Wisconsin-Milwaukee

May, 2014

ABSTRACT
EXPERIMENTAL AND ANALYTICAL CHARACTERIZATION OF REGENERATED/NANO CELLULOSE COMPOSITES

by

Issam I A Qamhia

The University of Wisconsin-Milwaukee, 2014
Under the Supervision of Professor Rani Elhajjar

Fiber-reinforced composite materials are increasingly used for structural and engineering purposes. In particular, composites reinforced with natural fiber systems are becoming more and more popular due to their biodegradability and abundance; added to that other properties such as transparency, dimensional stability and good mechanical behavior. However, major issues remain to properly understand their behavior and enable their widespread use.

In this thesis, the mechanical behavior of cellulose fiber/epoxy composites is investigated. The natural fiber systems studied fall into three categories: unidirectional regenerated cellulose fibers, triaxially braided quasi-isotropic regenerated cellulose fibers and micro-fibrillated cellulose in the form of nanocellulose scaffolds. Different methods of fabrication including wet layup, resin infusion, hot pressing and combinations of the three processes were investigated. Mechanical testing of tension coupons or three-point bending was performed to assess the mechanical behavior. When permitted, mechanical testing was accompanied by other validation techniques to help understand the mechanical behavior including digital image correlation (DIC) and acoustic emission. The effect of temperature and loading frequency on the mechanical behavior was also investigated by performing short beam testing using Dynamic Mechanical Analysis

(DMA). Environmental effects, mainly the effect of moisture on the behavior of the fibers and the composites was also investigated. Additionally, the effect of the level of cure of the resin was found to have a detrimental effect on the mechanical behavior of the composites and was studied using DMA and Digital Scanning Calorimetry (DSC). Finally, the experimental results were extended and validated using numerical solutions and finite element simulations. Results show that thermal and mechanical properties are highly sensitive to the different factors being investigated; mainly humidity, temperature, manufacturing procedure and parameters, fiber content, as well as the level of curing of the epoxy.

TABLE OF CONTENTS

LIST OF FIGURES

LIST OF TABLES

ACKNOWLEDGEMENTS

First I would like to offer my sincere gratitude to my mentor and advisor, Dr. Rani Elhajjar, who contributed to every step in preparing this thesis. Without his contribution and encouragement, this thesis could not have been possible. I could not ask for a more knowledgeable and understanding advisor than Dr. Elhajjar and I am glad that I had the chance to work under his supervision.

Second, I would like to acknowledge the help of the USDA Forest Service Forest Products Laboratory (FPL) in Madison-WI, who provided seed funding for this research. I would like to especially acknowledge the help of Dr. Ronald Sabo and Dr. Craig Clemons who contributed to this thesis by providing the nanocellulose scaffolds used in this study and for performing impact testing.

My gratitude also goes to my lab partners at the Engineering Mechanics and Composites Laboratory at the University of Wisconsin-Milwaukee for their support and knowledge sharing. I would like to especially thank Sadegh Shams and Peng Yang for their help in the work done in this thesis.

Many thanks for Tom Ellingham (UW-Madison), Alexandria Surrett (UW-Milwaukee) for the SEM images, Ms. Eileen Norby and the University of Wisconsin Student Solid Waste Research Program for supporting this research, Dr. Steven Hardcastle at the Advanced analysis Facility-UWM and to all the guys at the machine shop for their help and contribution.

Finally, I would like to thank my parents and my brother for their encouragement and support for me while I was doing my Masters. I dedicate this thesis to them as an appreciation for their support.

# 1. INTRODUCTION

## 1.1 Research Objectives

The renewable and biodegradable nature of natural fibers makes them an attractive reinforcement in composite materials for several product applications [1-3]. Regenerated cellulose fibers such as Rayon or Lyocell can offer less variability in the fiber properties compared to other natural fiber systems [4]. Regenerated cellulose fibers are seen as having good potential as reinforcement in polymeric composite materials due to their light weigh, natural origin, abundance, and acceptable mechanical properties for some applications. In addition, a new class of regenerated cellulose fibers made by dissolving cellulose and spinning the solution from a spinneret can result in cellulose fibers with a high degree of crystallinity. These fibers may potentially be processed at high temperatures thus opening the possibility of advanced composite manufacturing systems such as processing these materials in autoclaves or as a potential reinforcement in high temperature thermoplastics.

Recently, cellulose nanomaterials derived from natural resources, have generated interest for application to composite materials. Advantages include good transparency, dimensional stability and good barrier properties [5-14]. Cellulose nanocomposites can offer transparency due to the small cross-section of the fibers that does not result in light scattering even at high reinforcement ratios. Biodegradable cellulose nanocomposites are a potential material for replacing synthetic materials in the food packaging industry as they can be used to improve the mechanical and barrier properties of bio-polymers and also provide antimicrobial activity, enzyme immobilization and biosensing [15].

The challenges of fabricating and characterizing cellulose-based composites call for a need for new fabrication and new analysis methods. In this thesis, combinations of static and dynamic mechanical testing techniques as well as analytical and numerical solutions are used to analyze and characterize the behavior of novel cellulose-based thermosetting composites. In addition, one of the main goals for this thesis is to develop methods and baseline test data that can be ultimately used for composites based on nano cellulose-based regenerated cellulose fibers. This will add up to joint efforts at United Stated Department of Agriculture Forest Products Laboratory (USDA-FPL), the University of Wisconsin-Milwaukee and the University of Wisconsin-Madison to fabricate and characterize these fibers and their composites.

### 1.2 Research Program Overview

The research program is divided into three related components. In the first part of this research, the results of a computational and experimental investigation on the tensile behavior of uniaxial regenerated cellulose /bio-based epoxy composites are presented. A unit cell finite element model is proposed for the microstructure and related to the macro-properties of the composite. The unit cell model is based on using experimental results for the fibers and the resin as inputs for the mechanical properties of the constituents of the unit cell model. The mechanical properties of Lyocell tows are investigated for tensile properties under dry conditions to characterize the constitutive behavior. The composite is then prepared using wet layup and resin infusion to investigate the effects on the mechanical behavior. The p-version finite element analysis is used to generate the unit cell model incorporating the elastic-plastic bilinear constitutive response for the

regenerated fibers and is proposed within a possible framework for possible modeling of composite products made from these materials. Experimental data is used to calibrate and verify the FE model for this composite system and its predictive capability is assessed. In addition, the effect of moisture on the mechanical properties of the fibers and the composites is investigated on fiber bundles and composite coupons.

In the second part, a composite system consisting of a triaxially braided regenerated cellulose fibers and a high bio-based epoxy is investigated. A discrete three-layer analytical model based on classical lamination plate theory is proposed to predict the mechanical properties using a micro to macro mechanics approach. The model is validated by mechanical testing of longitudinal and transverse coupons prepared by resin infusion. Several trials for fabrication to obtain composites with the highest fiber content, good wetting and low porosity are examined. A digital image correlation technique is used to investigate the load redistribution using a full-field study of the deformation behavior. A passive acoustic emission technique is used to examine the damage initiation and propagation through the braided composite test specimens. The implications of the analytical model and experiments performed on this natural material are assessed. The effects of the braider angle, aspect ratios, crimp angle, and the yarn spacing on the elastic properties of the braided composite are also investigated. In addition, the strength of these composites is studied by fabricating and testing notched samples in the longitudinal and transverse directions. The viscoelastic properties of the triaxially braided regenerated cellulose composites are investigated using dynamic mechanical analysis. Samples of longitudinal and transverse coupons are tested under dry and wet conditions for a wide range of temperature and loading frequencies. The behavior of the composites is

compared to that of pure epoxy resin for changes in the storage, loss moduli and the *tan* $\delta$ curves. The effects of temperature, wetting, loading frequencies and direction of reinforcement are investigated.

Finally, we examine the reinforcement potential of novel nanocellulose-based scaffolding reinforcements constituting of microfibrils 5-50 nm in diameter and several microns in length. The cellulose nanofibril reinforcement is manufactured to produce three-dimensional scaffolding. Different techniques are proposed to manufacture and characterize these composites until composites are successfully made using a hybrid two step approach of Vacuum Assisted Casting followed by Hot-Pressing (VAC-HP). The manufactured samples are characterized for the mechanical properties using three point bending. Shore-D hardness testing and Differential Scanning Calorimetry (DSC) are used to investigate the curing response and its relation to mechanical properties. The viscoelastic properties for this composites system are investigated with DMA to assess the effects of nanocellulose on the elastic modulus and the glass transition temperature ($T_g$). A p-version finite element analysis model for the microstructure of composites made of directionally oriented microfibrillated cellulose scaffolds with epoxy is also presented. The expected mechanical properties for different loading scenarios are investigated and the model is proposed to predict the elastic mechanical properties for these composites.

# 2. LITERATURE REVIEW

## 2.1 Regenerated Cellulose Fibers and Composites

Bio-based composites have long been manufactured from natural fibers and bio-based polymers such as Poly- (lactic acid), natural oils and various epoxies with large bio-based sources. Natural fibers reinforcements for composites are increasingly attractive for many product applications [1, 3, 16, 17]. One class of natural fibers is regenerated cellulose fibers which are produced by dissolving cellulose, then regenerating it by extrusion and precipitation. Regenerated cellulose fibers have generally less variable properties compared to other natural fibers and result in more uniform shape, tensile strength, diameter, and failure stress [4]. Adusumali et al. compared single fibers of several types of regenerated cellulose fibers to glass and flax fibers for modulus of elasticity, tensile strength and interfacial shear strength with polypropylene [18]. They found that regenerated cellulose fibers could exceed both flax and glass fibers in their strain to failure; making them particularly useful for composites applications in which a higher fracture toughness is required. Cheng et al. [1, 19] investigated the effects of process and source of cellulose fibrils by measuring its elastic modulus using atomic force microscopy on the fibrils. The research estimated the elastic modulus of Lyocell (Tencel; Lenzing Fibers Inc., Axis, Alabama, USA) to be approximately 98±6 GPa for fibrils with diameters ranging from 150-180 nm. The modulus, however, drops dramatically for fibrils with diameters exceeding 180 nm. Gindl and Keckes studied the strain hardening of Lyocell and viscose forms of regenerated cellulose fibers by straining fibers under cyclic tensile tests and observing the increase in tensile modulus [4]. The strain hardening was larger for Lyocell that showed more crystallinity and fiber

orientation of cellulose chains in addition to a 47% increase in its modulus compared with only 28% for viscose. Research into regenerated cellulose based composites has also been reported in the literature as well as using recycled cellulose for its generation [20]. A surface selective dissolution method to prepare high modulus all-cellulose composites from Lyocell and Bocell fibers was investigated by electron microscopy, tensile testing and X-ray diffraction [3]. The fibers were found to have excellent mechanical properties that can be tuned depending on preparation parameters. The use of regenerated fibers for composites was also addressed by several studies. Graupner and Mussig [16] used compression molding to prepare cellulose composites with Kenaf and Lyocell in poly(lactic acid) (PLA) and poly(3-hydroxybutyrate) matrices. Lyocell-PLA composites showed the highest Young's modulus (9.3 GPa) with 30% Lyocell by mass. They also found that Lyocell- poly (3-hydroxybutyrate) had the highest impact strength at 70kJ/$m^2$. Other testing has showed that Lyocell-PLA composites have high tensile and impact strength as well as a high Young's modulus although achieving a good bonding between the fibers and the matrix was problematic [21]. The tensile and flexural properties of chopped Lyocell-polypropylene composites prepared by wet layup and compression molding were also investigated [22]. The Lyocell produced with steam exploded wood fibers showed a retention of 90% of the flexural strength and 98% of the tensile modulus at 41.2% of the cost of the reference based Lyocell composite. Raman spectroscopy analysis of the molecular deformation of regenerated cellulose fibers in epoxy and polyester has shown the presence of large interfacial shear stress between the fibers and the resin [23]. Use of biocompatible resins has been found to result in higher tensile strength when incorporating regenerated cellulose fibers [24].

## 2.2 Triaxially Braided Composites

Braided composites are a type of textile composites that can be produced in 2D and 3D fabric textures for improving the out-of-plane properties and impact resistance. The fiber preform produced by the braiding operations is unique and can be easily impregnated with a thermosetting resin using various techniques such as resin transfer molding, vacuum assisted transfer molding or in preimpregnated forms. Braided composites are less susceptible to delamination due to increasing the through-the-thickness yarn interlacing properties under components of out of plane resistance [25]. The out-of-plane resistance improvement and the net shape capability of braided composites compared to other types of composites like uniaxial tape fabric and filament wound composites have resulted in wide applications [26]. One additional advantage of Braided preforms is that they can be used to form complex shapes at high rates through automation techniques [27].

The design of triaxially braided architectures is performed by using three fiber orientations for the axial and the braider yarns in distinct directions and quantities in order to obtain the targeted properties. The axial yarn size, the braider yarn size, the braider angle, and the axial yarn spacing are the most effective parameters that determine the properties of the braided preform. Braided preforms can be constructed to obtain quasi-isotropic properties through the optimization of the fiber preform. The properties of the fibers, matrix, the interface mechanical properties and fabric architecture typically determine the stiffness and strength properties of the composites. Due to the undulations in the tows of the bias yarns, the direct application of classical lamination plate theories is challenging. Other Macromechanical and micromechanical approaches based on energy

methods, finite element analysis and classical lamination plate theory methods are proposed to model the elastic response [28-32]. A fiber inclination model is developed by Yang et al. [29] as a method for predicting the elastic properties of three-dimensional textile structural composites. Other general purpose micromechanics analysis models based on an iso-strain assumption by using a 3-D stress averaging technique within a representative unit cell (RUC) have been proposed to compute the overall composite properties [31, 33]. The effects of the fabric architecture for 2-D triaxially braided textile composites have been investigated, both analytically and experimentally. Analytical models for 2-D thermo-elastic properties of woven fabric composites are proposed by Chou and Ishikawa [34-36] based on the classical lamination theory, mosaic, fiber undulation and bridging models. Whitney and Chou [37] used the fiber inclination model to predict the in-plane elastic properties of composites reinforced with 3-D angle-interlock textile preforms. Challa and Shivakumar [38] used a similar approach for 3-D, 4-Step and circular braids. Sankar and Marrey [39] proposed a selective averaging method in which both stiffness and compliance coefficients can be averaged selectively depending on iso-stress or iso-strain conditions. Bowman et al. [40] examined two triaxial-braid architectures (0°±60°, 0°±45°) with the M36 epoxy resin and evaluated the tension, compression, and shear behavior. The 0°±45° configuration composites showed better response for measurements parallel to the axial tows. The composites with the 0°±60° arrangement, on the other hand, behaved better for measurements made perpendicular to the axial tows.

An analytical model based on iso-strain and interfacial continuity conditions is proposed by Zhang et al [41] . For the model, a sinusoidal path of the braider yarn is

defined as a function of the braider angle and the variation of the braider yarns' undulation period for a particular zone. A macro-level finite element-based model is proposed by Goldberg et al. [42] using four parallel shell elements; each element is modeled as a laminated composite developed to simulate the mechanical and impact response of triaxially-braided polymer matrix composites. The effects of the radius of curvature of a unit cell on the elastic constants of 2D braided tubular composites are investigated by Ayranci and Carey [43]. Hwang et al. [44] presented a micromechanical model for 2-D triaxially braided composites. The arrangements of the tows in the representative unit cell are modeled by using analytical optimization to solve the packing problem. Quek et al. [32] proposed a representative unit cell (RUC) model of the braided architecture that took into account the tow undulation and the bias tow angle through its constituents. This was performed by separating the axial and bias yarns into separate layers with subsequent averaging. Shokrieh and Mazloomi [45] proposed a modified equation to better capture the shear properties. Both of the reported models assumed an identical thicknesses of all three layers El-Hajjar et al. [46] evaluated the three-layer analytical representations for application on triaxially braided models for glass fiber composites. The correlation with experiments indicated that consistent predictions with experimental results are obtained by the three layer representation approach.

### 2.3 Nanocellulose Composites

Nanocellulose-based reinforcements constitute a relatively new class of naturally sourced reinforcements. Nanofibrillated cellulose (NFC) or cellulose nanofibrils (CNFs) are used to describe fibrillated cellulose with a nano-scale structure, and these are typically created by some combination of chemical, enzymatic, and/or mechanical

treatments of lignocellulosics materials, such as wood. CNFs have a complex structural hierarchy with fibril bundles from about 5-50 nm in diameter and up to several microns in length [47]. Strong tendency of cellulosic nanomaterials to hydrogen bond can lead to challenges in re-dispersing them if they are dried but can also result in fairly strong and stiff films that can be used in laminated composites [48]. Cellulose nanomaterials are very hydrophilic [49], which can create difficulties in dispersing them and bonding them to some thermosets due to swelling during composite manufacture. Thermosetting composites can be cured with low or no heat applied, which can be advantageous since nanocellulose has limited thermal stability. The curing in thermosets may be initiated through heat, radiation or through a chemical reaction (e.g. a two part epoxy). Uncured thermosetting materials can have low viscosities, which is a critical feature in the construction of composites that allows for infiltration and wetting of the fibers. Distributed or particulate composites based on nanocellulose benefit from the interactions with the resin and the relatively high aspect ratios of the cellulose particles or fibers. Ruiz et al. [50] manufactured cellulose nanofibril composites with aqueous suspensions of epoxy. The CNFs displayed large aspect ratios and an ability to associate by means of H-bonds.

The effect of fiber content on the mechanical and thermal expansion properties of bio composites based on CNFs have also been reported [51]. A linear increase in Young's modulus was observed at fiber contents up to 40 wt. %, using a phenolic resin. The results also showed a correlation between the coefficient of thermal expansion (CTE) relative to fiber content, indicating the effective reinforcement attained by the CNFs. In another example, Ruiz et al. found that adding CNFs up to about 2% in an epoxy resin

increased the mechanical properties but further addition of CNFs led to agglomeration and reduced thermal and mechanical properties [50]. The pressing method has been found to be the most common in the literature for processing of thermosetting composites with CNFs reinforcements. Regarding the mechanical properties of these composites; Siro et al. [52] reported that the tensile modulus for Nanofibrillated cellulose films can range from 3 GPa to 20 GPa, while the tensile strength ranges from 70 MPa to more than 300 MPa. Ruiz et al. [53] discussed the recent developments and challenges of nanocellulose based bio-nanocomposites. They reported that NFC/epoxy composites with up to 2% NFC showed an increase in the mechanical properties. Larger NFC contents, however, reduced the thermal and mechanical properties due to agglomeration. Jue Lu et al. [54] reported an increase in the storage modulus (E'), measure by DMA, from 2.6 GPa for neat epoxy to 3.1 GPa for 5 % by weight microfibrillated cellulose/epoxy film at 30 °C. To make more use of the reinforcement potential of the nanocellulose; the nanofibers can be oriented in one direction and a significant enhancement in the mechanical properties can be seen along that direction for the films [55, 56]. For example, Sehaqui et al. reported an increase in the tensile strength from 185 MPa for random NFC films to over 400 MPa for one case of the oriented films.

# 3. UNIDIRECTIONAL REGENERATED CELLULOSE FIBERS & COMPOSITES

## 3.1 Unit Cell Model for Unidirectional Composites

In this section, a multi-scale analysis approach is used for the simulation of unidirectional regenerated cellulose/bio-based epoxy composites. A representative unit cell where the behavior of the constituents is independently recognized is used for the first step. The result is then a homogenized behavior of the composites that can be used for a structural level analysis. The modelling approach is shown in Figure 1. This modeling approach is implemented in a p-version finite element analysis (p-FEA) approach.

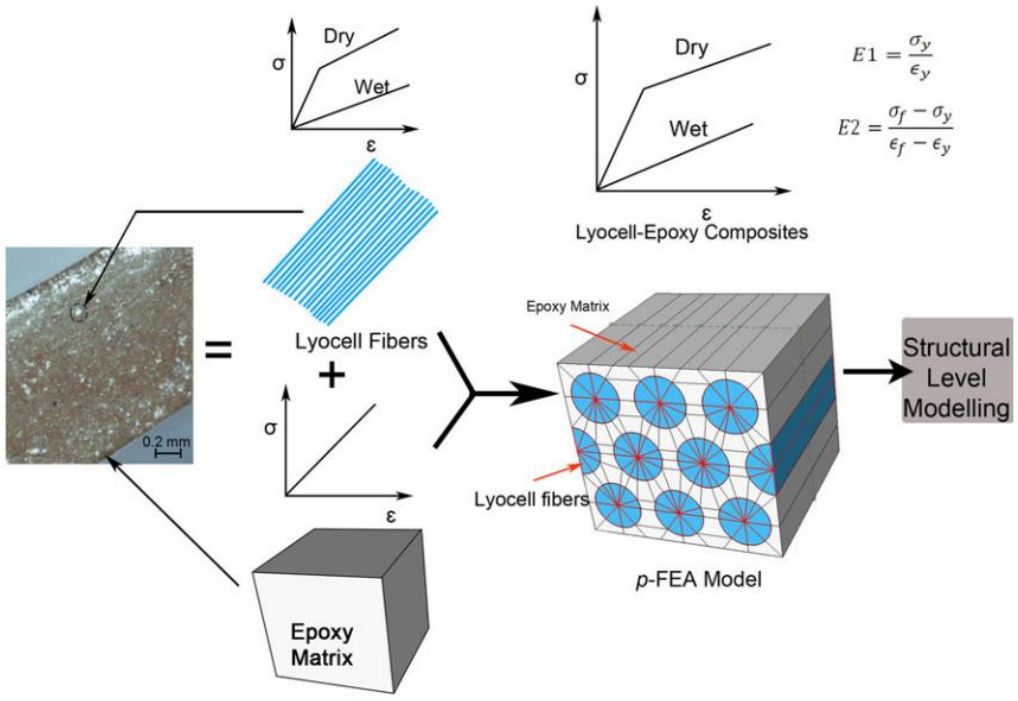


**Figure 1** Schematic of analysis approach for Lyocell/epoxy composites with bilinear elastic–plastic fiber response (*Elhajjar and Qamhia, 2013*)

In p-FEA, the refinement is achieved by increasing the polynomial degree of the elements, which is directly related to the degrees of freedom in the model. The primary advantage of this approach is the ability to check the convergence of the solutions with increasing element order, reducing the dependency on the mesh size. Increasing the polynomial degree of the elements is related to the error of approximation. These errors are reduced exponentially as the number of degrees of freedom is increased. The global energy norm is calculated for each polynomial order as an indicator of the convergence of the solution. In addition to the global energy norm, the quantity being investigated is also checked for convergence with each polynomial order solution. The energy convergence of the unit cell model for the regenerated cellulose/epoxy composites was checked and is shown in Figure 2. Commercially available p-FEA software is used for the simulations of the micromechanical models (Stress Check V9.0; ESRD, St. Louis, Missouri, USA). The typical unit cell model used for the hexagonal packing contained 178 elements consisting of 72 hexahedral and 106 pentahedral elements. A hexagonal packing geometry was considered the most representative for the models performed, although other packing geometries such as a square packing can also be considered.

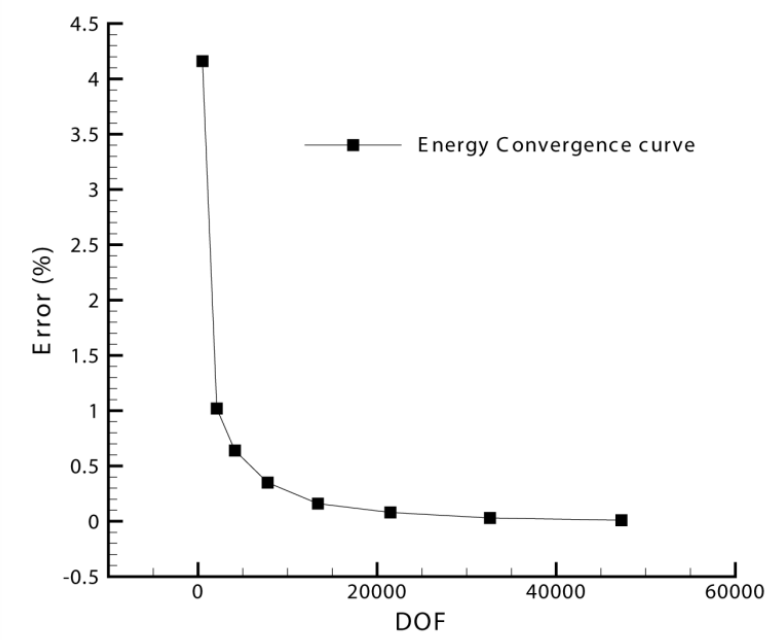


**Figure 2** Energy convergence curve for FEA model (19% fiber volume fraction trial)

The nonlinear material properties of the Lyocell fibers are accounted for by using a bilinear elastic-plastic stress-strain relationship to the experimental data. The polymeric epoxy matrix is assumed to be linear, where the modulus of elasticity was calculated experimentally by testing tension dog bone-shaped coupons using ASTM ID: D638 standard[57]. The p-FEA model proposed was calibrated for one set of experimental values using the specimens having a fiber content of 33 % (FVF of 0.33). The model was then run with different FVF for validation purposes of the modeling capability. The loading was applied to the model in the form of a constant displacement on one face in the fibers direction. Boundary conditions were applied to restrict in and out-of-plane displacement on the opposing face. No restrictions to the out of plane boundary conditions on the other four faces were applied to account for Poisson ratio effects as a

tension load is applied in fibers direction. The results from a trial of the model with 33% FVF are shown in Figure 3.

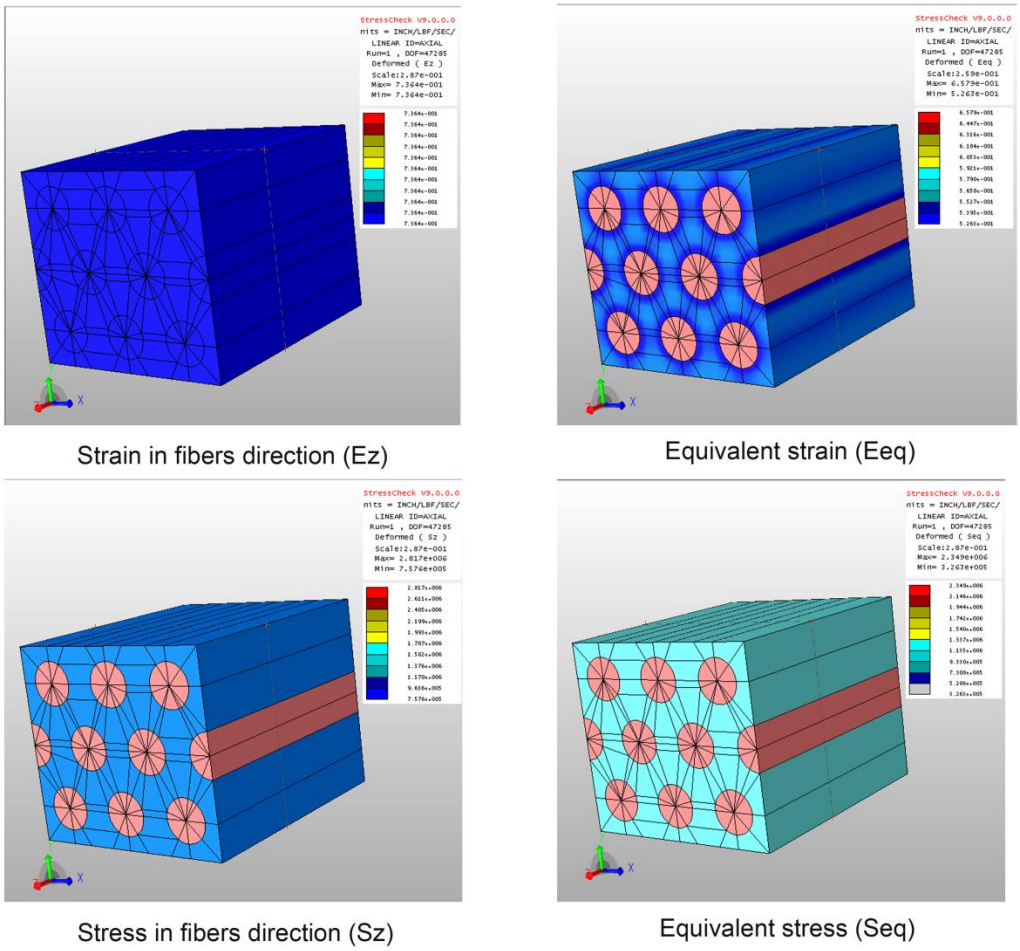


**Figure 3** FEA model results for unit cell with 33% fibers by volume.

For all fiber volume fractions, convergence was achieved rapidly in all cases with the error less than 0.01% achieved using 20,000 degrees of freedom. The results of p-FEA modeling were compared to those obtained by experiments in the fiber direction by calculating the average stress resulting on the loaded surfaces. The predictive properties of the model are shown in the stress strain graphs in Figure 4 superimposed with the FEA

calibration curve. The results show some variation in the plastic region; nevertheless, an approximate bilinear behavior can still be seen for the composites. The results of p-FEA modeling were compared to those obtained by experiments in the fiber direction by calculating the average stress resulting on the loaded surfaces. The p-FEA model was successfully used to capture the experimental stress-strain behavior of the composites and the FE model was calibrated to average the differences seen in the plastic region for the samples. The results show that it is possible to reproduce accurate results for different fiber volume fractions. The model was run with the same parameters, boundary conditions and material properties used to produce the calibration curve except for the fiber volume fraction which was reduced from 33% to 19%. The verification model shows a good match to the experimental values with a little overestimation of strength and elasticity in the plastic region.

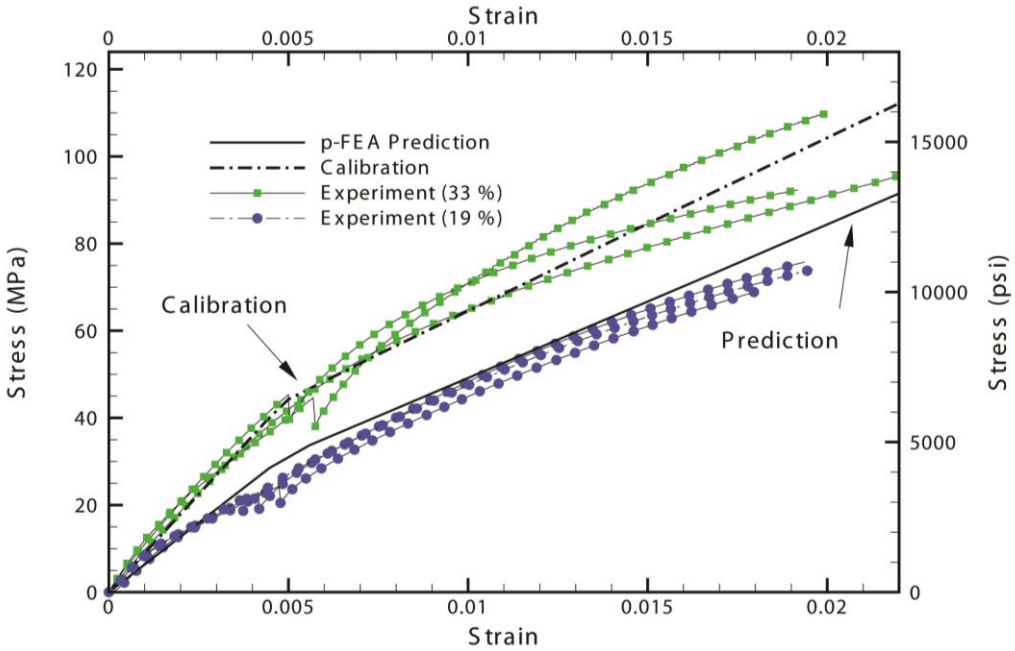


**Figure 4** Calibration & prediction of stress–strain response for dry Lyocell/epoxy composites (*Elhajjar and Qamhia, 2013*)

Changes in the elastic and plastic modulus of Lyocell-epoxy composites with different fiber contents are shown in Figure 5. A linear change is seen which can be attributed to the use of a bilinear stress-strain curve for Lyocell and a linear one for epoxy. This characteristic is expected to change with the wet composites where the non-linearity of the Lyocell loading curve is expected to lead to nonlinearity in the stress-strain curve of the composites. From experimental results for the soaked composites for 2 hours, the deterioration in the mechanical behavior under wet conditions was less pronounced due to the resin barrier. More variability, however, is seen in the results for the wet composites.

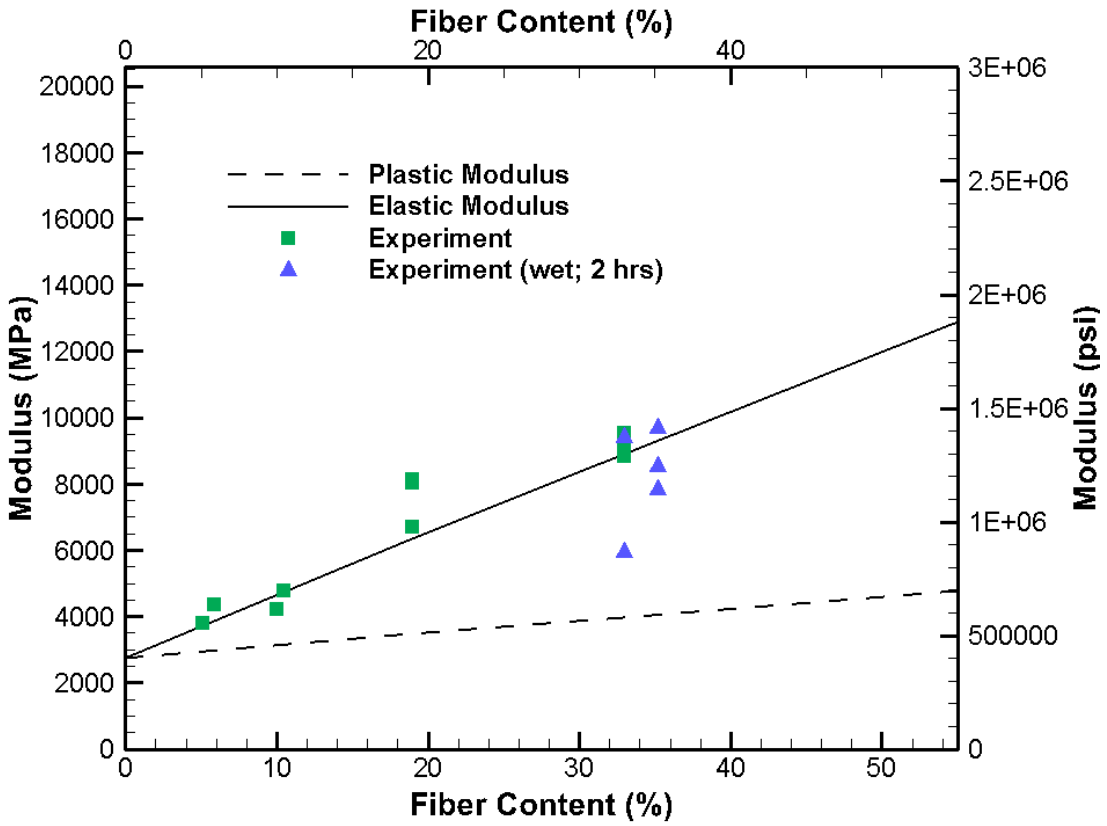


**Figure 5** Experimental and analytical results of the effect of FVF on the elastic modulus of Lyocell/epoxy composites (*Elhajjar and Qamhia, 2013*)

### 3.2 Specimen Fabrication and Test Setups

The experimental portion of this study consisted of studying the tension behavior of dry and wet Lyocell fibers and composites made with different fiber volume contents. The fiber tows obtained were in an uncrimped and unbleached state. The ASTM ID: D3822 [58] standard was used for determining the fiber properties.

The composite specimens were prepared using a wet layup and resin infusion methodology. The epoxy chosen for this study is a high bio-content based epoxy resin (Super Sap 100 Epoxy; Entropy Resins Inc., Gardena, California, USA). As opposed to traditional epoxies that are primarily made of petroleum-based materials, this resin formulation contains bio-renewable materials sourced as co-products or from waste streams of other industrial processes, such as wood pulp and bio-fuels production. The resin is reported by the supplier to have a 37% bio-content and is classified as a United States Department of Agriculture (USDA) Bio Preferred Product using ASTM D6866 [59]. The mixed resin has a pot life of 25 minutes at 25 degrees Celsius with an initial viscosity of 725 cps. The performance properties of this resin specified by the vendor as of 04-May-2012 revision (version no. 4) are shown in Table 1.

Several methods were investigated for producing the composite materials. In order to produce higher fiber volume fractions for the Lyocell-epoxy composites, the manufacturing of panels using a resin-infusion process was introduced (Figure 6). Resin infused samples were prepared by uniformly spreading a known mass of unidirectional fibers between two Teflon sheets in a vacuum bag and applying vacuum pressure up to 635.0 mm Hg (25 in. Hg) from a vacuum pump. The manual layup panels on the other

hand were prepared by wet layup, folding the cloth over the panel and using squeegees to uniformly distribute the resin over the fibers and removing the excess resin. The panels produced using wet layup and resin infusion resulted in a volume fraction of approximately 0.3. Specimens of lower fiber content were also manufactured for use in analysis and predictive purposes. Testing of composite coupons was performed under direct tension according to the ASTM ID: D3039 [60]. Strain properties were measured across a 25.4 mm (1.0 inch) gage length in the middle of coupons by the use of an extensometer for a subset of the specimens.

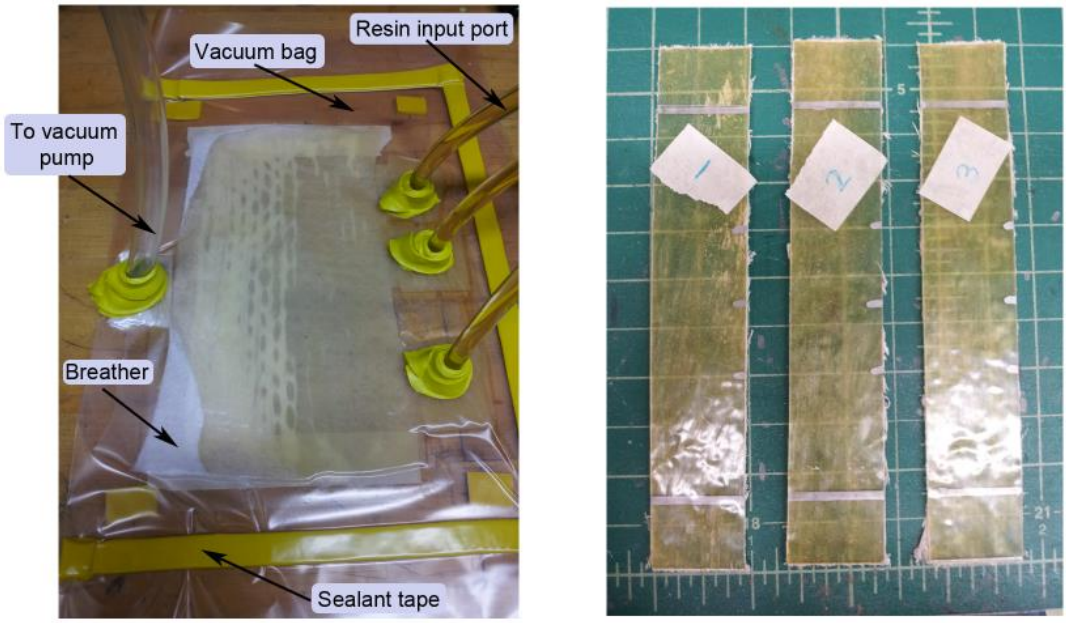


**Figure 6** Fabrication techniques for Lyocell/epoxy composites showing (a) a resin infusion panel and (b) specimens prepared by manual layup

**Table 1** Performance properties for Super Sap 100 epoxy with Super Sap 1000 hardener system as reported by Entropy resins (Revision date: 04-May-2014, version no. 4)

| **Property** | **Value** | **ASTM standard (used to determine property)** |
|---|---|---|
| Tensile modulus (psi) | 380,000 | ASTM D638 |
| Tensile strength (psi) | 8,200 | |
| Flexural modulus (psi) | 330,000 | ASTM D790 |
| Flexural strength (psi) | 11,170 | ASTM D638 |
| Onset $T_g$ by DSC (ºF) | 116 | ASTM D3418 |
| Ultimate $T_g$ by DSC (ºF) | 186 | ASTM D695 |
| Hardness (Shore D) | 70-80 | ASTM D2240 |

### 3.3 Effects of Moisture on Fibers and Composites Behavior

Moisture can have a detrimental effect on the mechanical behavior of cellulose-based natural fibers. The effect of moisture on the behavior of regenerated cellulose fibers and composites was investigated. Single Lyocell fiber tows (Tencel; Lenzing Fibers Inc., Axis, AL, USA) were used for the study. The tensile properties of the fibers were obtained using the ASTM 3822 [60] standard. Cardboard carriers with a gauge length of 25.4 mm (1.0 in) were cut and used to support and ease the handling of the samples before they are tested on a general testing machine. Fiber tows having the same weight and properties were cut and attached to the cardboards using epoxy resin at both ends. The fibers were exposed to different wetting degrees before being tested. The dry fibers were tested under normal air humidity conditions ranging between 30 and 35%. The wet fibers were wetted by soaking the cardboards with the fibers attached in a water bath for a

determined amount of time. The first set was soaked for two hours and the second set was soaked for four hours. The error margin in the soaking time for both sets was ± 5 minutes. All samples were soaked and tested at room temperature of 21˚C (70 ˚F) and an approximate humidity of 30%. The swelling in the fibers was noted by recording the change in weight of surface dried fibers soaked for the same length of time under the same environmental conditions.

Samples were tested under direct tension by applying load from an electro-mechanical loading machine and using a load cell having a maximum capacity of 2224 N (500 lb.). The test setup is shown in Figure 7-a. In order to account for the compliance of the loading machine; samples of different gauge lengths were prepared for the Lyocell tows. Samples of gauge lengths of 127, 50.8 and 14.0 mm (5, 2 and 0.55 in.) were prepared and tested in the same manner described above and under the same conditions. The data was processed to plot the graph of compliance in mm/N (in. /lb.) versus nominal gauge length in mm (in.). The best-fit straight line was plotted for the data points, and compliance of the loading machine was calculated as the y-intercept for the equation of the linear graph (Figure 7-b).

The load versus crosshead displacements for these tests is shown in Figure 8 for both dry and wet conditions. The soaking of fibers represents a severe case in which the fibers are not protected from moisture by any polymer encasement and are totally submerged in water. For the dry fibers, a bilinear load-displacement behavior in the loading curve can be seen with a dent (a knee) in the loading curve in the middle. The loss of modulus as the fibers are wetted is clearly shown by the loading curves. Some variability is shown for 2 hours soaking in the behavior of the fibers during loading. The results are more

consistent, however, for 4 hours soaking and show a drastic loss in modulus and a non-linear behavior of the fibers. The specimens have a lower failure stress, yet tend to show a higher strain to failure. Additionally, the dent seen in the loading curves for the dry fibers is shifted toward the (0, 0) point of the curves as the level of moisture increases in the fibers due to the removal of the hydrogen bonds [61]. Thus, the constitutive response of the regenerated fibers is very dependent on the moisture condition and under moisture exposure; the elastic response gradually dissipates and results in a largely plastic unrecoverable behavior.

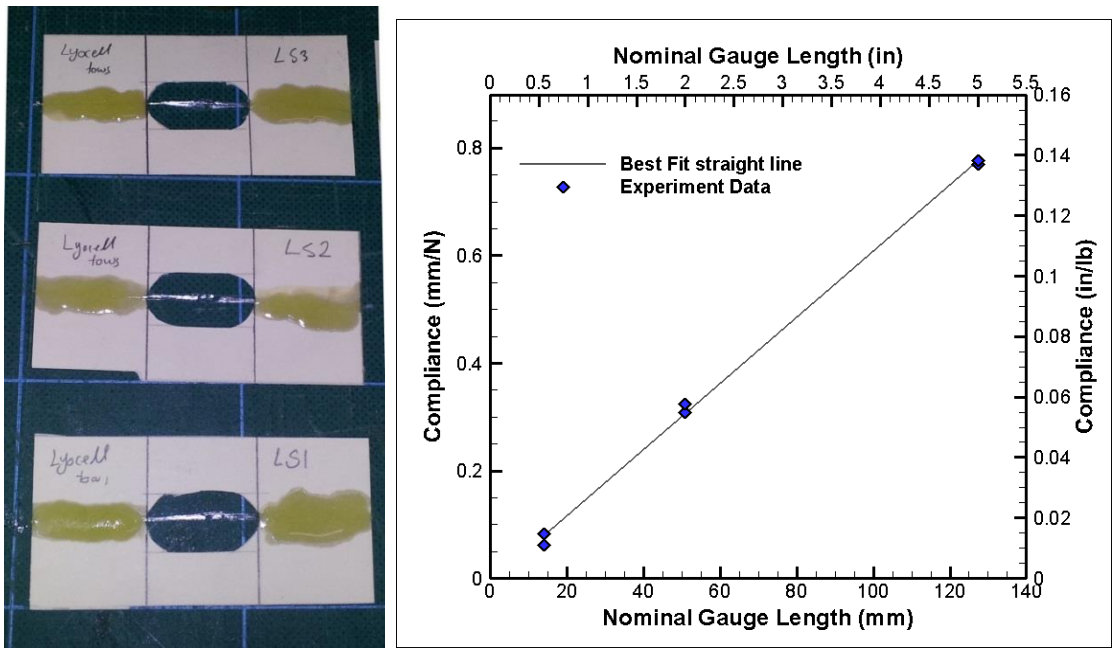


(a) (b)

**Figure 7** (a) test samples for single fiber bundles and (b) correction curve for loading machine compliance

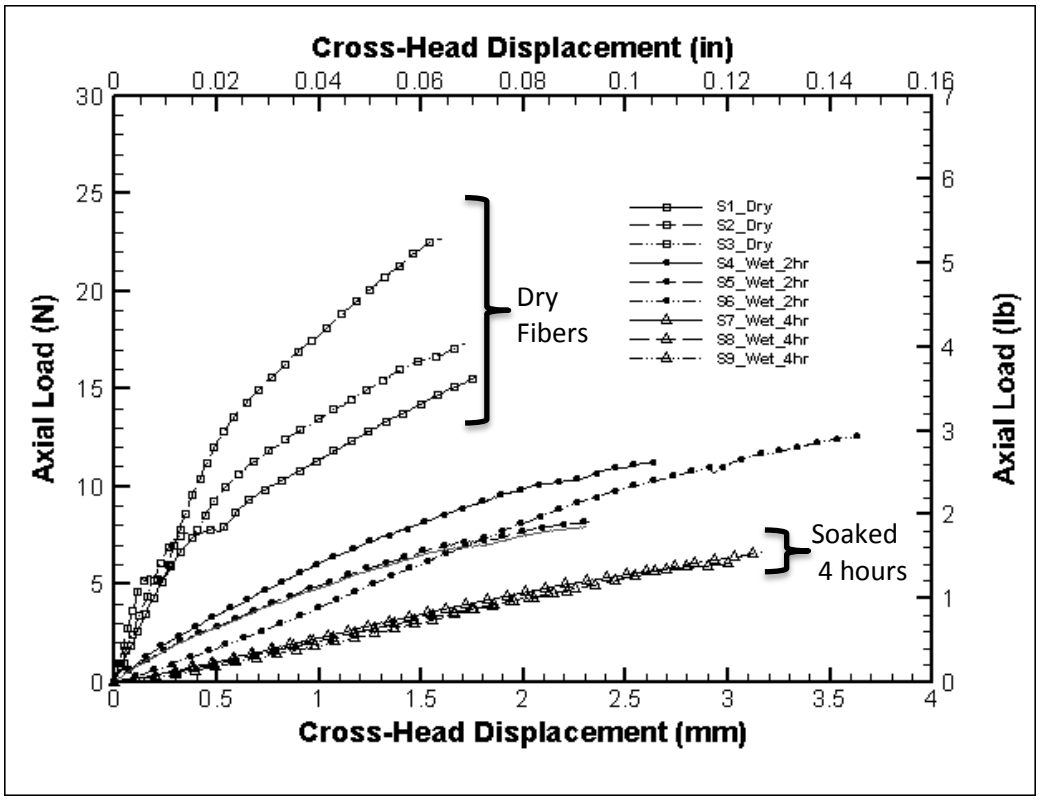


**Figure 8** Load versus cross-head displacement response of dry and wet Lyocell tows

# 4. TRIAXIALLY BRAIDED CELLULOSE FIBERS & COMPOSITES

## 4.1 Specimens Fabrication

Braided natural fiber composites materials can have several benefits including an improved out-of plane behavior and impact resistance compared to filament wound composites or uniaxial fiber composites. The braided preforms also allow obtaining quasi-isotropic elastic properties and can be used to form complex shapes at high rates by automation techniques. For the purposes of this study, a regenerated cellulose fiber called BioMid (BioMid; GSC and ENC, Inc., Burnaby, BC, Canada) was used. The regenerated cellulose fibers are reported to have a 95 percent degree of crystallinity and the ability at high temperatures up to 360 °C (680°F) compared to other natural fibers that start to degrade at 150 °C (302°F) [62]. The quasi-isotropic braided sleeve consisting of axial and +60/-60 degrees bias yarns was specially manufactured by A&P Technology (Cincinnati, Ohio, USA). The triaxial braid fiber architecture is produced by having the bias yarns alternating two over and two under the axial yarns. The bias angle and spacing of the axial and bias yarns were designed to yield similar properties in the axial and transverse directions. The spacing between the bias yarns was at 2.6 mm, whereas between the axial yarns the center-to-center spacing was 5.2 mm. The axial bundle would fill a space of approximately 2.5 mm in width between the bias yarns. For this architecture of braiding with quasi-isotropic properties, the percentage by weight in each bias and axial yarn is equal. The braiding architecture is shown in Figure 9. Following the braiding process, the braided sleeve was subsequently slit into a flat sheet to allow for further processing.

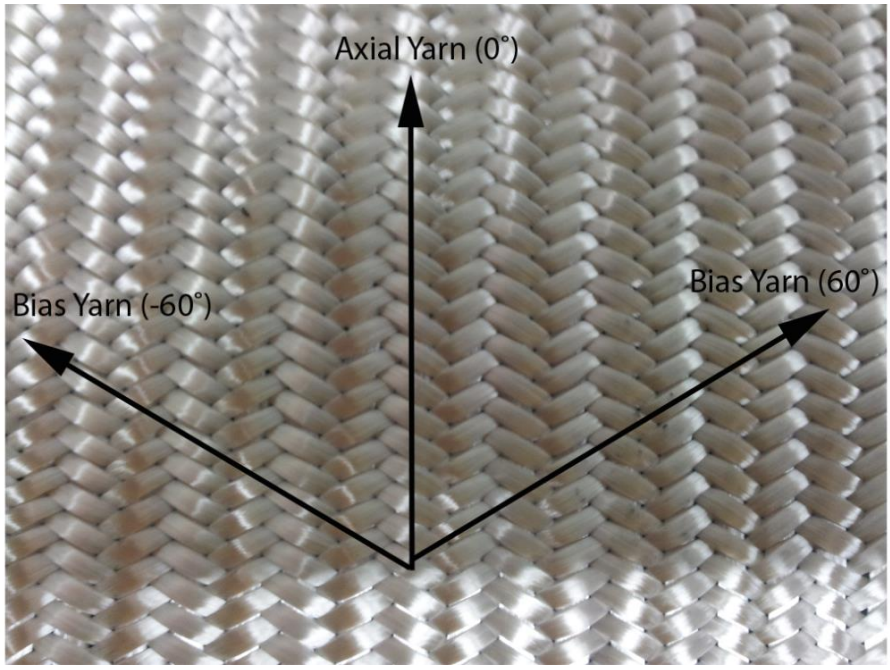


**Figure 9** Triaxially braided regenerated BioMid preform showing axial and bias yarns

Composite panels were prepared from BioMid and a high-bio content epoxy resin system (Super Sap 100/1000; Entropy Bio-Resins, Gardena, California, USA). The performance data supplied by the vendor was reported in Table 1 in chapter 3. The material properties for the used fibers and resin and the triaxial braiding properties for the fibers are summarized in Tables 2 and 3 respectively.

**Table 2** Regenerated cellulose fibers (BioMid) and epoxy matrix properties

| | Regenerated Cellulose Fiber | Epoxy |
|---|---|---|
| $E_x$ GPa (Msi) | 46 (6.67) | 1.45(0.21) |
| $E_y$ GPa (Msi) | 46 (6.67) | 1.45(0.21) |
| $G_{xy}$ GPa (Msi) | 18 (2.61) | 0.53 (0.076) |
| Poisson's ratio | 0.23 | 0.35 |

**Table 3** Triaxial braiding parameters for regenerated cellulose (BioMid) quasi-isotropic ply

| | |
|---|---|
| Braided angle (degree) | 60 |
| Undulation amplitude (mm) | 0.0005 |
| Yarn Aspect Ratio | 0.18 |
| Fiber Volume Fraction (%) | 60.5 |
| Raw Fiber Yield – Braider Yarns (yds/lb) | 2653 |
| Raw Fiber Yield – Axial Yarns (yds/lb) | 2653 |
| Material Content in Axial Yarns (% by volume) | 33.4 |
| Material Content in Braider Yarns (% by volume) | 66.6 |

The fiber volume fraction of the composites is determined by using the volume measurements of the matrix and fiber constituents [63], resulting in an average fiber volume fraction of $0.60 \pm 0.02$. Prior to processing, the regenerated fibers were stored at room temperature and a humidity level of 30%. A vacuum assisted resin infusion method was used to manufacture the composite panels with minimal levels of porosity. For the early trials, a wet layup technique was used to prepare the composites, but the fibers weren't fully infused, especially the axial yarns. The increased difficulty in processing may be attributed to the swelling of the fibers. The modified process used silicon connectors for the resin introduction and a flow mesh to improve the wetting process (Figure 10). The panels produced were 200 mm by 305 mm and were infused under room temperature conditions. Panels were cut into 305 mm long by 38 mm wide coupons in transverse and longitudinal directions.

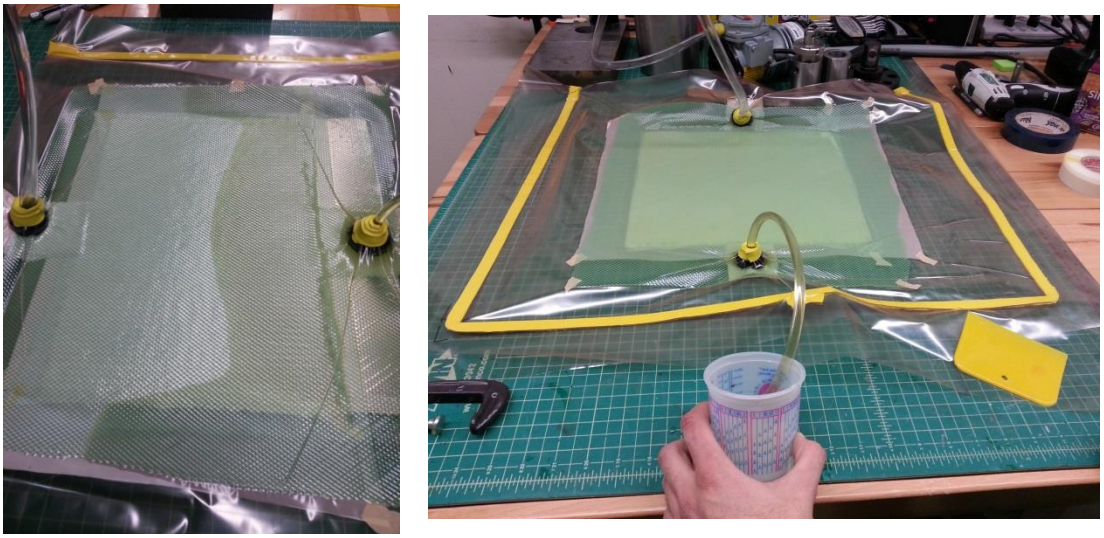

**Figure 10** Resin infusion process for a triaxially braided regenerated cellulose panel. A flow mesh is used to facilitate resin flow and the silicon connectors help to eliminate leakage.

### 4.2 Analytical Model for Braided Composites

An analytical model is presented for quasi-isotropic triaxially braided regenerated cellulose composite with the epoxy resin. The prediction of the mechanical properties is carried out by predicting the effective macroscopic properties from the constituent microscopic material characteristics by using a representative unit cell (RUC) for the macrostructure. The analytical model used in this study is the discrete three-layer models. The model was developed by Shokrieh and Mazloomi [45] and evaluated by El-Hajjar et al. [46] for application on triaxially braided models of glass fiber/epoxy composites. In the discrete three-layer models, the total stiffness of the unit cell is composed of three separate composite layers. The unit cell consists of two layers for the bias yarns and one layer for the axial yarns (Figure 11). The elastic mechanical properties of each layer can be obtained by using the rule of mixtures or by experimental measurements to obtain the

ply-level properties. Each layer of the composite is considered to be made of a transversely isotropic material.

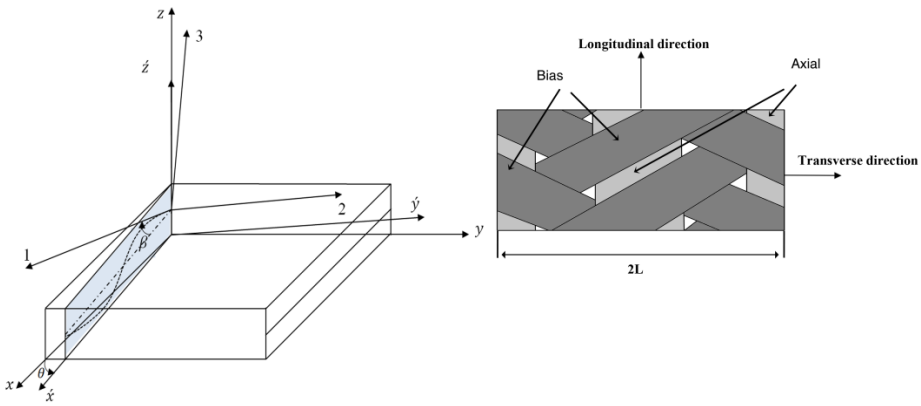


**Figure 11** Unit cell and orientation of axial and bias yarns in a braided preform (Qamhia et al., 2014)

The crimp effect of the braider yarns is taken into account by applying the following sinusoidal function to the bias layers [32, 45]:

$$\tan(\beta) = \frac{\pi A}{L}\cos(\frac{\pi x'}{L}) \qquad (1)$$

The local coordinates of the undulating yarn along a ply is defined by the 1-2-3 local coordinates [32]. Two sets of rotation transformation matrices are used around the y-axis and z-axis for the braider yarns for alignment in the global axes (Figure 11). The first two rotations are used for considering the crimp effect and the second set is for the bias angles that are shown in equations 2–6, respectively:

$$\hat{T}_1 = \begin{pmatrix} \cos(\beta)^2 & 0 & \sin(\beta)^2 & 0 & 2\cos(\beta)\sin(\beta) & 0 \\ 0 & 1 & 0 & 0 & 0 & 0 \\ \sin(\beta)^2 & 0 & \cos(\beta)^2 & 0 & -2\cos(\beta)\sin(\beta) & 0 \\ 0 & 0 & 0 & \cos(\beta) & 0 & \sin(\beta) \\ -\cos(\beta)\sin(\beta) & 1 & \cos(\beta)\sin(\beta) & 0 & \cos(\beta)^2 - \sin(\beta)^2 & 0 \\ 0 & 0 & 0 & \sin(\beta) & -2\cos(\beta)\sin(\beta) & \cos(\beta) \end{pmatrix} \quad (2)$$

$$\hat{T}_2 = \begin{pmatrix} \cos(\beta)^2 & 0 & \sin(\beta)^2 & 0 & \cos(\beta)\sin(\beta) & 0 \\ 0 & 1 & 0 & 0 & 0 & 0 \\ \sin(\beta)^2 & 0 & \cos(\beta)^2 & 0 & -\cos(\beta)\sin(\beta) & 0 \\ 0 & 0 & 0 & \cos(\beta) & 0 & -\sin(\beta) \\ -2\cos(\beta)\sin(\beta) & 1 & 2\cos(\beta)\sin(\beta) & 0 & \cos(\beta)^2 - \sin(\beta)^2 & 0 \\ 0 & 0 & 0 & \sin(\beta) & 0 & \cos(\beta) \end{pmatrix} \quad (3)$$

The stress-strain relation can be obtained by using the averaged transformed local stiffness calculated over one wave-length [45]:

$$\{\sigma\} = \frac{1}{2l}\int \left[\hat{T}_1\right]^{-1} [C] \left[\hat{T}_2\right] dx \{\varepsilon\} \qquad (4)$$

And the second rotation, as seen in Figure 11, for the braider angle transformation is given by[32]:

$$T_1 = \begin{pmatrix} \cos(\theta)^2 & \sin(\theta)^2 & 0 & 0 & 0 & 2\cos(\theta)\sin(\theta) \\ \sin(\theta)^2 & \cos(\theta)^2 & 0 & 0 & 0 & -2\cos(\theta)\sin(\theta) \\ 0 & 0 & 1 & 0 & 0 & 0 \\ 0 & 0 & 0 & \cos(\theta) & -\sin(\theta) & 0 \\ 0 & 0 & 0 & \sin(\theta) & \cos(\theta) & 0 \\ -\cos(\theta)\sin(\theta) & \cos(\theta)\sin(\theta) & 0 & 0 & 0 & \cos(\theta)^2 - \sin(\theta)^2 \end{pmatrix} \quad (5)$$

$$T_2 = \begin{pmatrix} \cos(\theta)^2 & \sin(\theta)^2 & 0 & 0 & 0 & \cos(\theta)\sin(\theta) \\ \sin(\theta)^2 & \cos(\theta)^2 & 0 & 0 & 0 & -\cos(\theta)\sin(\theta) \\ 0 & 0 & 1 & 0 & 0 & 0 \\ 0 & 0 & 0 & \cos(\theta) & -\sin(\theta) & 0 \\ 0 & 0 & 0 & \sin(\theta) & \cos(\theta) & 0 \\ -2\cos(\theta)\sin(\theta) & 2\cos(\theta)\sin(\theta) & 0 & 0 & 0 & \cos(\theta)^2 - \sin(\theta)^2 \end{pmatrix} \quad (6)$$

The stress-strain relation in the global stiffness axes is given as[45]:

$$\{\sigma\} = [\mathrm{T}_1]^{-1}[\bar{\mathrm{C}}][\mathrm{T}_2]\{\varepsilon\} \quad (7)$$

Where $[\bar{\mathrm{C}}]$ is the stiffness matrix obtained from rotation around y-axis. After calculating the stiffness matrix of each layer, the stiffness matrix of the unit cell can be determined as [45]:

$$[C^{RUC}] = t^{+\theta}[C_{global}]^{+\theta} + t^{-\theta}[C_{global}]^{-\theta} + t^{0}[C_{global}]^{0} \quad (8)$$

where $t^{+\theta}, t^{-\theta}$ and $t^{0}$ are specified as the thickness of each layer to the thickness of the laminate. Previous studies have considered these thicknesses to be identical [45]. For this work, the actual thicknesses of each layer are measured from microscopic images of the cross sections of the actual triaxially braided regenerated cellulose/ epoxy composites prepared using resin infusion. A cross-section micrograph of the composite showing the necessary dimensions is shown in Figure 12.

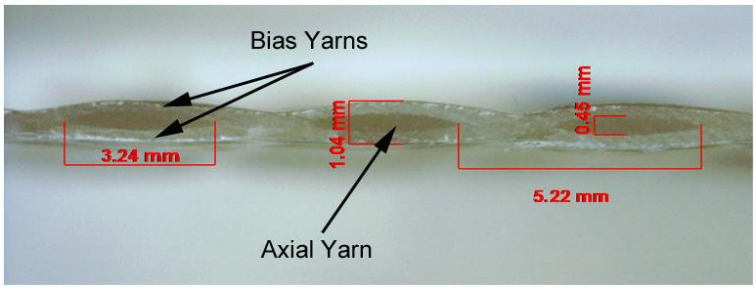


**Figure 12** Cross section micrograph for the cured triaxially braided regenerated cellulose/ epoxy composite

A brief summary of some of the results that can be obtained using the analytical solution are shown in Figure 13.

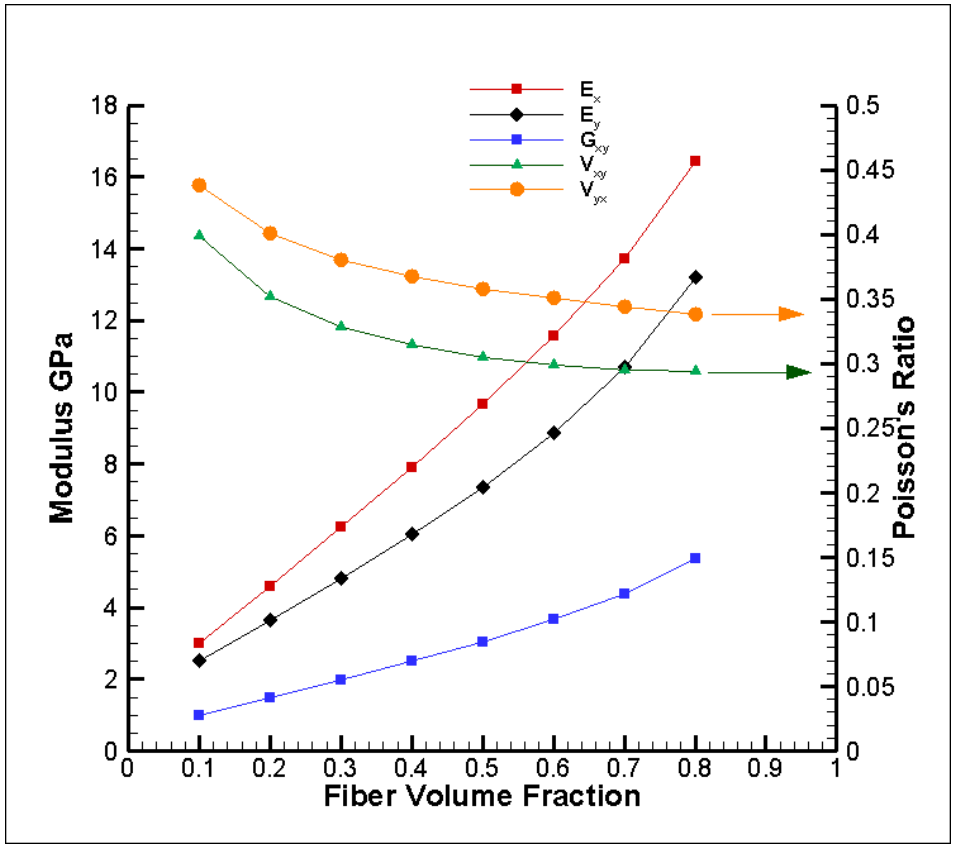


**Figure 13** Analytical model results for the effect of changing the fiber volume fraction on the elastic moduli ($E_x$, $E_y$, $G_{xy}$) and Poisson's ratio ($\upsilon_{xy}$, $\upsilon_{yx}$)

In order to validate the results given by the discrete-three layers analytical solution, composite panels for regenerated cellulose triaxially braided composites were prepared and tested for the mechanical properties; mainly the elastic modulus in the axial and transverse directions and the Poisson ratios. The mechanical testing experiments were performed in a displacement-controlled mode at a displacement rate of 1.3 mm/min (0.05 in/min). Both axial and transverse coupons with an approximate width of 38 mm (1.5 in) were tested (Figure 14). The load on axial and transverse specimens was applied using an electromechanical test system with a 97.8 kN (22.0 kips) capacity. An extensometer was used for recording the elastic deformation behavior along a 25mm length at the middle of the specimens. The stiffness properties are extracted within the 0 to 0.6 percent of the strain range from extensometer readings. The maximum error of the recorded load was within ± 0.022 kN (5.0 lb). For each orientation of axial fibers, three replicates were investigated.

Simultaneous mechanical testing, 3D-Digital Image correlation (DIC), and Acoustic Emission (AE) tests were carried out on a subset of the specimens. DIC was used to capture the strains on the surface of the composite specimen and to confirm the loading curves obtained by simple mechanical loading. The DIC technique uses a random speckle pattern applied to the specimen that is captured by using a couple-charged device (CCD) camera. These images are then processed by using correlation algorithms to compare strained maps with a reference image taken before the loading is applied. The procedure has been previously applied by El-Hajjar and Peterson by comparing strain results obtained from 3D-DIC with finite element predictions for carbon/epoxy laminates with through thickness cutouts [64]. More details about this method can be also found in

Schreier et al. [65].The digital image correlation tests were performed by using the Dantec Dynamics Q-400 system. A resolution of 5 megapixels was used for the two CCD cameras, together with a 30 mm Schneider Xenoplan lens. Acoustic emission was used to investigate damage initiation and damage propagation through the study of cumulative energy versus time of the recorded acoustic emissions during mechanical loading. A Mistras 2001 data acquisition system was used for recording the data, including waveforms. A Physical Acoustics WS-alpha transducer was used for measuring the AE signals. The sensor has an operating frequency of 100-1000 kHz with a 63.74dB peak sensitivity occurring at 523.23 kHz. In order to improve the quality of the captured signals; a pre-amplifier coupled with a bandpass filter adjusted to pass frequencies in the range of 10-1200 kHz was used.

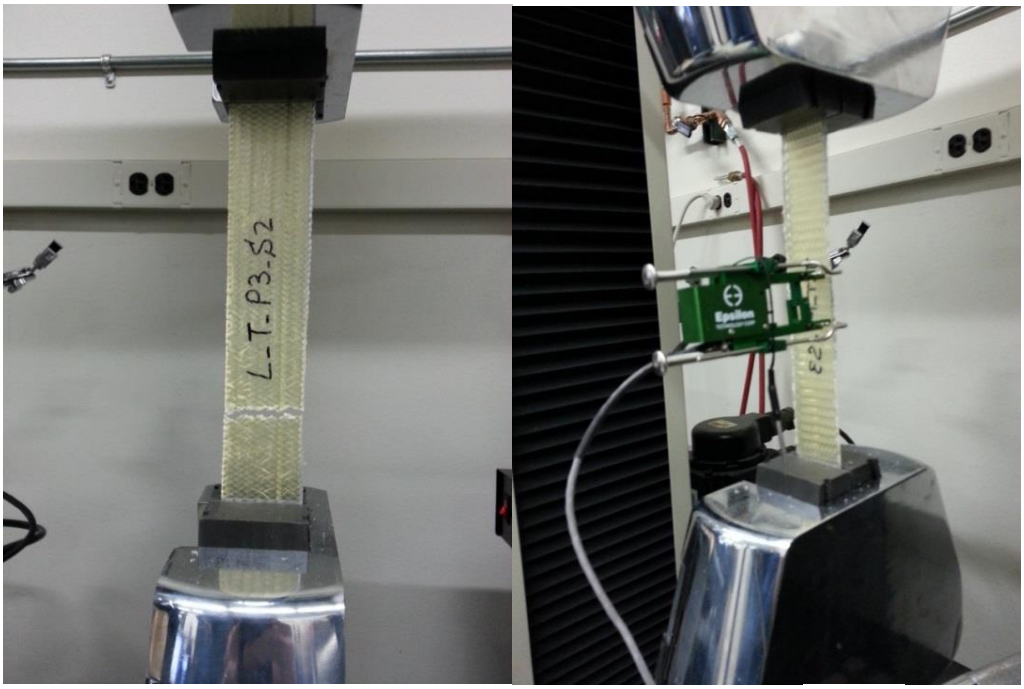


(a) (b)

**Figure 14** Mechanical testing of (a) an axial and (b) a transverse braided composite specimens

**Comparison of Experimental and Analytical Results**

The stress versus strain curves for longitudinal and transverse specimens loaded in tension shows that two regions can be identified (Figures15 and 16). The predictions provided by the three layer discrete model [32, 45] show a high correlation with the test results. Differences in stiffness between experimental and model results were found to be less than 4% in both longitudinal and transverse directions.

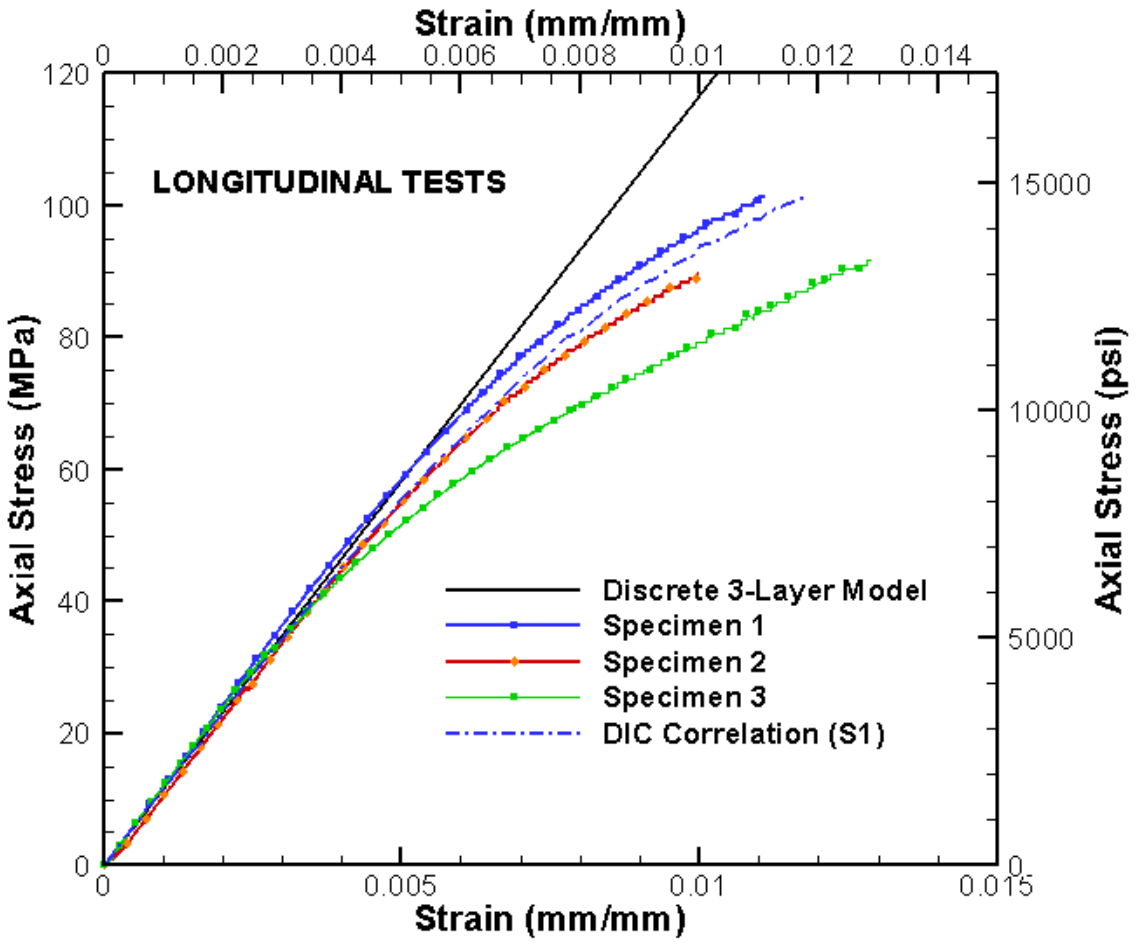


**Figure 15** Stress versus strain plots of regenerated cellulose/epoxy quasi-isotropic composites showing model prediction (longitudinal)

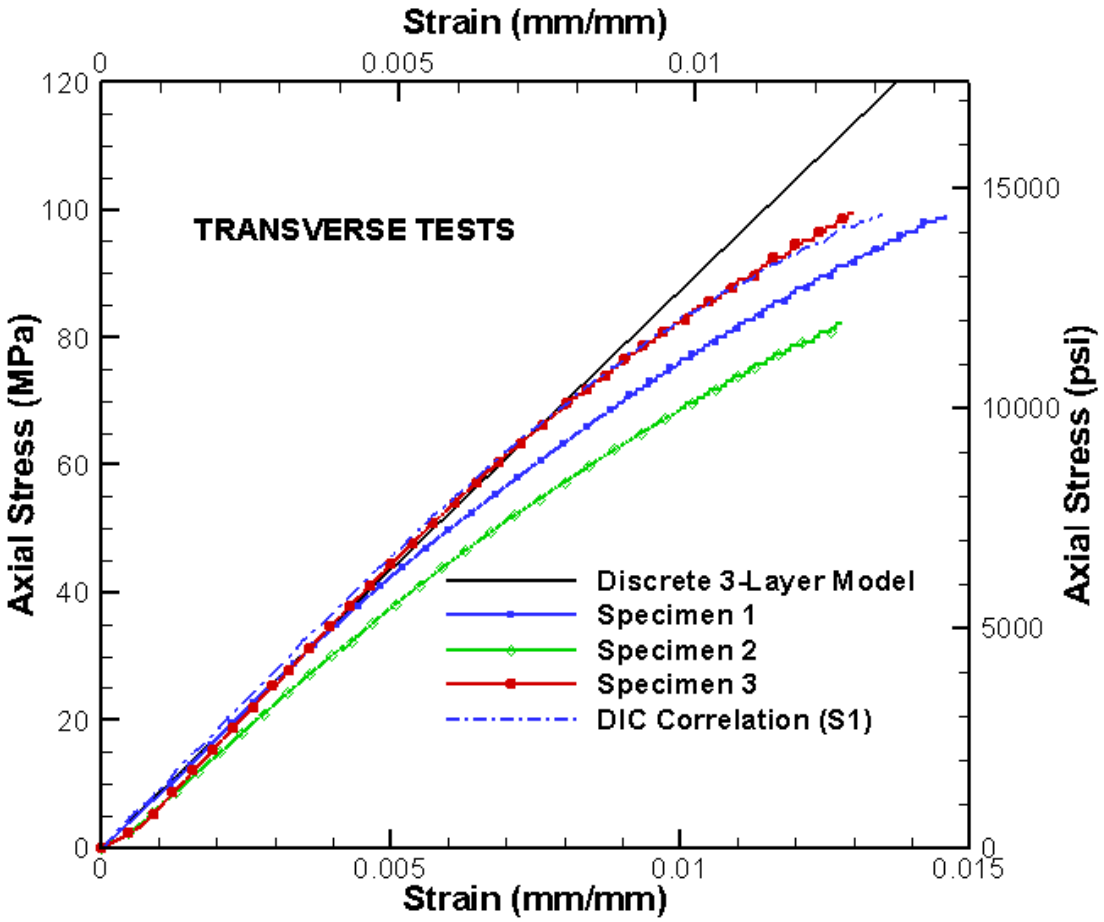


**Figure 16** Stress versus strain plots of regenerated cellulose/epoxy quasi-isotropic composites showing model prediction (transverse)

The results also show how the in-plane fiber architecture of the quasi-isotropic triaxially braided composite yields close stiffness in both the axial and transverse directions. Two regions can be immediately identified for the loading curve in which the first is linear elastic and the second is the region with a lower stiffness. The loading properties are similar to other regenerated cellulose composites, e.g. Lyocell/epoxy composites discussed in the earlier sections of this chapter.

Using the analytical model, the effects of fiber volume fractions (FVF) on the elastic properties can be investigated. The variation of longitudinal and transverse elastic modulus with respect to the fiber volume fraction shows good correlation with the experimental data (Figure 17). The same is observed for the Poisson ratio predictions by the model (Figure 18). A nonlinear relationship between fiber content and elastic properties is predicted by the model. The relationship is a direct proportion between FVF and elastic moduli and an inverse relationship with Poisson's ratio.

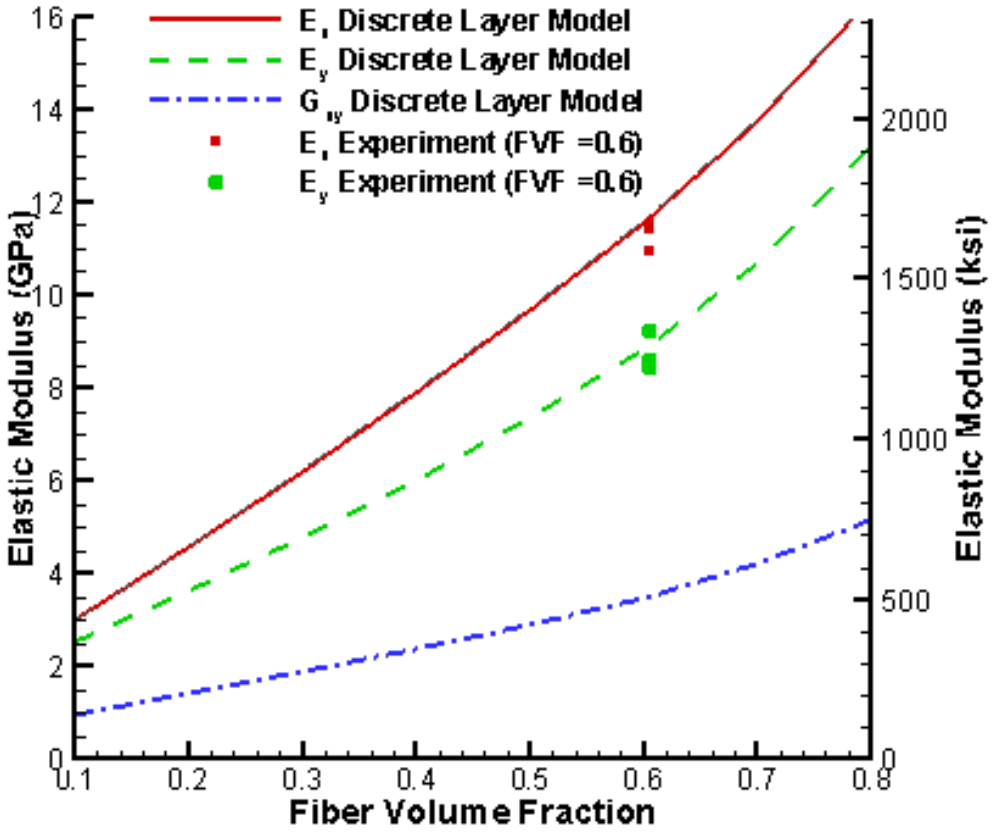


**Figure 17** Prediction of stiffness properties versus fiber volume fraction

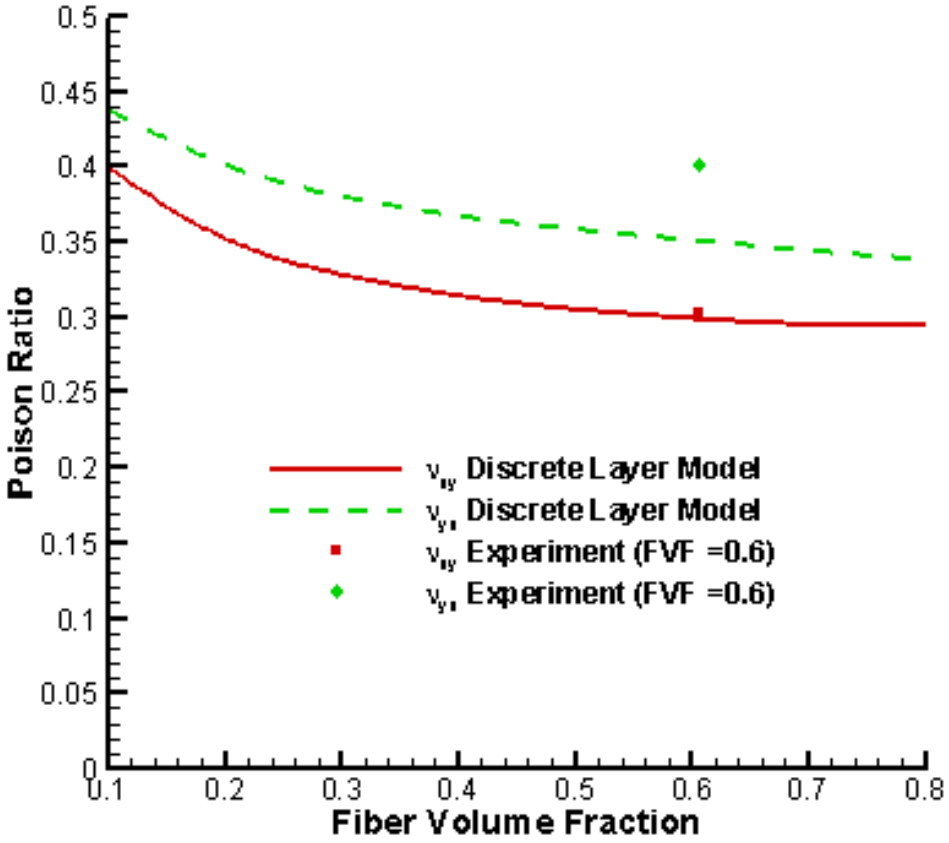


**Figure 18** Prediction of Poisson's ratio versus fiber volume fraction

The effects of the crimp angle on the mechanical constants were also investigated. Figure 19 shows a relatively high sensitivity of the transverse modulus of elasticity to the crimp in the bias yarns. However, there is not a significant variation of predicted longitudinal stiffness with the crimp angle as the behavior in that direction is dominated by the longitudinal fibers that have no undulations. In contrast with $E_X$ ; $E_Y$ decreases by increasing the aspect ratio since this parameter affects the bias yarns that have a larger contribution in the transverse direction (Figure 19). Note that there is a physical limitation on the aspect ratio as this is a function of the yarn spacing and the fiber volume fraction of the composite. In addition, a comparison of the effects of changes in the

aspect ratio shows less of an effect on the predicted properties of the quasi-isotropic material compared with other braided systems [32]. Similar results are shown for the effect of crimp angle on Poisson ratio, where the Poisson ratio in the transverse direction is more sensitive than in the longitudinal direction (Figure 20). The test results show that the microstructure effects are pronounced in the transverse specimen largely due to the relatively large spacing between the axial yarns.

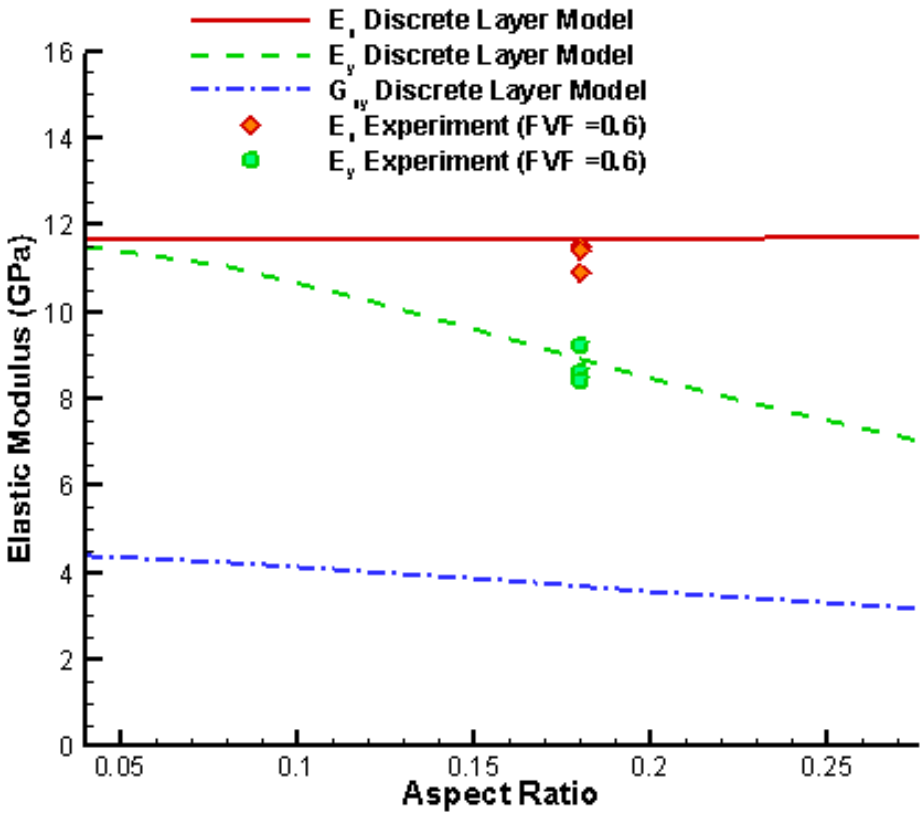


**Figure 19** Effect of aspect ratio in the bias yarns on the elastic modulus

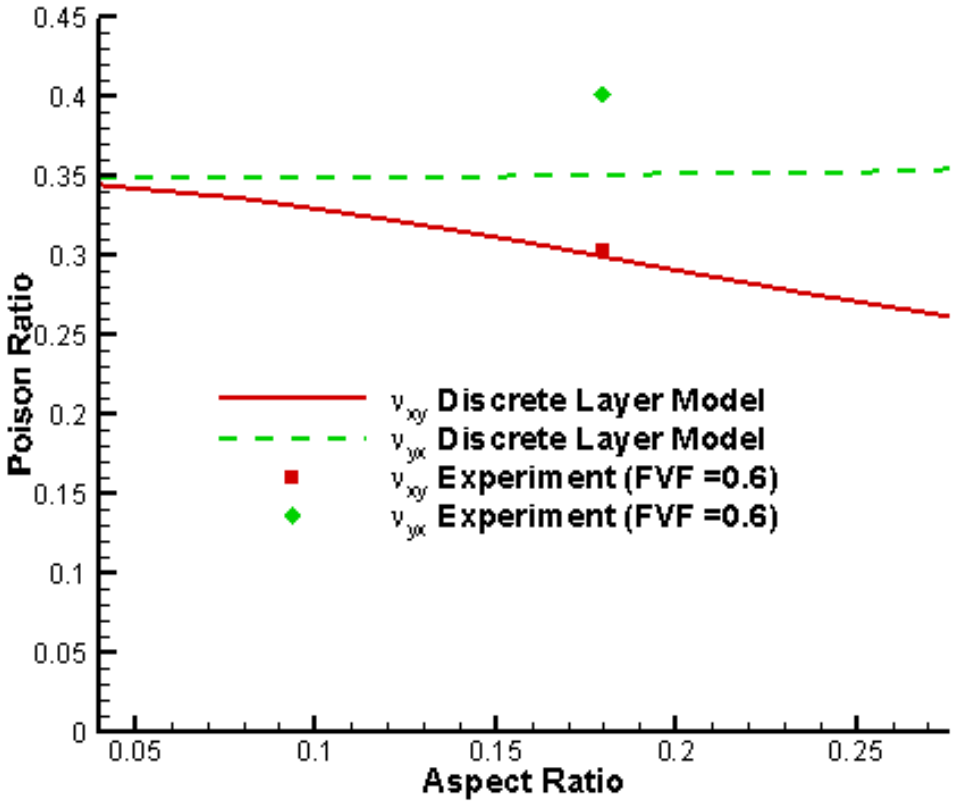


**Figure 20** Effect of aspect ratio in the bias yarns on Poisson's ratio

The 3D Digital Image Correlation results show a high correlation between loading curves obtained by mechanical loading and the full-field strain measurements. The strain fields from DIC are also included in Figures 15 and 16 above to show the correlation with the extensometer measurements. The strain fields were averaged over the area of the specimen and were used to obtain the Poisson ratios, $\nu_{xy}$ and $\nu_{yx}$ (Table 4). The same table also shows a summary of the results of the mechanical results predicted by the analytical solution and the experimental results for a 60% fiber content by volume.

**Table 4** Predicted and experimental results for triaxially braided regenerated cellulose/epoxy composite system (FVF = 60%)

| Mechanical Property | Discrete 3-Layer Model | Experiments |
|---|---|---|
| $E_x$ GPa (Msi) | 11.67 (1.69) | 11.22 (1.63) |
| $E_y$ GPa (Msi) | 8.74 (1.27) | 9.06 (1.31) |
| $\nu_{xy}$ | 0.296 | 0.303 |
| $\nu_{yx}$ | 0.351 | 0.401 |
| $G_{xy}$ GPa (Msi) | 3.46 (0.52) | - |

**Other Significant Results**

The results of cumulative acoustic emissions superimposed with the stress strain curves (Figure 21) show that the initiation of damage starts at a much lower stress level in the transverse specimens compared to the first emissions observed in the longitudinal specimens. The initial emissions are likely due to the matrix cracking. Higher energy emissions before failure are observed for the longitudinal specimens where the final cumulative energy at failure is 35% higher. This is believed to be associated with the fracture of the axial fibers oriented in the direction of loading. While a distinction between initial and final ply failure cannot be directly made, the incidence of high acoustic emissions can be used as an indication of the point of detrimental irreversible damage.

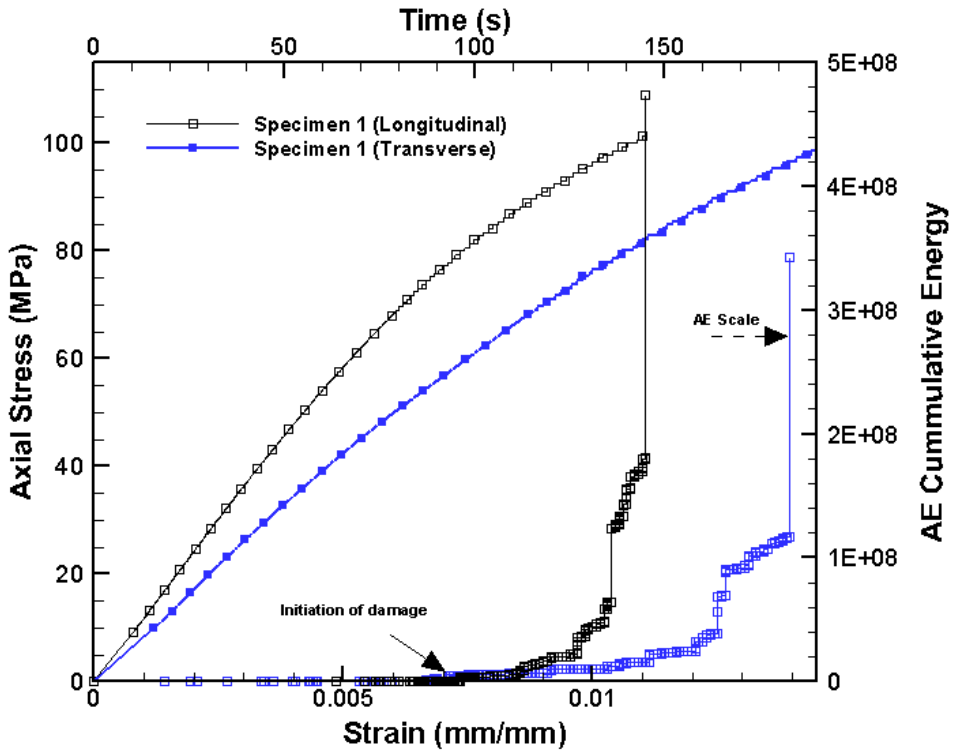


**Figure 21** Stress versus strain and acoustic emission cumulative energy plots of regenerated cellulose/epoxy quasi-isotropic composites (longitudinal and transverse specimens)

Figure 22 shows the damage progression in longitudinal and transverse coupons using the DIC method. Figure 22 (a) shows that the load in the longitudinal tension tests is uniformly distributed. Consequently, the interlaminar shear stresses as a result of increasing the shearing stresses in the axial and bias yarn interface are believed to be causes of the interfacial matrix cracking [66]. The strain patterns in the transverse specimens show a significant effect of the microstructure, especially at the edges. The specimens show large areas of low stress in the regions between the axial yarns. These patterns are also associated with deflections in the out-of-plane of the image as the

coupon is loaded in tension. The pattern indicates the stresses associated with this deformation pattern can contribute to edge damage.

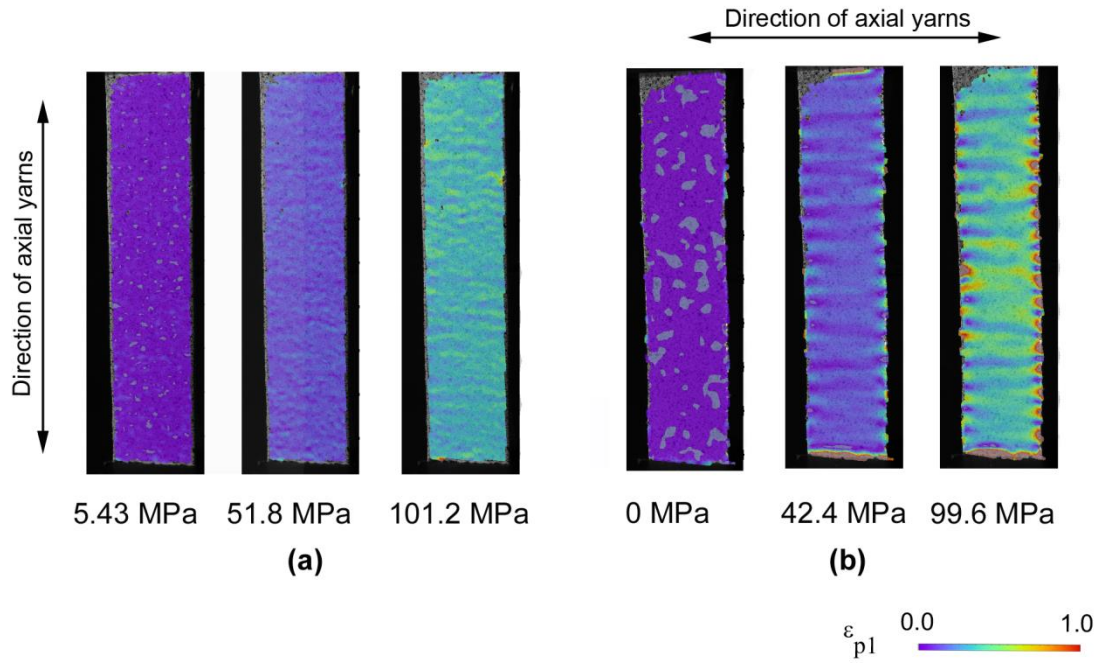


**Figure 22** Progression of principal strain distribution in (a) longitudinal specimen (b) transverse specimen

The full field strain measurements show the limitations of the rectangular coupon in capturing the transverse deformation behavior due to the abnormal behavior at the specimen edges. This abnormal behavior results in significant out-of-plane deformation creating areas of stress concentration at the edges from which failure can propagate. They also reduce the effective width of the specimen.

### 4.3 Fracture Study

It is difficult to obtain reliable strength properties for triaxially braided composites due to failure mode inconsistencies. Notched specimens are more suited to strength

measurements[67] and are expected to result in higher strength values than test coupons. For the purpose of this research, notched and unnotched specimens were tested for strength properties, and the results were compared. In addition to the mechanical tests described above, the strength of the triaxially braided regenerated cellulose/ epoxy composites was evaluated using notched specimens. For the notched specimens, the specimens were 152 mm (6 in) long by 76 mm (3 in) wide. Two notches were machined at each side leaving an uncracked ligament of 36mm (1.4 in). The preparation and testing of notched samples is shown in Figure 23.

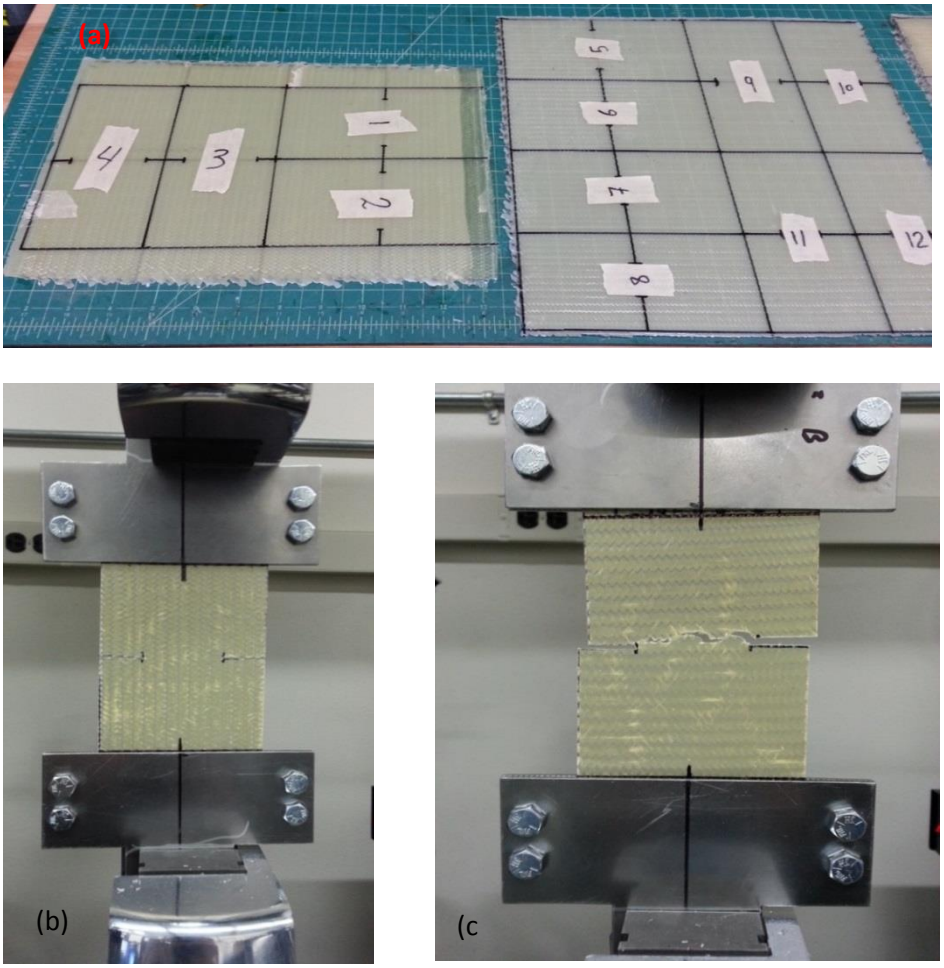


**Figure 23** (a) Preparation and testing of (b) an axial and (c) a transverse notched samples

A simple finite element model was used to study the behavior of the notched specimens. The model was generated in commercially available p-FEA software (Stress Check V9.0; ESRD, St. Louis, Missouri, USA). The typical notched sample used 24 quadrilateral elements. The notches were modeled by creating two independent nodes at the farthest end of each crack tip. The two adjacent elements were created by attaching the nodes so that each element is attached to one of the two independent nodes. This way, the two adjacent elements are continuous at the crack tip but move independently at the end of the crack. Boundary conditions were applied to restrict all in-plane movements of the sample at one edge in the loading direction and to restrict the in-plane movement perpendicular to the loading direction at one point towards the center of the constrained edge. The load was applied as a traction force, linearly distributed on the opposite edge. The model is parameterized for several changes that affect the notched mechanical properties including the size of the notches, the height, thickness and width of the sample, and the value of the applied load. A description of the model parameters is shown in Figure 24. The tensile test results for notched and unnotched samples and the FE results are shown in Figure 25. The proposed analytical model shows a reasonable prediction of the elastic properties within the range of the properties measured. Notched specimens are also seen to have 15-20% higher elastic modulus values compared to unnotched specimens. One explanation might be that the better engagement of the notched specimens in the wedge grips and the gripping on all biased and axial yarns has resulted in better test conditions in which slipping was minimized and higher mechanical properties were obtained.

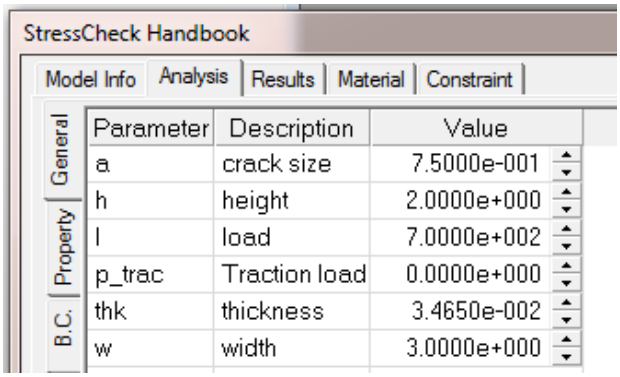


**Figure 24** Parametric parameters for the notched p-FEA model

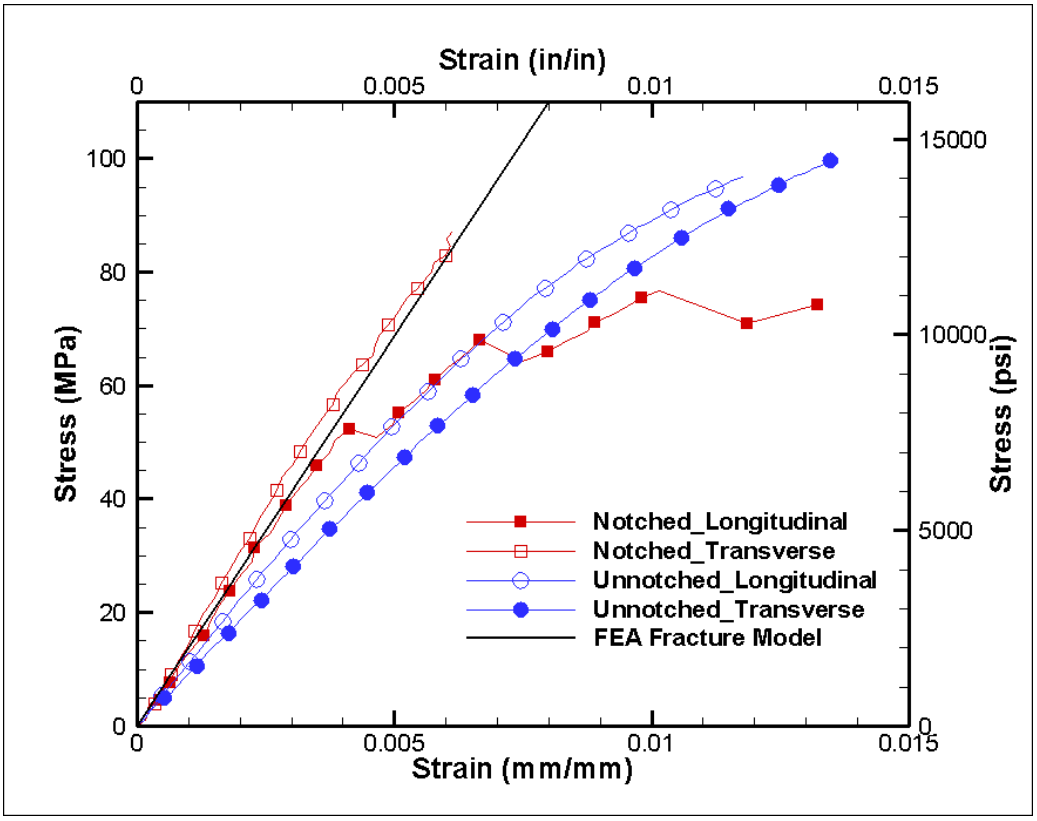


**Figure 25** Stress strain behavior of notched and un-notched triaxially braided regenerated cellulose composites.

The results of the tension strength (Figure 26) show some interesting observations both related to notched and un-notched behaviors as well as the comparison amongst

transverse and axial properties. A comparison of the acoustic emissions and loading curves indicating initiation damage show these to occur at a much earlier load in the unnotched specimens. This can be attributed to the edge deformations seen in Figure 22 demonstrated previously; especially related to the transverse specimens. The notch concentrates the deformations in a smaller area thus limiting the edge influences and also results in less variability in the test results. It thus results in a higher initiation damage load level. However, the increased stress concentration at the notch is likely the cause for the slightly reduced ultimate strength in both orientations.

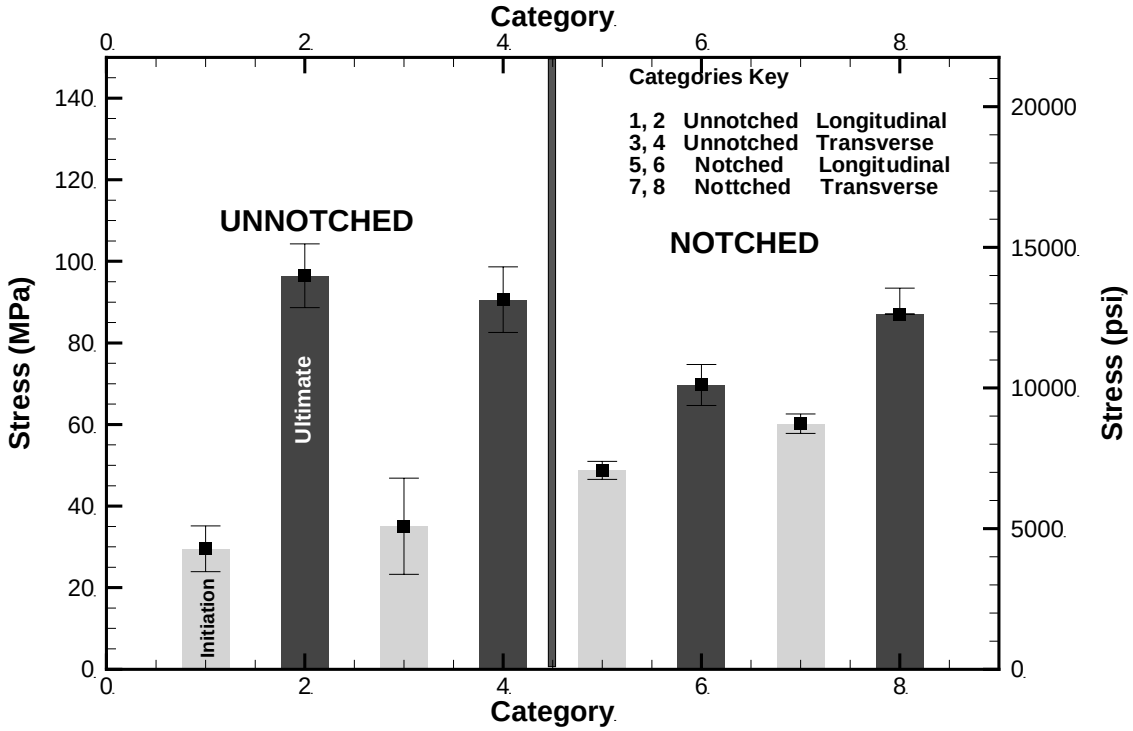


**Figure 26** Initiation and ultimate failure of unnotched and notched RF/epoxy specimens (Qamhia et al., 2014)

After the results of the p-FEA model were validated with the experimental results for the 0.8 inch crack size, and the results were found to match the experimental measurements; the model was run for different notch sizes to evaluate the effect of notch sizes on the strain energy release rate ($J_I$). The results were evaluated for different stress levels for three crack sizes: 12.7, 19.1 and 25.4 mm (0.5, 0.75 and 1.0 inch respectively). Sample runs are shown in Figure 27 and the comparison of the results for different crack sizes is shown in Figure 28. The critical strain energy release rate ($J_{1c}$) was determined by running the model with the experimented notch sizes and applying a load equivalent to the ultimate load withheld by the experimental notched samples. The J-integral values are computed in StressCheck for linear and elastic-plastic solutions of isotropic materials and for linear solutions of orthotropic materials. The values are computed by specifying the radius of a circle that represents the integration path. The radius is selected such that the circle remains in the solution domain. The influence of the size of the extraction circle on the results is generally very small if proper meshing is utilized [68].

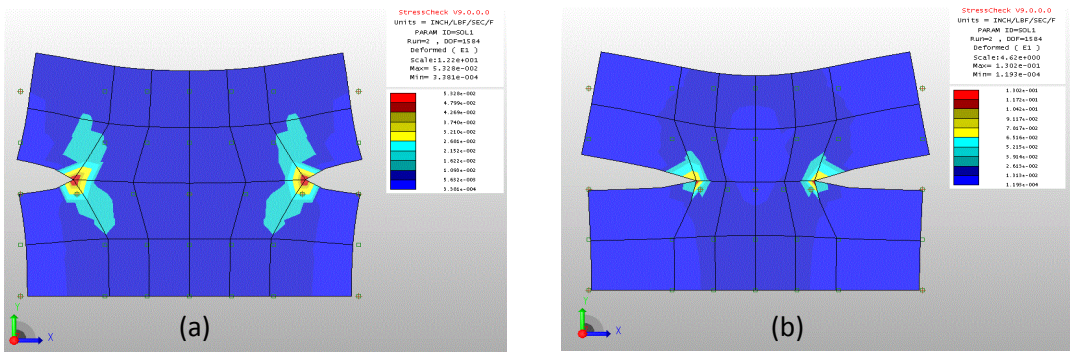


**Figure 27** p-FEA fracture model for (a) 12.7 mm (0.5 in) notch and (b) 25.4 mm (1.0 in) notch sizes

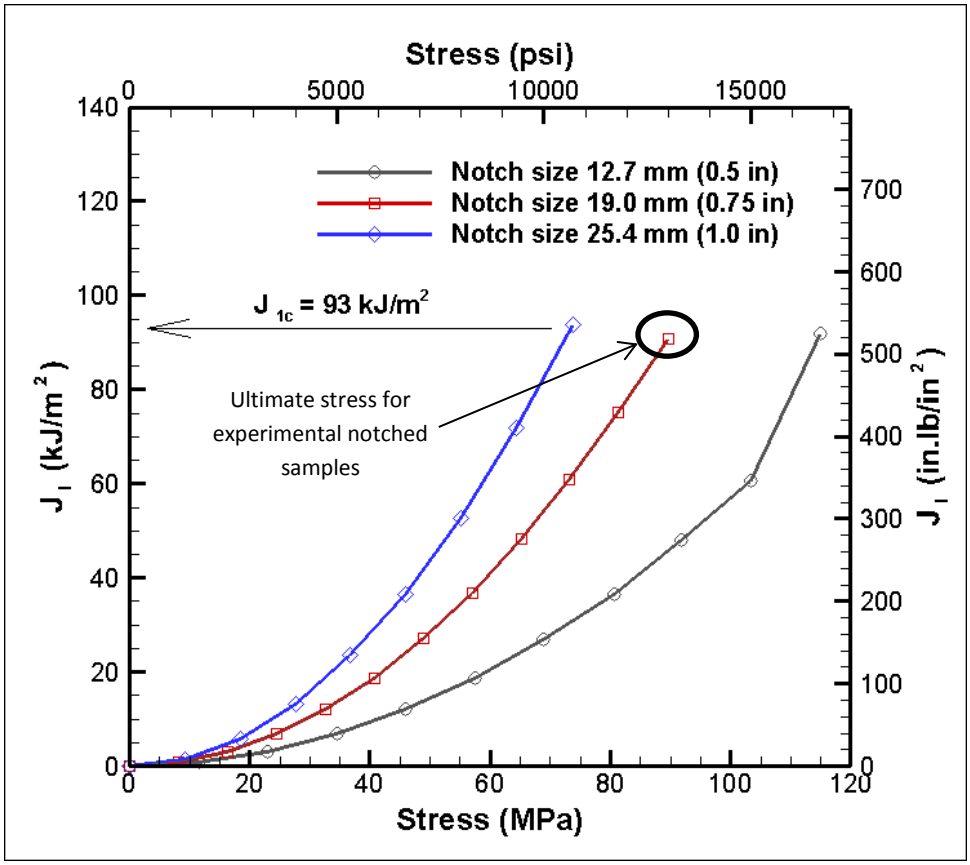


**Figure 28** J-integral results for notched triaxially braided regenerated cellulose samples with different notch sizes

### 4.4 Viscoelastic Behavior of Triaxially Braided Composites

The use of viscoelastic techniques such as DMA to characterize cellulose and regenerated cellulose composites have been previously reported. Bledzki et al. studied the effect of fibrous reinforcement incorporation of regenerated cellulose fibers produced in chemical–technical viscose processes and natural abaca fibers on the dynamic-mechanical performance of native Polylactic acid (PLA) and its composites [69]. They found out that the incorporation of fibers enhances the $T_g$ to a higher temperature due to the altered mobility of the polymer chains. Soykeabkaew et al. used dynamic mechanical

analysis to investigate the effect of temperature on the storage modulus of three different types of regenerated cellulose composites; namely: low draw ratio Lyocell, high draw ratio Lyocell and Bocell fibers [3].

Bocell composites were found to have outstanding mechanical and thermal performances over Lyocell; seen by a higher elastic modulus over the tested temperature range. Tajvidi et al. studied the dynamic mechanical properties of natural fiber / polypropylene (PP) composites [70]. The natural fibers used included wood flour, Kenaf fibers, rice hulls and newsprint. A decrease in the mechanical loss factor was observed for all the composites as compared to the pure PP resin indicating a more elastic behavior of the composites. The latter two studies show the suitability of DMA to characterize regenerated cellulose composites and its efficiency as a materials characterization comparison tool between similar composites. Jacob et al. [71] investigated the effect of fiber weight fraction and alkali treatment on the thermo-mechanical properties of a natural fiber-reinforced natural rubber composites by dynamic mechanical analysis.

Dynamic mechanical analysis is a thermo-mechanical technique that monitors property changes due to a temperature and/or a frequency or a time change. The technique measures the total energy stored and dissipated in the material due to a dynamic stimuli. DMA separates the viscoelastic properties into an elastic part and a viscous part. The elastic part is measured by the storage modulus (*E'*), which accounts for the energy stored in the material due to the dynamic response. The loss modulus (*E"),* on the other hand, measures the energy dissipated in the material due to the viscous part of the dynamic response. This energy is lost due to friction and internal motions. The equations of the storage and loss modulus are given by Menard [72] as follows:

$$E' = \frac{\sigma_0}{\varepsilon_0}\cos(\delta) = \frac{f_0}{bk}\cos(\delta) \qquad (9)$$

$$E'' = \frac{\sigma_0}{\varepsilon_0}\sin(\delta) = \frac{f_0}{bk}\sin(\delta) \qquad (10)$$

where $f_o$ is the force applied at the peak of the sinusoidal wave, $k$ is the sample displacement at the peak, $b$ is a term for sample geometry, $\sigma^o$ and $\varepsilon^o$ are the maximum stress and the strain at maximum stress respectively, and $\delta$ is the phase angle. The phase angle ($\delta$) is the primary DMA output. The phase lag between a sinusoidal applied stress (e.g. $\sigma = \sigma_o \sin \omega t$) and a measured strain (or vice versa) is due to the viscoelastic behavior of most materials. A fully elastic response produces an in-phase response while a fully viscous response produces an out of phase response. The tangent of the phase angle ($tan\ \delta$) is called damping and is defined as the ratio of the loss to storage modulus (Equation 3). Damping is a measure of how efficiently a material loses energy to molecular rearrangements and internal friction as a response to the dynamic stimuli.

$$\tan(\delta) = \frac{E'}{E''} \qquad (11)$$

For a three-point bending clamp, the model equation for a rectangular cross section sample is given as:

$$E = Ks\frac{L^3}{6I}\left[1 + \frac{6}{10}(1+\nu)\left(\frac{t}{L}\right)^2\right] \qquad (12)$$

Where $E$ is the elastic modulus, $Ks$ is the measured stiffness, $I$ is the moment of inertia of the rectangular cross section, $t$ and $L$ are the thickness and the length of the specimen

respectively, and $v$ is the Poisson's ratio. The equation assumes that the local deformations in the region of the supports are negligibly small that no correction factor between the measured stiffness (*Ks*) and the model stiffness (*K*) for a rectangular beam under three-point flexure.

### 4.4.1 Experimental Approach

Similar to the composite panels used for the validation of the analytical models discussed in the previous sections; the composite samples used for this study were also prepared from triaxially braided regenerated cellulose fibers (BioMid; GSC and ENC, Inc., Burnaby, BC, Canada) and a high-bio content epoxy resin system (Super Sap 100/1000; Entropy Bio-Resins, Gardena, California, USA). The regenerated fibers were stored at room temperature and a humidity level of around 30%. The panels from which the samples were cut were prepared by a vacuum assisted resin infusion technique. For comparison purposes, pure epoxy samples were prepared and tested under the same dynamic conditions. The pure resin samples were prepared by a wet layup technique from the excess resin that was used in preparing the composites panels. Using the same resin batch ensures consistency in the composition and sets an accurate control point to compare the behavior of the different triaxially braided regenerated cellulose fibers on the mechanical behavior of the composites. In addition, all prepared samples were post-cured in an oven for 240 ±5 minutes at a fixed temperature of 75 ˚C (167 ˚F) to ensure full cure of the resin.

The study was carried out on a DMA system (Q800; TA instruments, New Castle, Delaware, USA). A three-point bending mode with a controlled strain of 15 µm

(displacement) was used. A picture of the test setup is shown in Figure 29. For the first part of the study, pure epoxy samples and samples of triaxially braided regenerated cellulose reinforced composites were tested at a constant frequency of 1.0 Hz. A temperature range of 0-150 $^{o}$C (32-302 $^{o}$F) and a heating rate of 3 $^{o}$C/min (5.4 $^{o}$F/min) were chosen. The tested regenerated cellulose/epoxy samples were approximately 35 x 10-12 x 0.8 mm (1.4 x 0.4-0.5 x 0.03 in) in length, width and thickness respectively. Neat epoxy samples were approximately 35 x 11 x 1.3 mm (1.4 x 0.45 x 0.05 in) in length, width and thickness respectively. The supported span width was 20 mm (0.8 in). The test parameters were chosen to comply with the general recommendations of the ASTM D4065-12 [73] and ASTM D5023-07[74] standards. For the regenerated cellulose reinforced composites, the effect of moisture on the behavior of the composites was investigated by soaking samples in water at a room temperature of 22 $^{o}$C (72 $^{o}$F) for a period of 120±5 minutes. The change in mass for the surface dry composites was recorded and the wetted samples were tested in DMA to investigate the effect of soaking on the viscoelastic properties. In the second series of tests conducted for the frequency effects, the same DMA loading and running parameters discussed above were used except as discussed below. The loading frequency values were selected at 1,10, and 50Hz. The temperature and frequency ramping were performed simultaneously. The frequency effects study was carried out on a temperature range of 20-135 $^{o}$C (68-275$^{o}$F).

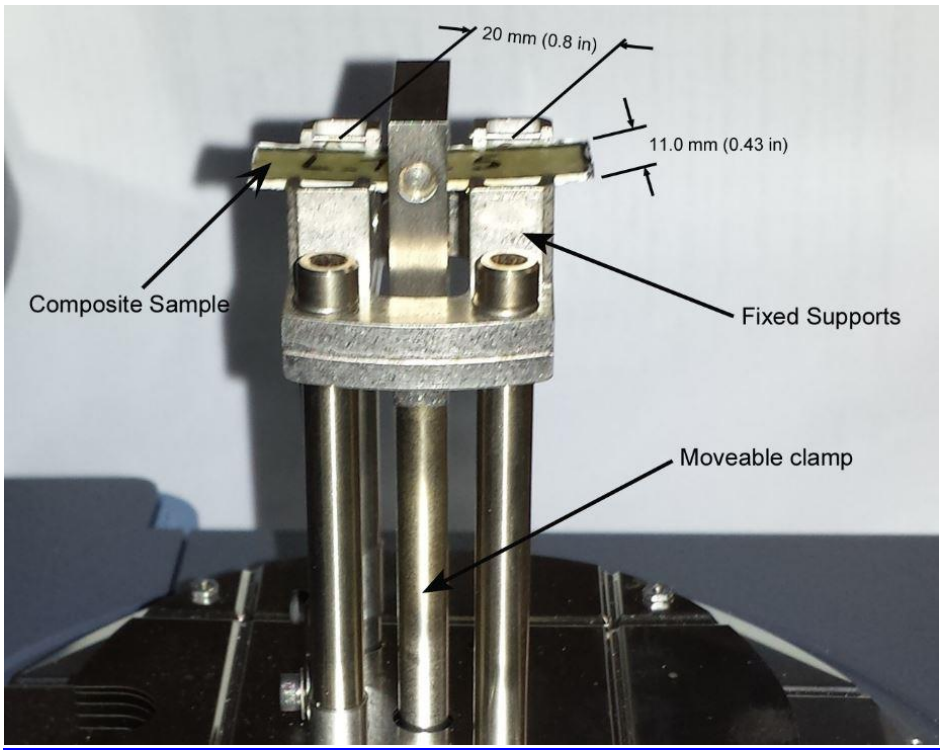


**Figure 29** DMA three-point bending test setup

### 4.4.2 Results and Discussion

The waviness in the bias yarns makes the thickness variable across the specimens (Figure 12). In our calculations, the average thickness was used for the DMA calculations of storage modulus. The results of the first part of the study by DMA are shown in Figures 30-35. Figure 30 shows the variation in the storage modulus with temperature. For the three sets of samples, a nonlinear degradation in the storage modulus is observed as the temperature increases. As expected, the neat epoxy specimens show the highest degradation in modulus as these were held as controls. The wet specimens showed the second largest drop. The epoxy specimens were found to lose all of their elastic properties at a temperature of 70 ºC (158 ºF), while the dry and wet regenerated composites retained 11% and 15% respectively of their storage modulus for a

temperature up to 140 ºC (284 ºF); double that for epoxy. Due to the degradation of the mechanical properties of the fibers as they absorb water; soaking the samples for two hours is seen to reduce the storage modulus significantly at the lower temperatures. At higher temperatures, the storage properties of the wet and dry composites are similar. One explanation might be that the fibers recover some of their mechanical strength as the water evaporates. One general observation was that for the same testing parameters, the wet composite samples were slightly warped after testing while the dry samples didn't show any obvious curvature. The curvature results from the uneven swelling of the cellulose fibers. Note that the values of the storage modulus at room temperature obtained for the triaxially braided regenerated cellulose/epoxy composites are significantly lower than the values of the elastic modulus obtained by the mechanical testing of uniaxial tension specimens shown in Table 5. This can be attributed to the nonlinearity in the load displacement response and the data reduction approach used in the analysis of the DMA results, which is based on a point measurement approach.

**Table 5** Elastic Properties of triaxially braided regenerated cellulose/epoxy composite system

| Mechanical Property | Analytical | Coupons | DMA* |
|---|---|---|---|
| $E_x$ GPa (Msi) | 11.67 (1.69) | 11.22 (1.63) | 3.5 (0.51) |
| $E_y$ GPa (Msi) | 8.74 (1.27) | 9.06 (1.31) | 3.0 (0.44) |
| $\nu_{xy}$ | 0.296 | 0.303 | - |
| $\nu_{yx}$ | 0.351 | 0.401 | - |
| $G_{xy}$ GPa (Msi) | 3.46 (0.52) | - | - |

* DMA values are for the storage modulus

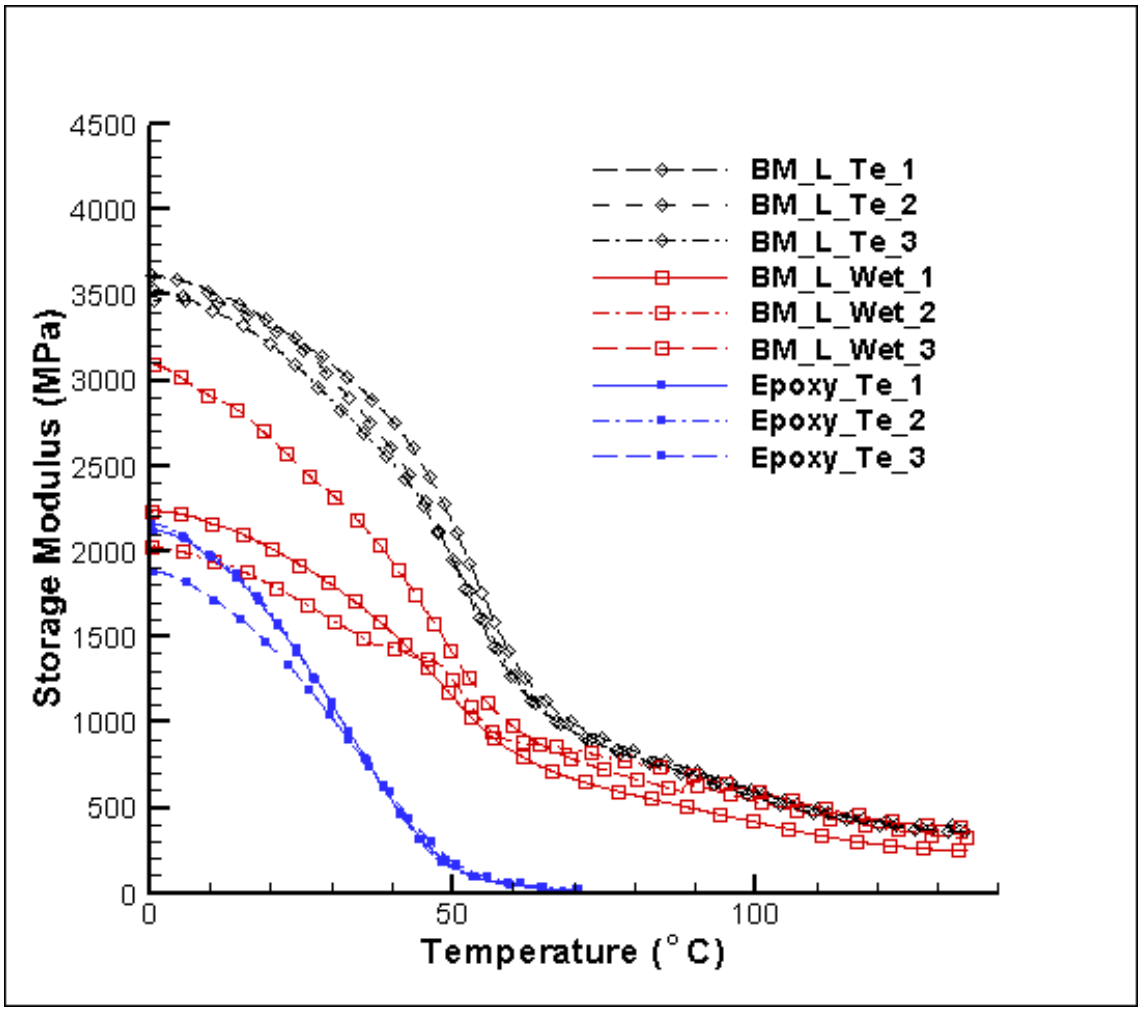


**Figure 30** Changes in the storage modulus of neat epoxy and wet and dry triaxially braided cellulose composite with temperature ramping.

For the loss modulus results (Figure 31), a shift in the peak is seen between the neat resin and the wet and dry regenerated cellulose/epoxy specimens. The same trend in peak shifts is also shown in the *tan δ* plots (Figure 32), where the glass transition temperature ($T_g$) is higher for the regenerated cellulose composites but drops with the wetting of the composites. The neat epoxy specimens also show higher damping characteristics as characterized by higher *tan δ* peaks.

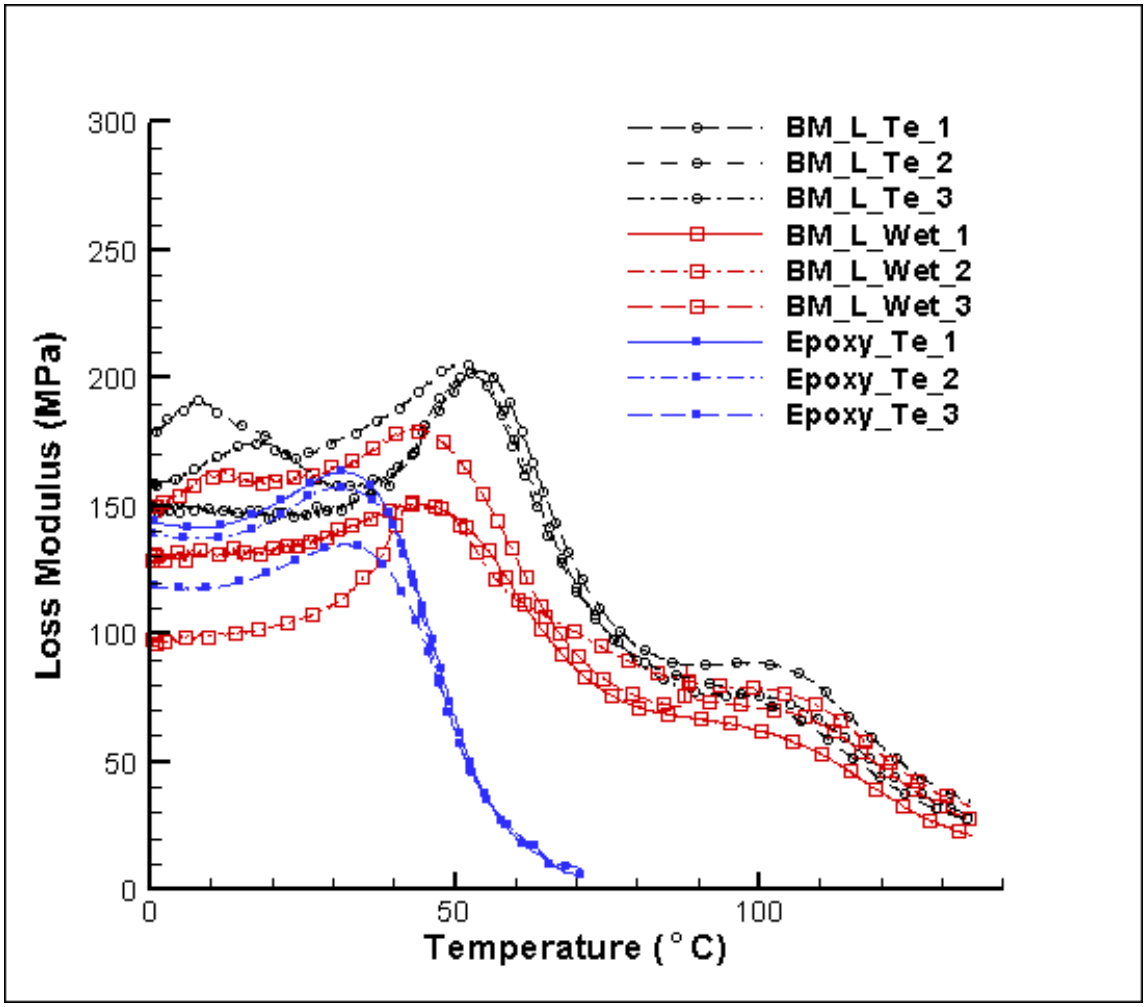


**Figure 31** Changes in the loss modulus of neat epoxy and wet and dry triaxially braided cellulose composite with temperature ramping.

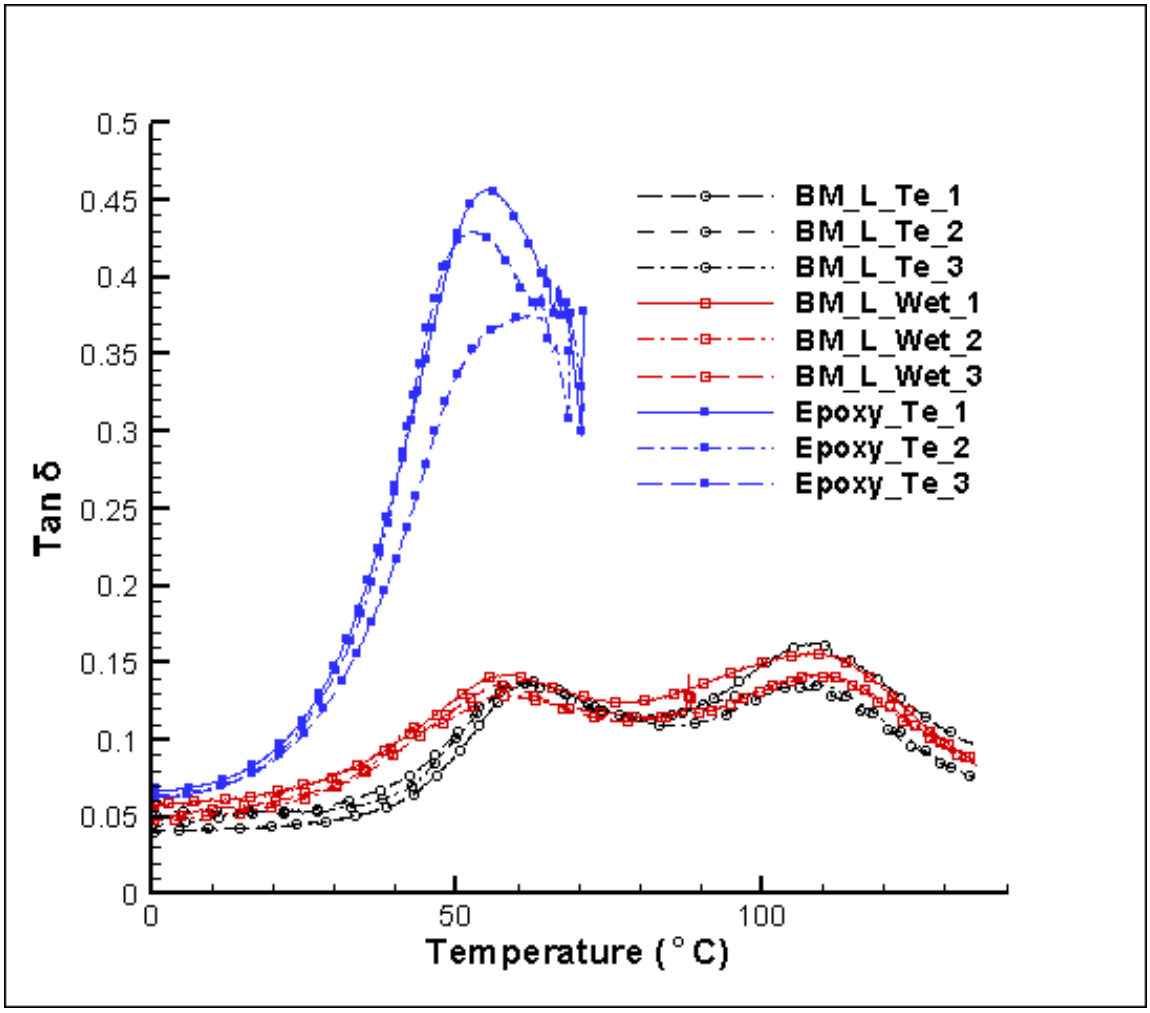


**Figure 32** Changes in *tan δ* of neat epoxy resin, wet and dry triaxially braided cellulose composite with temperature ramping

A second peak is observed for both the wetted and dry composites at a temperature of around 110 ºC (230 ºF) in the curves of *tan δ* and the loss modulus. Initially, this peak was thought to indicate an incomplete cure in the resin, as it was reported by Margem et al. [75]; thus a second heating of one of the composites sample was carried out (Figure 33) to investigate the reasons behind the peak. The curve for the second heating still showed the two peaks at relatively the same temperatures and damping rates; with the second peak shifted 5 ºC (9 ºF) to the right. Thus, this second peak is likely not due to

incomplete cure of the resin. Guo and Ashida observed similar duplications of peaks and reported that the *tan* $\delta$ versus temperature curves for composites materials of two phase systems can show two peaks characteristic of the $T_g$ of each of the components[76]. To investigate whether the second peak is a result from the BioMid fibers or the braiding architecture, samples of triaxially braided glass fibers were tested using DMA under the same loading and heating parameters described above. The results are shown in Figure 34. For glass fiber/epoxy composites, a second peak was also seen at 125 ˚C (257 ˚F); the peak is thus not distinct to BioMid fibers. The first peak observed was thus attributed to the glass transition in the epoxy matrix; the second peak might be due to a transition of the fibers. Geethamma et al. also reported that a small, broad peak can be observed between the two distinct peaks in the two phase system due to the interface region in the composite [77]. One explanation of this peak might be also that it is a secondary transition of the epoxy, which is quite common for polymers. Further, note that the second peak occurs after the $T_g$ of the resin, so it is not of main interest in this effort.

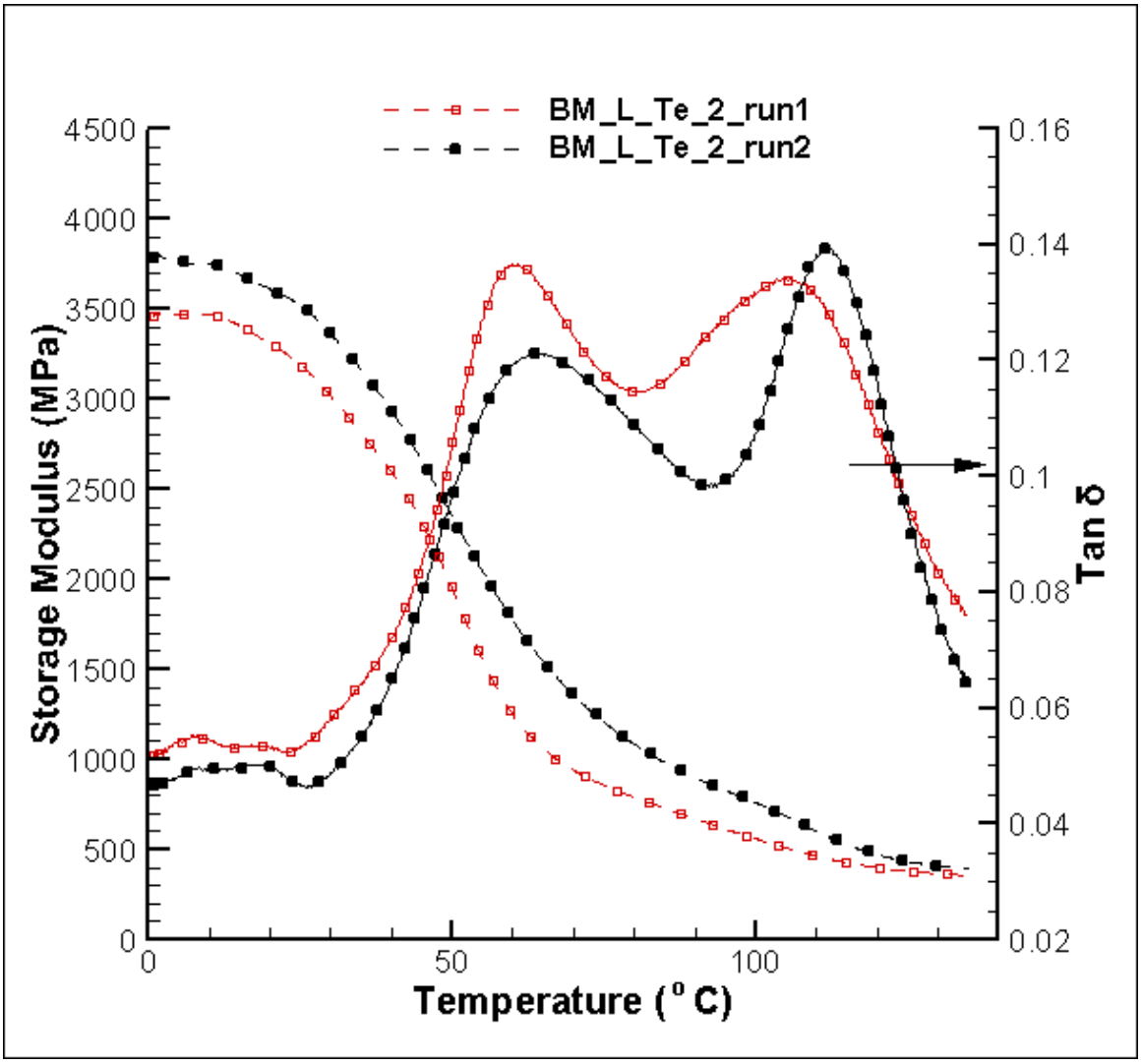


**Figure 33** Results for the first and second heating of triaxially braided dry regenerated cellulose/epoxy specimen

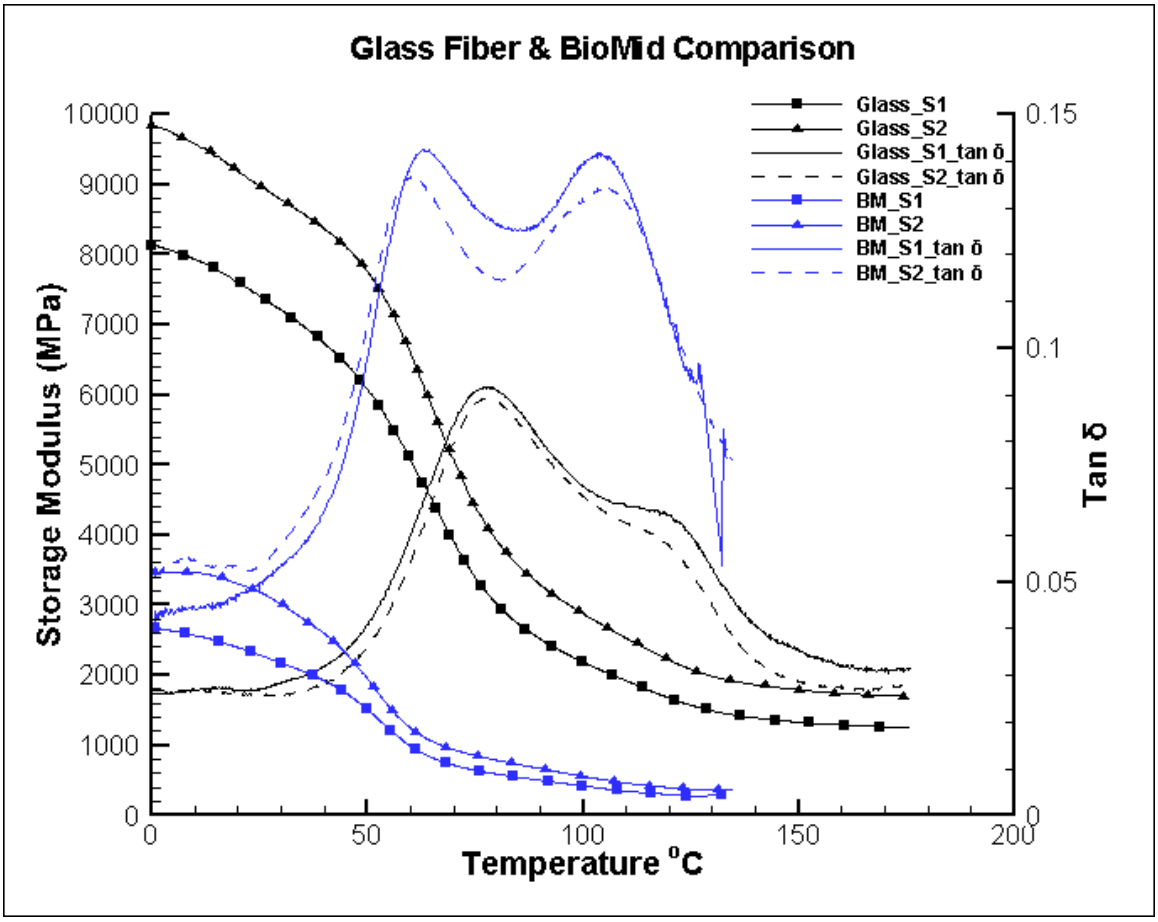


**Figure 34** DMA results for dry triaxially braided regenerated cellulose/epoxy and glass/epoxy specimens

In addition, a second heating was carried out for two of the originally wet samples to investigate changes in the viscoelastic behavior after the evaporation of water. The results for the storage modulus for both samples and *tan δ* for the first sample are shown in Figure 35. A slight enhancement in the storage modulus and a shift in the *tan δ* peaks are seen for the second heating. The storage modulus values however, do not recover to the values reported for the dry composites (Figures 30 and 33). Thus, part of the deterioration in the mechanical properties that is caused by exposure to water is irreversible if the composites are dried.

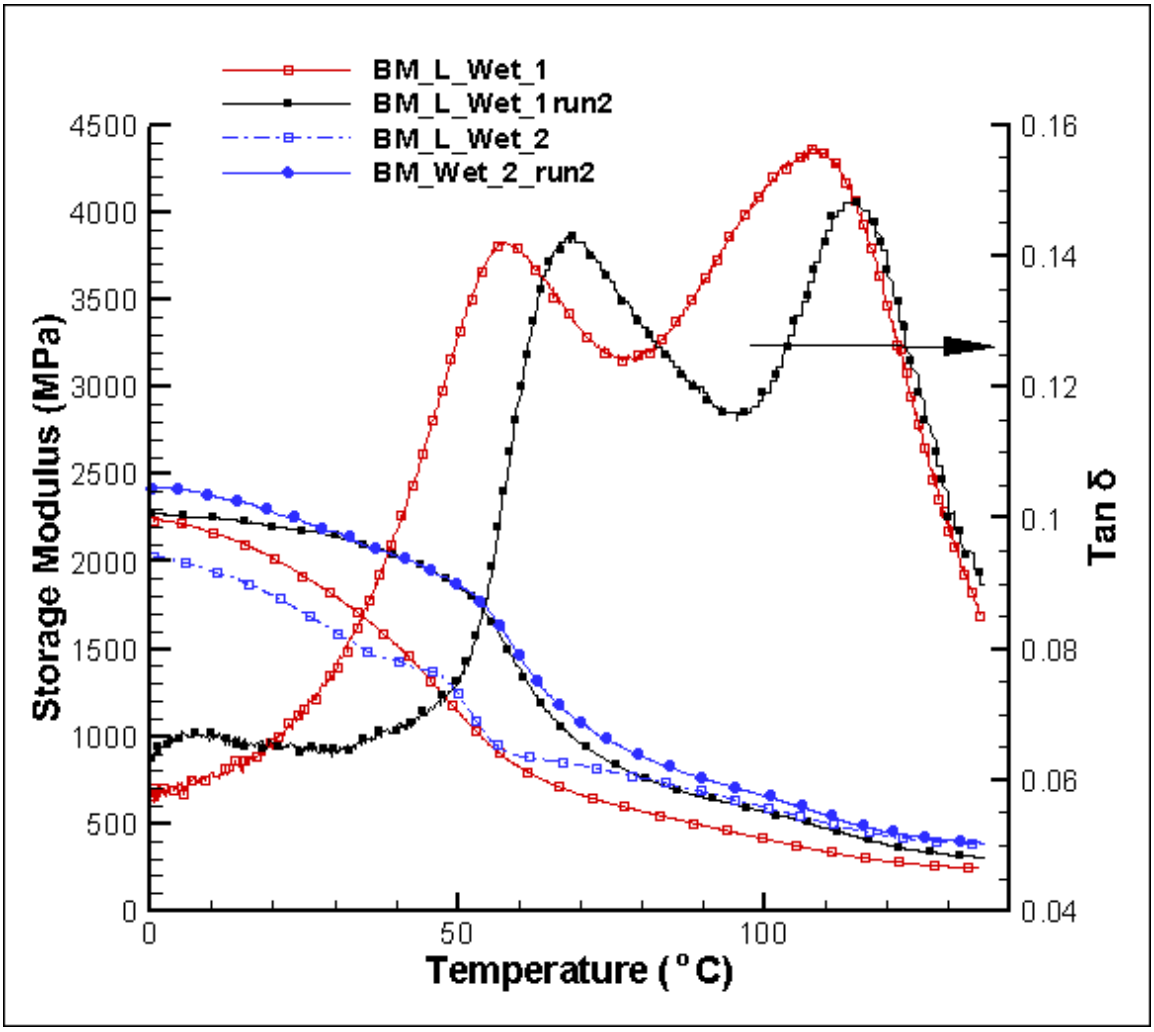


**Figure 35** Results for the first and second heating of wet regenerated triaxially braided cellulose/epoxy specimens

The second part of the dynamic study on the triaxially braided regenerated cellulose/epoxy composites was involved in the investigation of the damping effects under frequency loading in the composites. For this part of the study, the composites were tested in the axial and transverse directions. The results are shown in Figures 36 to 39. The results show a comparison of the thermo-mechanical behavior between one neat resin sample, and two composite samples: one in transverse and one in axial directions.

For the storage modulus results (Figure 36), a 10% increase in the storage modulus of the longitudinal and transverse braided BioMid composites at room temperature is observed as the frequency increases from 1 to 50 Hz. The increase is more significant at higher temperatures and is around 50% for the highest test temperature of 135 $^{o}$C (275$^{o}$F). Overall, the same trend in the degradation of the storage modulus for both epoxy and the longitudinal composites is seen at different frequencies. At room temperature and normal humidity levels, the storage modulus of the transverse composites is 12-15% lower than the longitudinal composites. This result is also seen in the previous sections on the results of the uniaxial mechanical testing of the braided regenerated cellulose/epoxy composites; where the average elastic modulus was 24% higher in the longitudinal direction due to the undulations of the bias yarns that dominate the behavior in the transverse direction. The results for the loss modulus and *tan* $\delta$ plots are shown in Figures 37 and 38. A significant increase in damping is seen for the composites and the neat resin at a frequency of 50Hz.

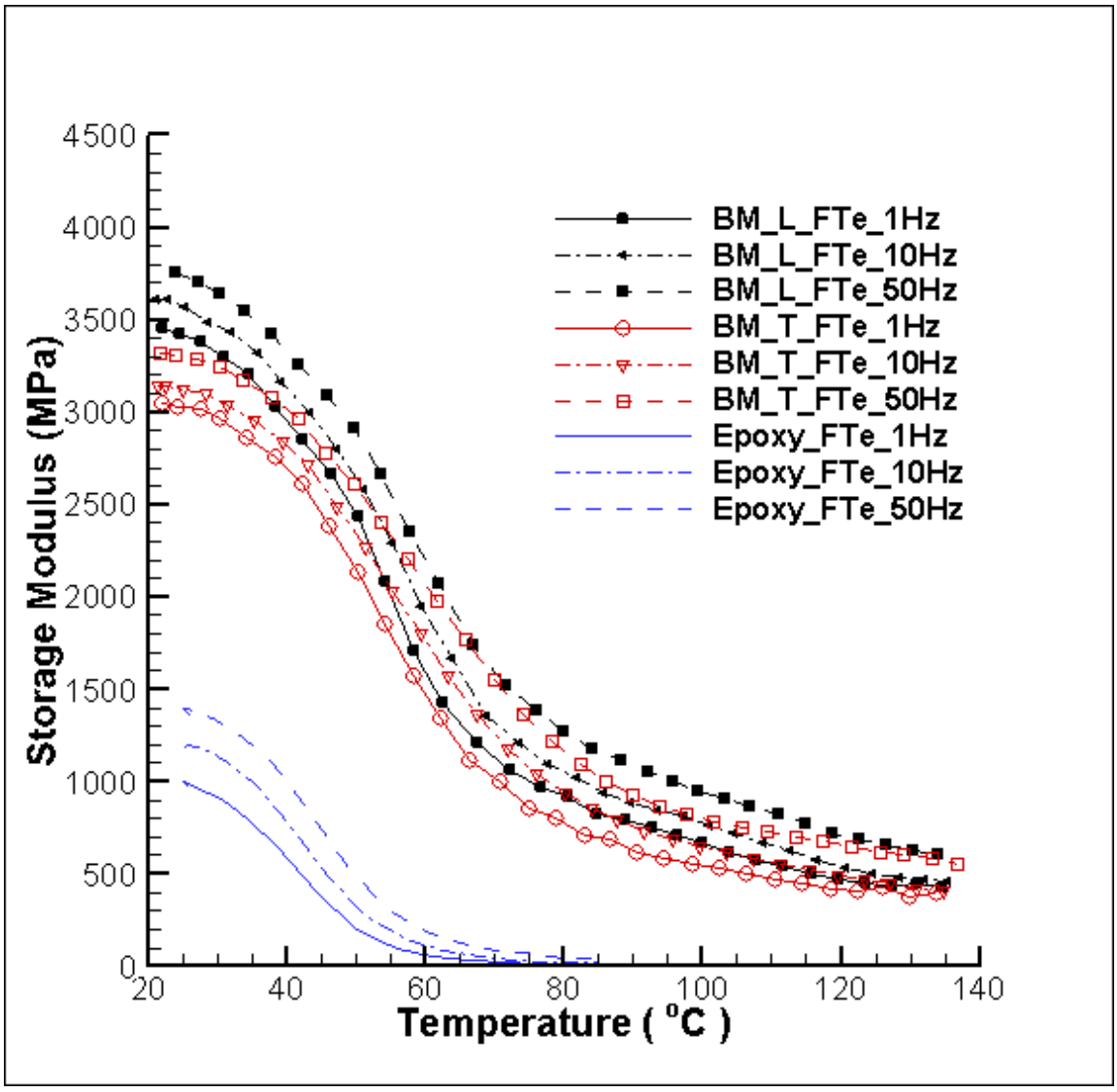


**Figure 36** Changes in the storage modulus of neat epoxy, longitudinal and transverse dry triaxially braided cellulose composites with temperature ramping at different frequencies

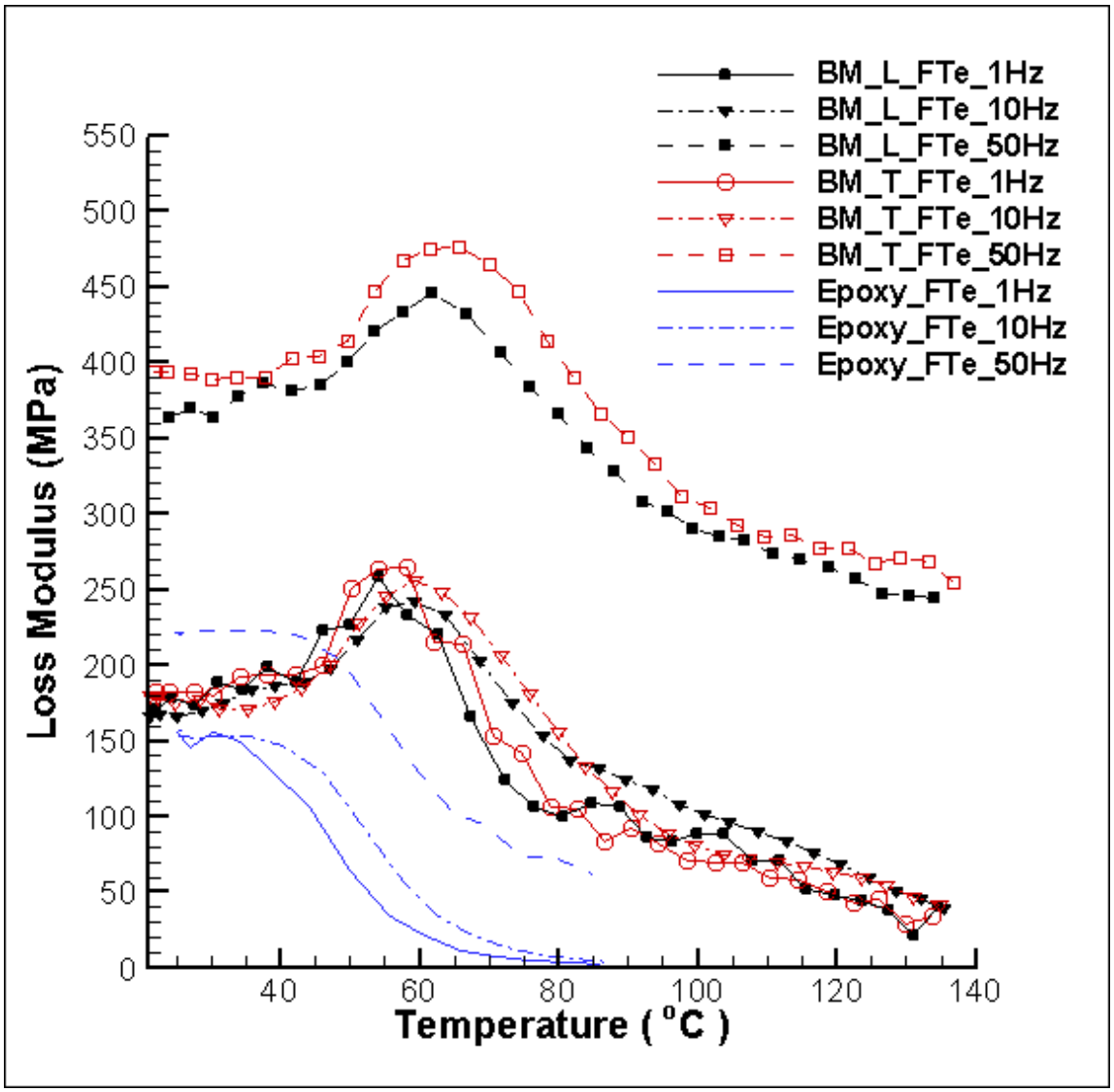


**Figure 37** Changes in the loss modulus of neat epoxy, longitudinal and transverse dry triaxially braided cellulose composites with temperature ramping at different frequencies

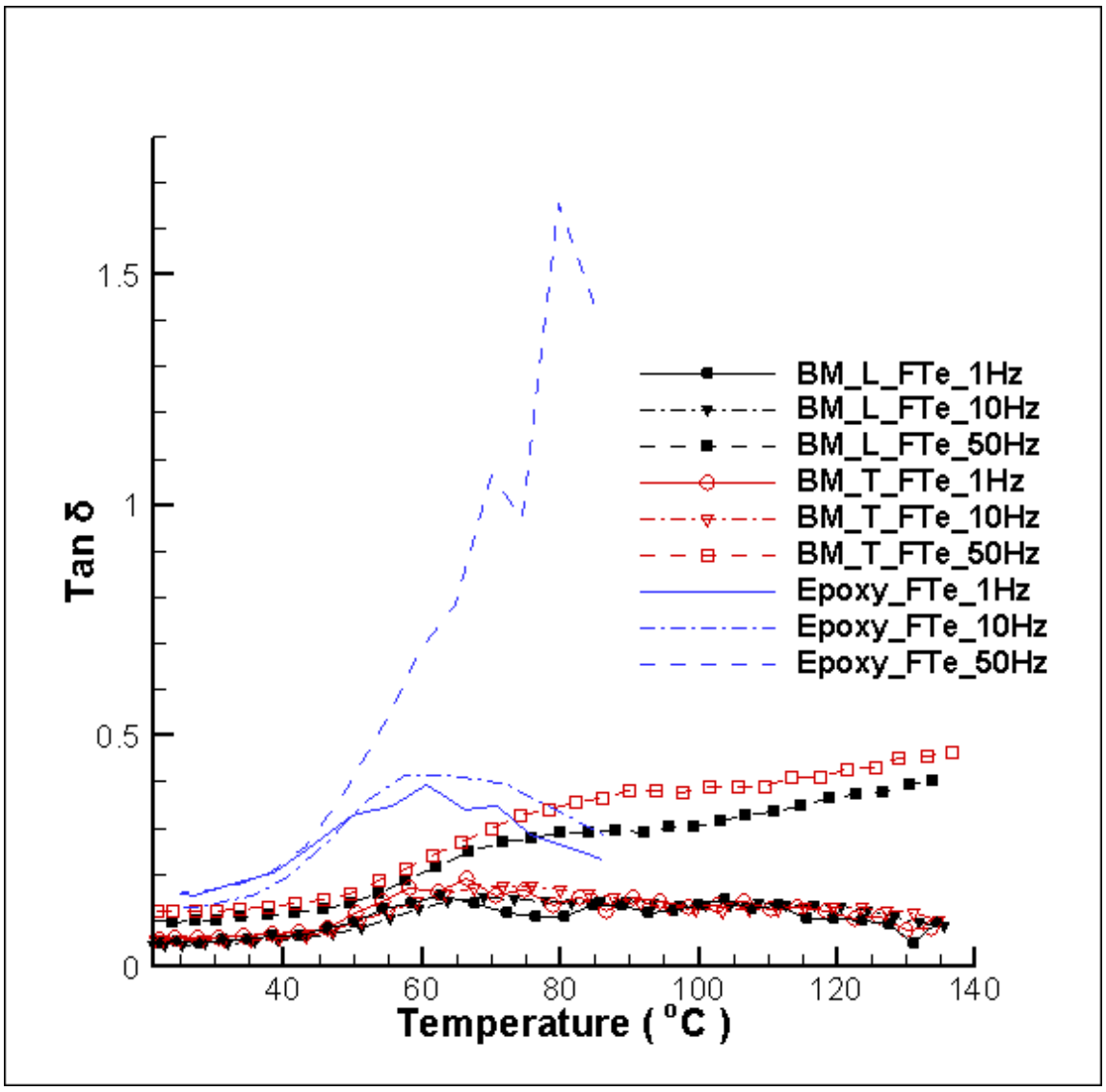


**Figure 38** Changes in *tan δ* plots of neat epoxy and longitudinal an transverse dry triaxially braided cellulose composites with temperature ramping at different frequencies

The behavior of samples at frequencies from 1Hz to 50Hz, incremented at 10Hz intervals was investigated for longitudinal and transverse braided specimens as well as for neat epoxy specimens (Figure 39). The significant increase in damping is shown only at the highest frequency (50Hz). On the other hand, no significant peak shifts (change in glass transition or other transformations) is observed with the change of loading

frequency. In addition, the plots for the storage modulus did not show significant drops or sniffs for the highest frequency of 50 Hz. This indicates that the increase in damping is most likely not due to the effect of a resonance frequency.

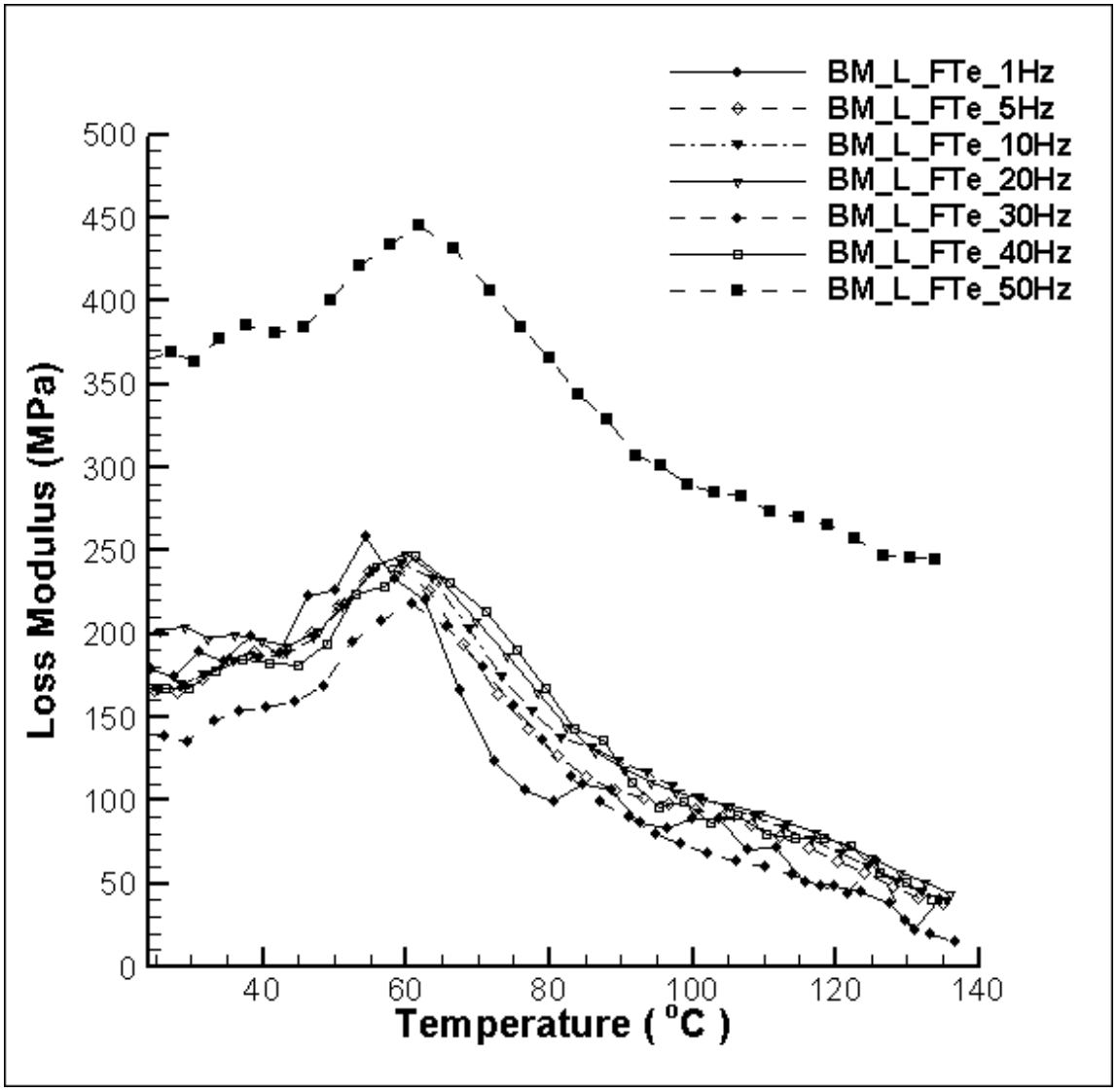


**Figure 39** Changes in the loss modulus for dry longitudinal triaxially braided regenerated cellulose composite at different frequencies

# 5. CELLULOSE NANOFIBRIL SCAFFOLD-BASED COMPOSITES

## 5.1 Production and Characterization of CNF Scaffolds

The work described in this section for the production and characterization of CNF scaffolds was carried out with collaboration at the USDA Forest Products Laboratory (FPL) in Madison, WI. The samples were obtained from Dr. Ronald Sabo. The procedure for the production of the nanocellulose scaffolds was previously reported [78]. TEMPO-oxidized cellulose nanofibrils (Figure 40) used in this study were prepared according to the work reported by Saito et al.[79]. The scaffolds (Figure 41) were created by freeze drying diluted suspensions of cellulose nanofibrils in a Vir Tis model 36DX84 tray-type freeze drier. Chilled suspensions were placed in trays, and the setpoint of the freeze drier was -20 °C. The condenser removed approximately 5-10 L of water per day, and the process was stopped once the material was dry, as indicated by rapid changes in the operating pressure and temperature of the chamber.

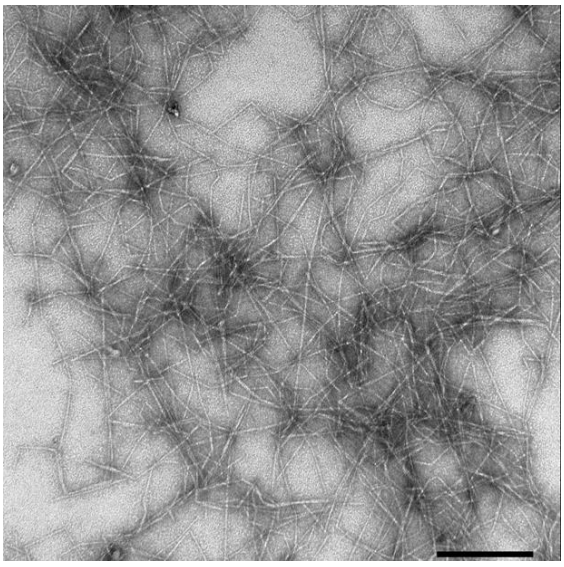

**Figure 40** Transmission electron micrograph of cellulose nanofibrils. The scale bar is 200nm. (*Qamhia et al., 2014*)

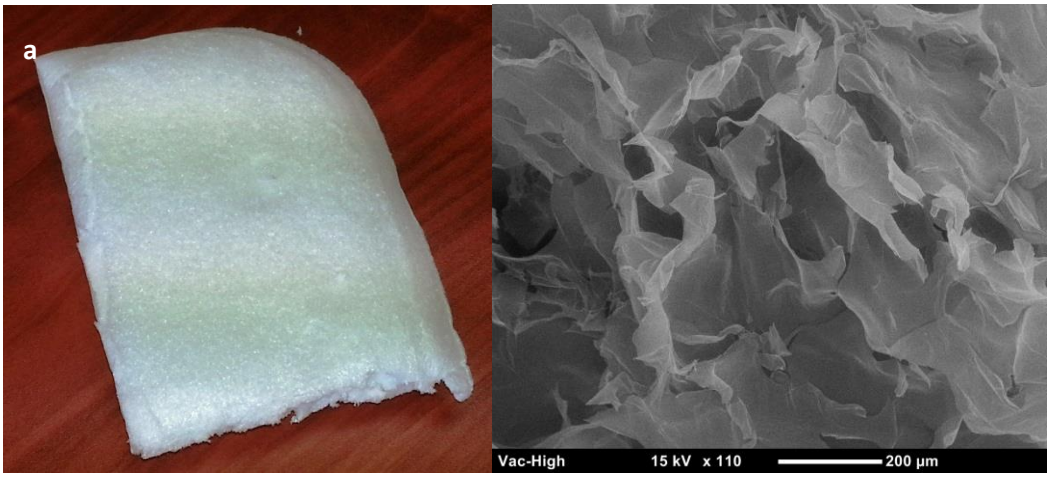


**Figure 41** Photograph (a) and scanning electron micrograph (b) of cellulose nanofibril scaffolds (*Qamhia et al., 2014*)

### 5.2 Fabrication of CNF/Epoxy Composites

In the initial trials of preparing CNF/epoxy composites, the resin system that was chosen was the high bio-content Super Sap epoxy resin (Super Sap 100; Entropy Resins, Hayward, CA, USA) used for the other studies in this thesis. The composites were initially prepared by soaking the CNFs in a resin bath inside a silicon mold containing the resin, flipping the sample around several times, and then curing on a hot plate at 70 ˚C (158 ˚F) for four hours. These initial trials with a relatively high viscosity resin (650 cps at 25 ºC (77 ºF)) resulted in samples having poor infusion (Figure 42) with a void content exceeding 60% for most of the prepared samples. A modification to the procedure was proposed in which the infusion was assisted by placing the samples in the resin bath in a vacuum chamber. Only slight improvements were seen, so a third more efficient procedure with a less viscous resin was proposed as it will be discussed below.

**Figure 42** A photograph of an early trial of making a CNF/epoxy composite specimen using wet layup and a high viscosity resin. Incomplete wetting of CNF is seen in the lower image.

In the modified fabrication technique; composites were fabricated from the nanocellulose scaffolds with the aid of a low viscosity thermosetting epoxy resin. The composites were manufactured using a low viscosity epoxy system (*Embed-It*™ Low Viscosity Epoxy; Polysciences Inc., Warrington, Pennsylvania, USA) with a viscosity of 65 cps when mixed and long working time (More than 48 hours if no heat is applied). Using the low viscosity epoxy, two fabrication methods were experimented for use on the nanocellulose scaffolds. The first is a Vacuum Assisted Casting followed by a heat curing (*VAC-H*). For this fabrication technique, nanocellulose scaffolds were placed in an epoxy resin bath under a vacuum pressure of 635.0 mm Hg (25 in. Hg) for 60 ± 2 minutes. After this step, the mold was placed over a heated plate to cure overnight (15-16 hours) at a temperature of 70 ºC (158 ºF). The resulting composites were polished

against a 320 SiC abrasive disc with a 250 RPM platen speed to ensure flat surfaces and to remove excess epoxy. The second composite fabrication technique (Figure 43) we refer to as the Vacuum Assisted Casting followed by Hot pressing (*VAC-HP*). In this method, the vacuum assisted casting is done in the same manner as before. However, for the resin curing a press-claving method using a Wabash hot press (GE30H-15-BCX, Wabash, Indiana) was used instead of the hot plate. The curing procedure consisted of increasing the temperature from 27 ºC (80 ºF) at a rate of 6 ºC/min (11 ºF/min). The temperature was then held at 120 ºC (250 ºF) for 210 minutes then cooled down at a rate of 6 ºC/min (11 ºF/min) to 27 ºC (80 ºF). During the whole curing time, a 445 N (100 lbf) compressive pressure was applied to the composite scaffolds to increase fiber volume fraction and reduce porosity. The curing of the resin system was found to be very dependent on the process parameters. The use of the *VAC-HP* method enabled higher cellulose content in the composites (up to 7.5% by volume) as compared to the VAC-H method.

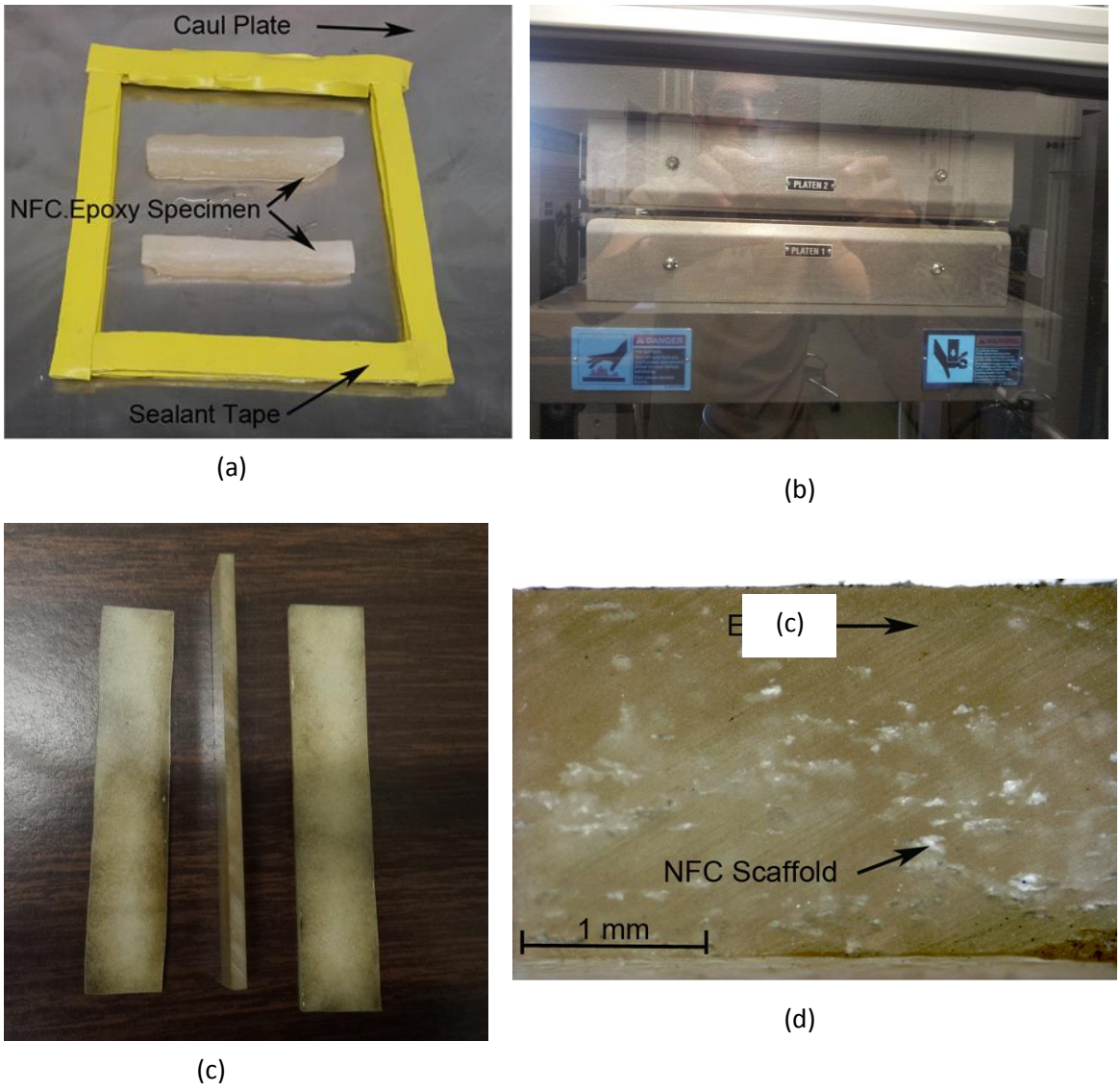


**Figure 43** Preparation of CNF/epoxy composites by VAC-HP method showing (a) wetted specimens, (b) hot press, (c) final specimens and (d) a cross section micrograph for one of the specimens

### 5.3 Mechanical and Thermal Characterization

Sample hardness was measured using the Shore-D hardness equipment. A hardness value of 70 was found to correlate to a fully cured sample as confirmed with differential scanning calorimetry (DSC) measurements. DSC was performed on cured specimens extracted from the pure epoxy and nano-cellulose reinforced specimens prepared by both the *VAC-H* and *VAC-HP* methods. DSC was used to investigate the physical and chemical changes that may occur when the nanocellulose is incorporated into the epoxy resin. In addition, three-point bending tests were performed on the pure resin and nanocellulose-embedded specimens. Samples dimensions and test setup were chosen to comply with the recommendations of the ASTM D790-10 test standard for flexural testing [80]. The simply supported beam had a 50 mm (2 in) span with a 10 mm (0.4 in) overhang. Samples were supported on 11 mm (0.4375 in) diameter supports and the loads were applied at mid-span. Tests were carried out using an electromechanical loading machine having a maximum loading capacity of 97.8 kN (22 kip) with a 2.2 kN (500 lb) capacity load cell. The specimens were loaded in a displacement-controlled rate of 1.3 mm/min. Simultaneous measurements for the load, displacement, and time were recorded. The flexural test setup is shown in Figure 44. The flexural stresses and strains were determined using a strength of materials approach using the relationships of ASTM D790-10 [80]. Scanning Electron Microscopy (SEM) was performed on the fractured surfaces of the CNF/epoxy composites to investigate the failure morphology (SM-300 SEM; TopCon, Japan).

The specimens prepared using VAC-HP method showed a significantly higher elastic modulus and strength compared to specimens prepared with the *VAC-H* method. The *VAC-HP* process resulted in a 15% average increase in modulus for reinforcement levels of 5-7.5% compared to neat resin properties. The strain to failure decreased from 5.5-6 % in the unreinforced specimens to 2.3 - 3.0% in the CNF/epoxy composites (Figure 45). The CNF-reinforced composites do not show much plastic deformation compared to the neat resin, so the yield strength for the neat and CNF-reinforced samples was similar.

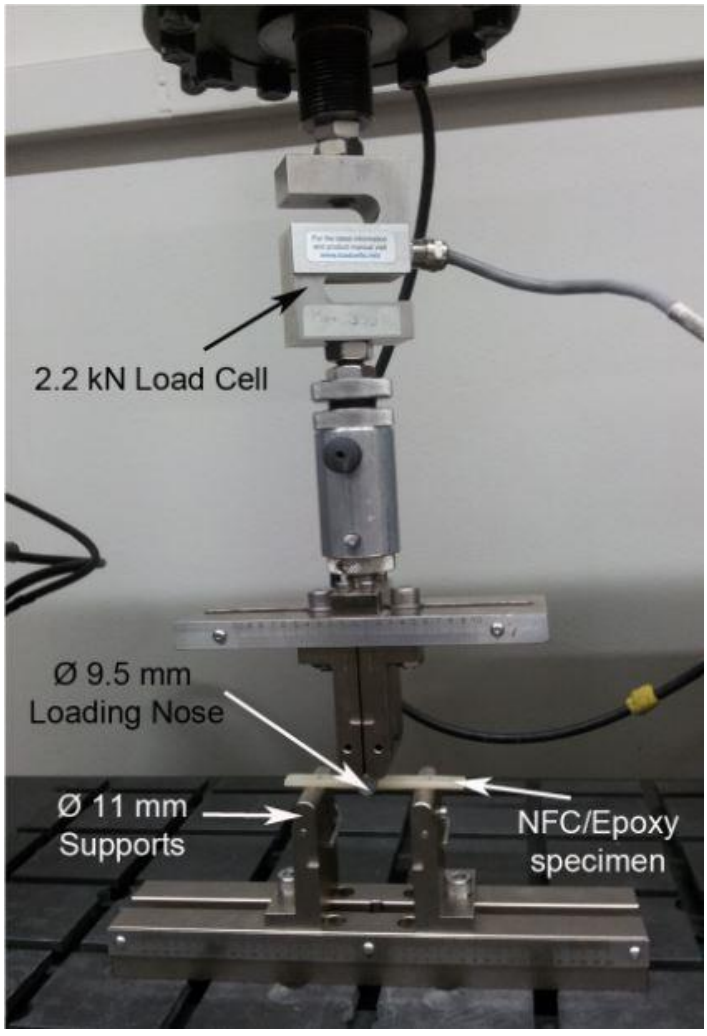


**Figure 44** Mechanical testing setup for three-point bending

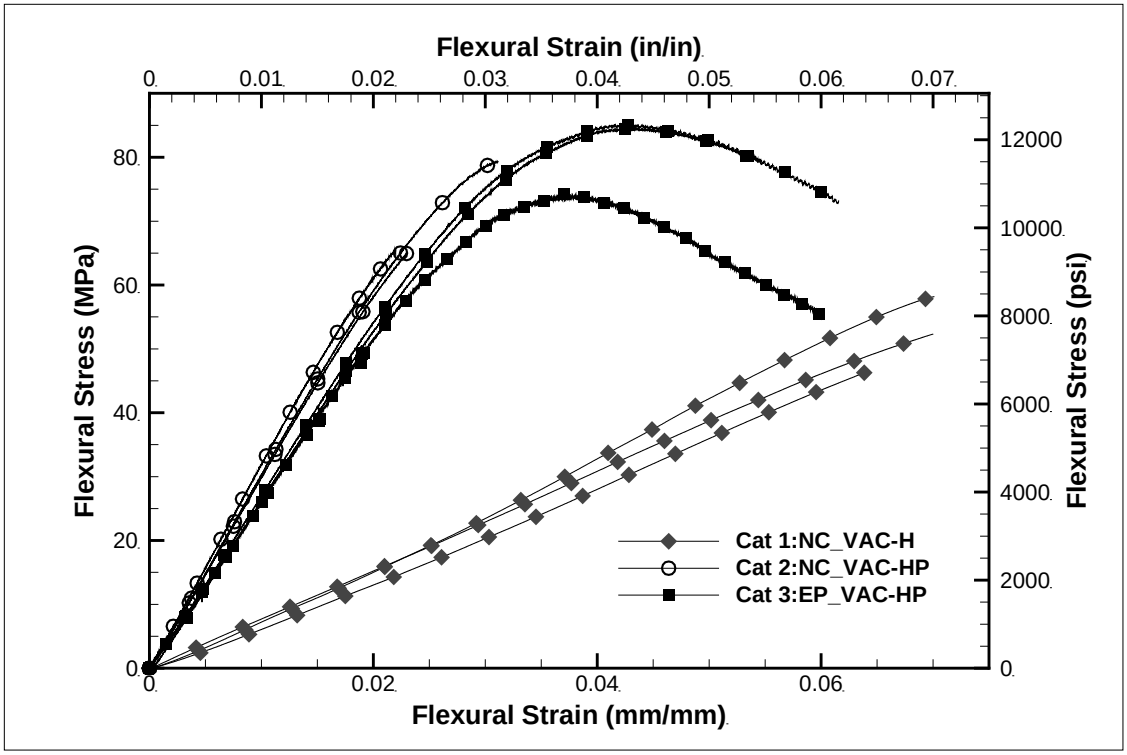


**Figure 45** The stress-strain response of pure epoxy and CNF/epoxy specimens using VAC-H and VAC-HP methods (Qamhia et al., 2014)

The results from these tests are summarized in Table 6. Previous work using films as reinforcements at 1-6% loadings in epoxy resulted in modest increases to the tensile modulus [81] similar to the increase in bending modulus seen in the present work with CNF scaffolds. However, in the case of films, delamination was observed between the CNF and epoxy layers. Having porous scaffolds is expected to improve the adhesion and entanglement between cellulose and epoxy and prevent such delamination, although more work is needed in that area as the SEM observations described later indicate that improvements in processing are still desired.

**DSC and SEM Results**

Figure 46 shows the results from DSC. Using DSC it is possible to determine the degree of curing and glass transition temperature ($T_g$) of the composite materials. The results from the *VAC-H* technique show an exothermic peak for CNF-reinforced specimens at a temperature of 170 ºC (338 ºF). The peak is nonexistent for pure epoxy specimens prepared by both techniques. It is interesting to note that for the CNF/epoxy composites using the *VAC-HP* method the exothermic peak was not observed. A clear drop in heat flow is observed for pure epoxy at 265 ºC (509 ºF). A change in slope at the same temperature is observed for nanocellulose specimens around this same temperature indicating a similar behavior (Figure 46). It is believed that this drop in heat flow is not due to a glass transition and might be due to the degradation of the resin. DSC experiments were run for pure resin samples and nanocellulose-reinforced composites prepared by VAC-HP method at lower temperatures and a clear $T_g$ was observed at a temperature around 60 ºC (140 ºF) for both categories (Figure 47). The nanocellulose does not appear to significantly affect the glass transition temperature of the composite. The glass transition temperature is also investigated with DMA, as discussed in the next section. These results reveal the importance of proper resin curing to the properties of the composites. No exothermic peaks are observed for samples prepared by *VAC-HP* compared to those obtained when using the standard curing procedure. The conditions in the *VAC-HP* result in complete curing as seen in both the improved mechanical properties and the disappearance of the exothermic peak in the DSC results. The DSC results show an exothermic peak at 170 ºC (338 ºF) only in the nanocellulose composites

when the resin was not cured properly. The peak is not seen for the materials processed using the *VAC-HP* method.

**Table 6:** Summary of results for the effects of CNF composites

| Resin | Nano-cellulose Form | Process | Strength (MPa) | Initial Elastic modulus (GPa) | Strain to failure (%) |
|---|---|---|---|---|---|
| Epoxy | No CNFs | Vacuum/ Press | 75-85 | 2.43-2.56 | 5.5-6 |
| Epoxy | CNF Scaffolding | Vacuum/ Press | 67-80 | 2.79-3.03 | 2.2-3.0 |

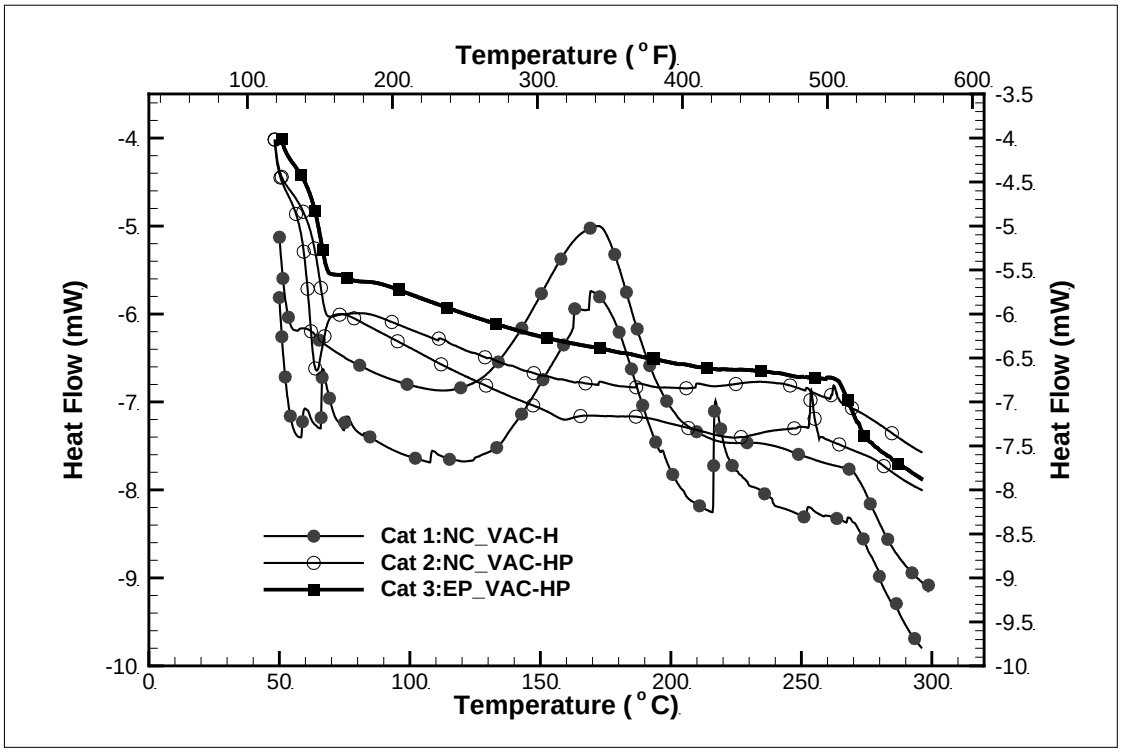


**Figure 46** DSC results on pure epoxy and CNF/epoxy specimens using both methods (Qamhia et al., 2014)

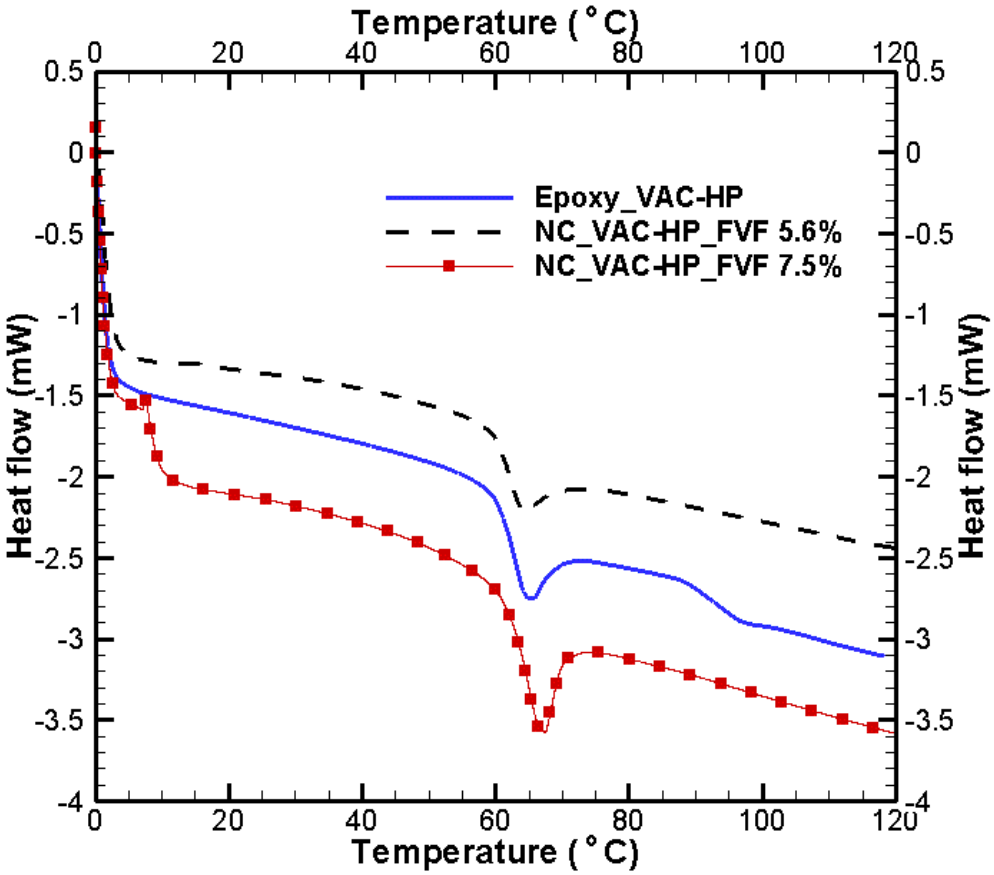


**Figure 47** DSC results on pure epoxy and CNF/epoxy specimens using VAC-HP for lower temperatures (Qamhia et al., 2014)

SEM micrographs (Figure 48) for epoxy and CNF/epoxy composites samples show a more ductile failure of the neat resin specimens compared to those reinforced with nanocellulose. Failures of the CNF/epoxy samples show a more brittle failure and the appearance of various sized voids on the fracture surface. This observation agrees with the behavior shown by the mechanical testing results (Figure 45) for which a lower strain to failure was seen for CNF/epoxy composites prepared by the VAC-HP method. Inspection of the cross-sections of the fracture surfaces of the CNF/epoxy composites also show only a partly uniform composite, in which some areas have more cellulose and

others have more resin. The presence of voids in the CNF composites and the lower strain to failure of the cellulose microfibrils might explain why the mechanical strength was not significantly increased by the addition of cellulose reinforcement. The voids in the microstructure may be preventing the nanocellulose from adequately bonding with the epoxy and developing full strength.

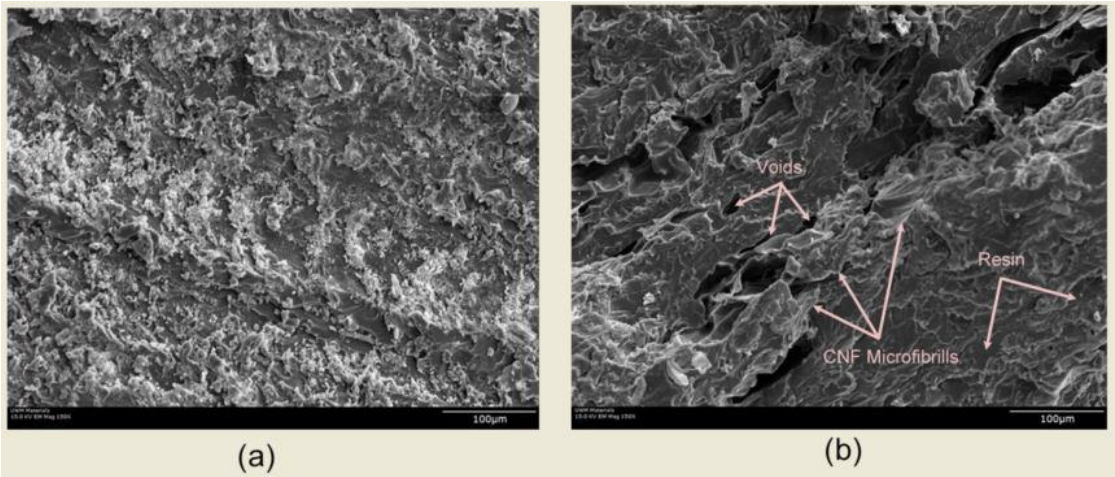


**Figure 48** SEM Micrographs for (a) neat epoxy (b) CNF/epoxy with fiber volume fraction of 5.6 % (Qamhia et al., 2014)

### 5.4 Viscoelastic Effects on CNF/Epoxy Specimens

The effect of nanocellulose reinforcement on the viscoelastic properties was examined using DMA. The study was carried on a Q800 DMA TA instrument (TA instruments, New Castle, Delaware, USA). A three-point bending mode with a controlled strain mode of 15 µm (displacement) was used. Pure resin samples and samples of nanocellulose/epoxy with different fiber volume fractions prepared by VAC-HP method were tested at a constant frequency of 1.0 Hz. A temperature range of 0-120 $^{o}$C (32-248

°F) and a heating rate of 5 °C/min (9 °F/min) were chosen. The tested samples were approximately 35 x 12-15 x 1.5-2.0 mm (1.4 x 0.5-0.6 x 0.06-0.08 in) in length, width and thickness respectively. The supported span width was 20 mm (0.8 in). The test parameters were chosen to comply with the general recommendations of the ASTM D4065-12 [73] and ASTM D5023-07 standards [74].

The results of dynamic mechanical analysis (DMA) are shown in Figures 49 and 50. Figure 49 shows an increase in the storage modulus for the nanocellulose-reinforced samples in the glassy state. The increase is directly proportional to the amount of nanocellulose reinforcement. A similar trend was seen for the elastic modulus as characterized by the three-point bending tests where a 15% increase in elastic modulus was observed. At room temperature, DMA results show an 18% increase in the storage modulus for the highest FVF of nanocellulose (7.5 % by volume) when compared to the pure resin. During the glass transition of the samples as the temperature is increased, the opposite scenario is seen, where the storage modulus is highest for pure epoxy and decreases with increasing the nanocellulose content. Figure 50 shows the effect of adding the nanocellulose on the *tan* $\delta$ plots. The trend is that the *tan* $\delta$ curves show a peak shift to lower temperatures with the increase in nanocellulose reinforcement. This peak shift indicates a reduction in the glass transition temperature with increasing the nanocellulose content in the nanocomposites. Other studies have shown the opposite behavior where the addition of nanocellulose increased the $T_g$ [82]. The glass transition temperature for pure epoxy as characterized by the *tan* $\delta$ curves peaks is around 85 ºC (185 ºF) and drops to 73 ºC (163 ºF) for the composite having 7.5% nanocellulose by volume. No significant changes were observed for the width of the *tan* $\delta$ peaks. The peak intensities are

remarkably lower for the nanocellulose composites compared to neat epoxy samples. This can be attributed to the interaction between the resin and the nanocellulose which restrict the segmental mobility of the polymer chains in the vicinity of the reinforcements [82, 83].

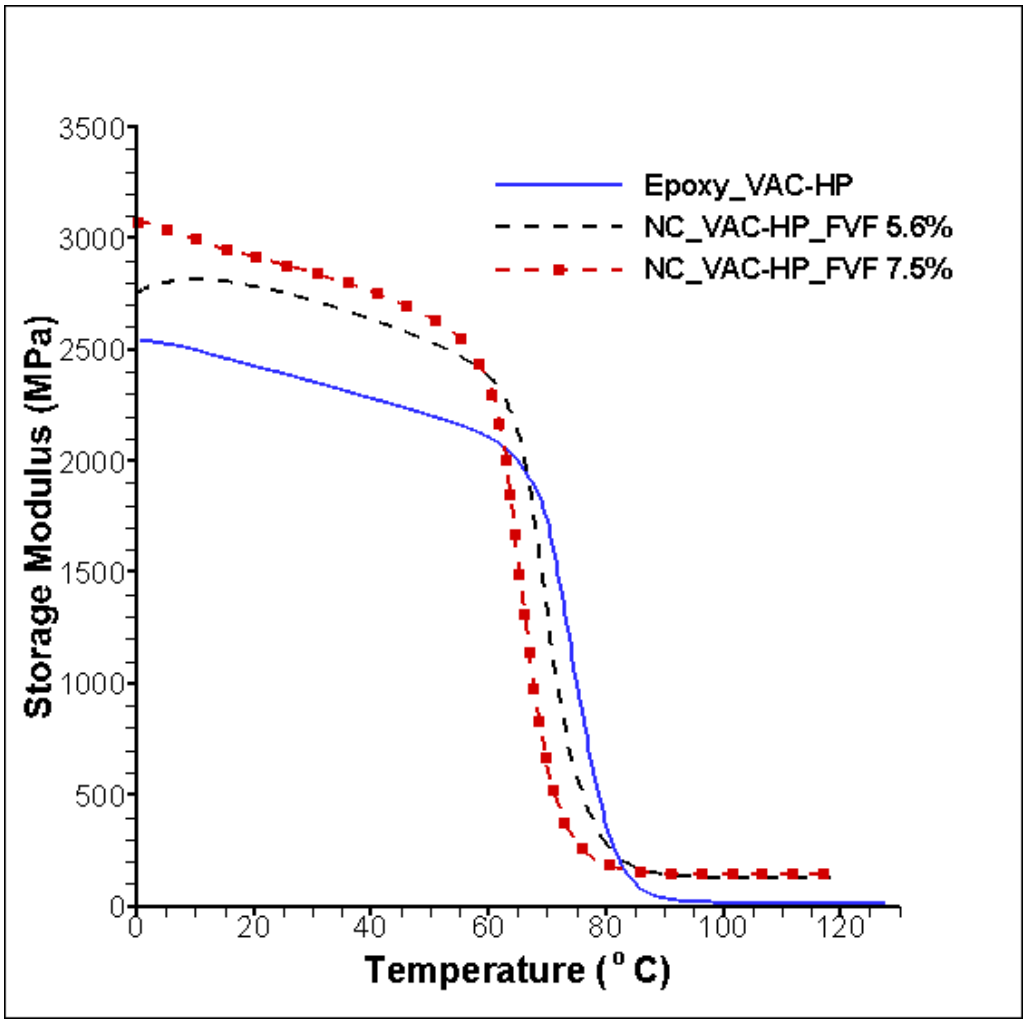


**Figure 49** DMA results on pure epoxy and CNF/epoxy specimens showing storage modulus curves

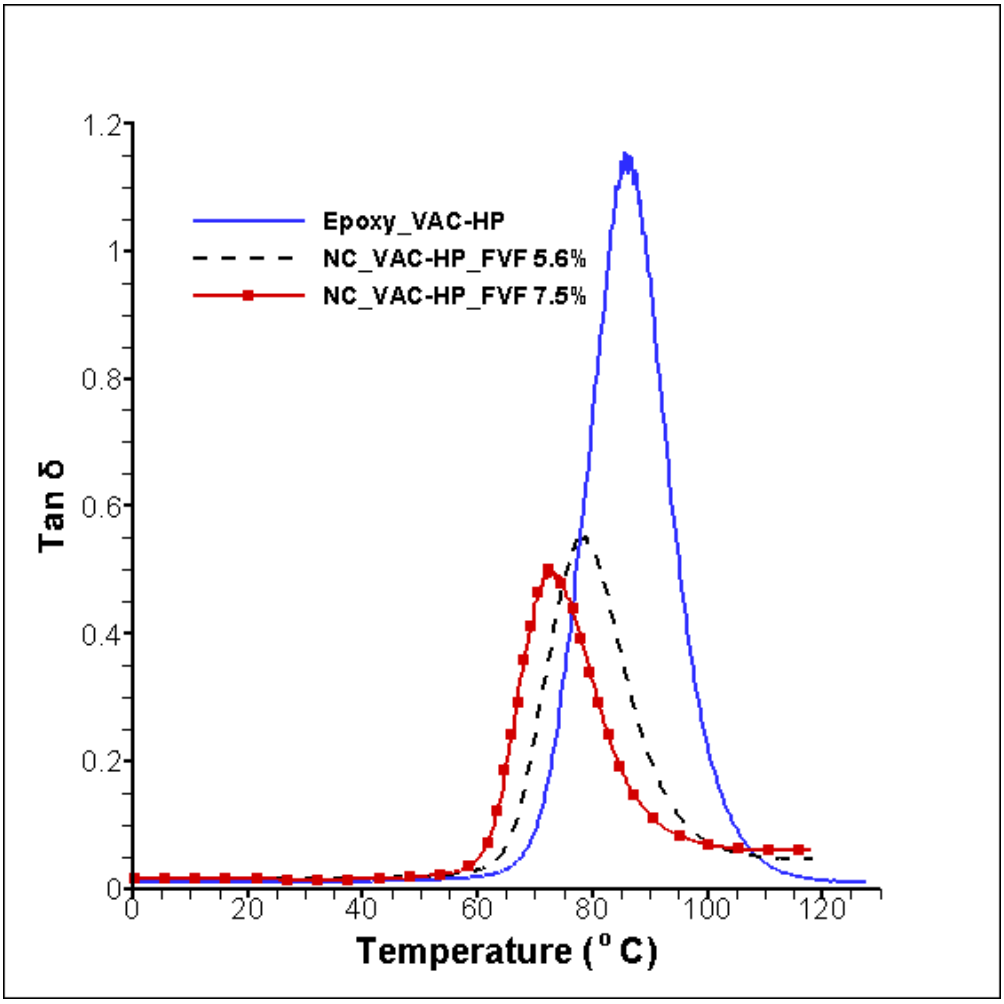


**Figure 50** DMA results on pure epoxy and CNF/epoxy specimens showing *tan δ* curves

### 5.5 Unit Cell FEA Model

The following section describes a computational finite element analysis model for the microstructure of a directionally oriented microfibrillated cellulose-based scaffold composite with an epoxy resin. The model adds up to continuing efforts at USDA Forest Products Laboratory-Madison and the universities of Wisconsin Madison and Milwaukee to create and characterize the scaffolds and the composites. The modeling approach is similar to that explained in Section 3.1 for unidirectional regenerated cellulose/bio-based

epoxy composites; in which a representative unit cell where the behavior of the constituents is independently recognized is utilized for the first step. The result is then a homogenized behavior of the composites that can be used for a structural level analysis. This modeling approach is also implemented using a p-version finite element analysis (p-FEA) approach. StressCheck software is used for the simulations of the micromechanical models (Stress Check V9.0; ESRD, St. Louis, Missouri, USA). The typical unit cell model used for the composites consists of 1224 elements consisting of 936 hexahedral and 288 pentahedral elements. The cross section of the unit cell model assumes a hexagonal packing of fibrillated cellulose. The sizes and shapes of typical unit cells were initially based on scanning electron micrographs for the actual directionally oriented CNF scaffolds (Figure 51). The proposed unit cell model is shown in Figure 52. The p-FEA model is parameterized for changes in the dimensions of the cross section, length, and loading (Figure 53). Parametric studies for the effect of the side length and thickness of the hexagonal walls were carried out to investigate their effects on the maximum equivalent stresses ($S_{eq}$) and strains ($E_{eq}$), as well as the first stress and strain invariants ($I$ and $J$ respectively) for normal stresses. The first stress invariant is the sum of the principal stresses ($S$) in the x, y and z directions and is a constant at any point irrespective of the considered axis. The equations for the stress and strain invariants and the equivalent stress and strain are shown below. The equivalent stresses and strains are related to the von Mises yield criterion.

$$I_1 = S_x + S_y + S_z = S_1 + S_2 + S_3 \qquad (13)$$

$$S_{eq} = \sqrt{\frac{1}{2}[(S_1 - S_2)^2 + (S_2 - S_3)^2 + (S_3 - S_1)^2]} \qquad (14)$$

$$J_1 = J_x + J_y + J_z = J_1 + J_2 + J_3 \qquad (15)$$

$$E_{eq} = \sqrt{\frac{1}{2}[(\varepsilon_1 - \varepsilon_2)^2 + (\varepsilon_2 - \varepsilon_3)^2 + (\varepsilon_3 - \varepsilon_1)^2]} \qquad (16)$$

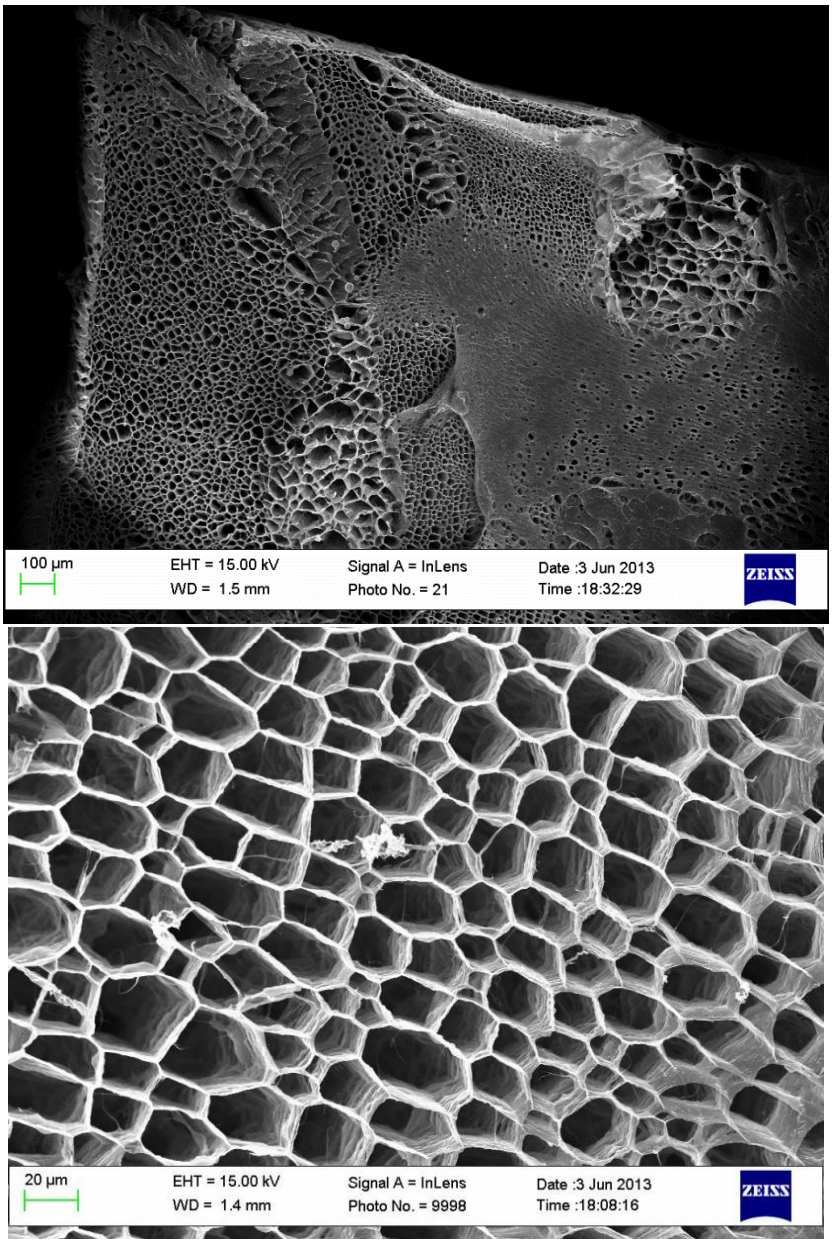


**Figure 51** SEM micrographs for directionally oriented microfibrillated cellulose scaffolds (photo credit: Tom Ellingham, UW-Madison)

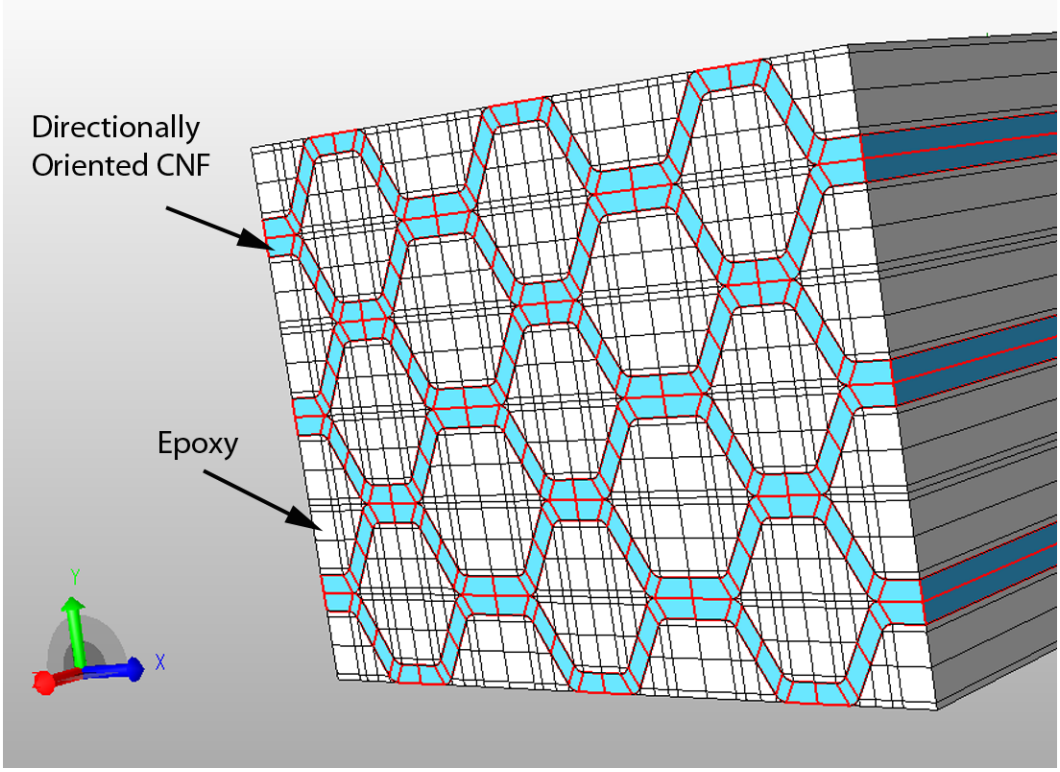


**Figure 52** Proposed directionally oriented CNF/epoxy microstructural p-FEA model

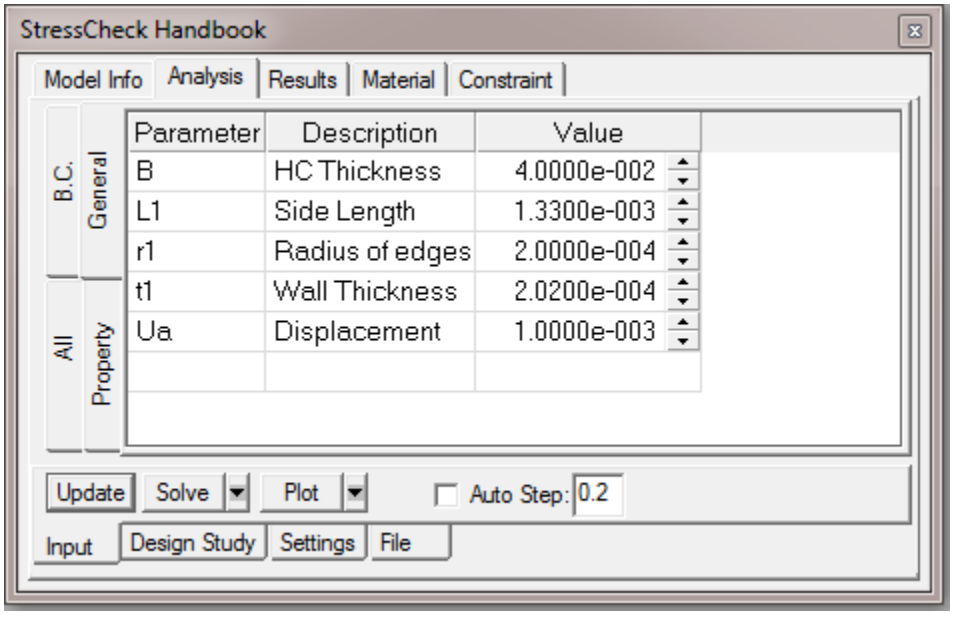


**Figure 53** Parameterized parameters for the directionally oriented CNFs unit cell model

The loading applied to the model was in the form of a traction load parallel to the direction of the oriented fibers at one face. Boundary conditions were applied to restrict in and out-of-plane displacement on the opposing face. Using these constraints, the Poisson's effects can also be captured. The material properties for the microfibrillated cellulose are accounted for by using a linear elastic material model. The modulus of elasticity is obtained by performing nanoindentation tests of Nanofibrillated CNF sheets having a small thickness of 0.14 mm (0.0055 in) using a 3-sided Berkovich tip indenter. Indentation was carried out on a Agilent Technologies G200 at a speed of 10 nm/s at an approach depth of 1000 nm. The target frequency used is 45 Hz, with a harmonic displacement of 2nm. A stiffness criterion was used and the sample was indented at four randomly selected locations. Samples were attached to the stage using crystal bond 509 amber wax. The results of the nanoindentation are shown in Figure 54. The results for average modulus and stiffness are also summarized in Table 7. The polymeric epoxy matrix is assumed to be linear elastic. The model was only verified for small traction loadings in the elastic regions for both the epoxy and the CNFs.

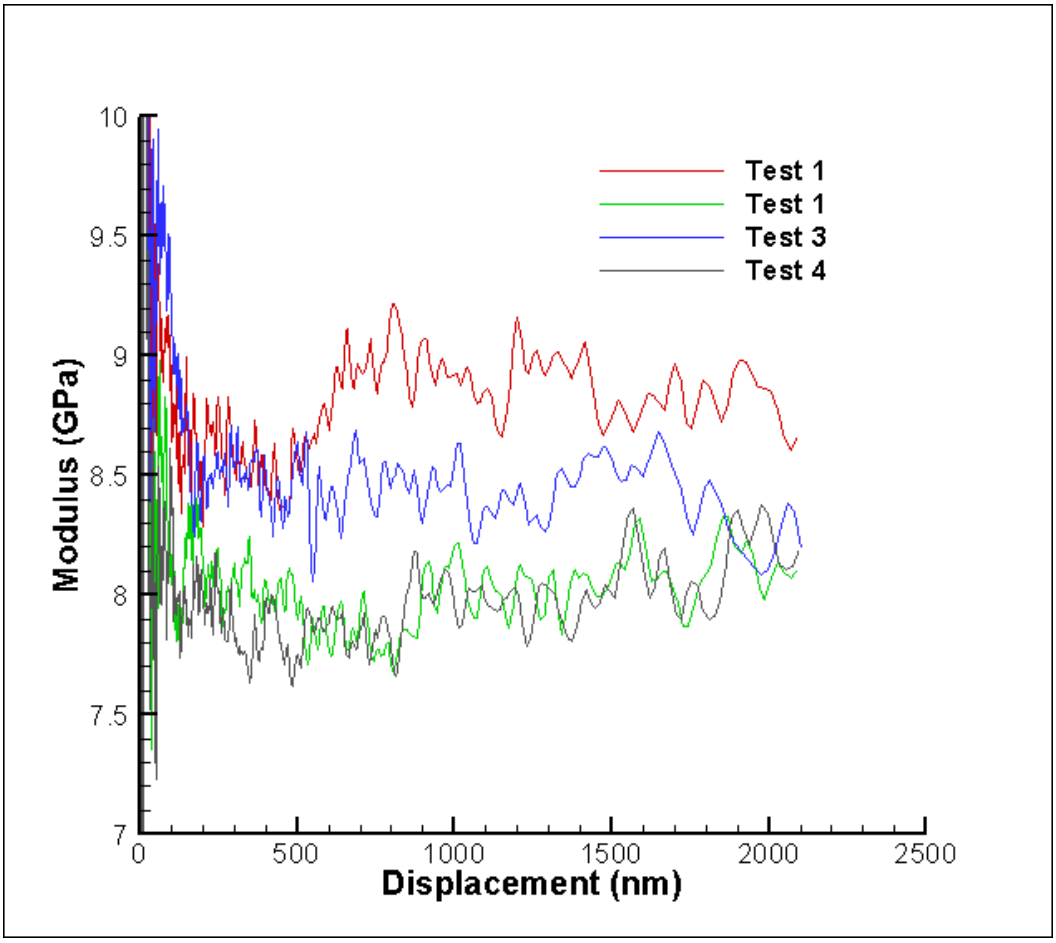


**Figure 54** Elastic modulus measurements using nanoindentation on CNF sheets

**Table 7** Average modulus and stiffness for CNF sheets

| **Test** | **Avg. Modulus** [600-1200 nm] GPa | **Avg. Hardness** [600-1200 nm] GPa |
|---|---|---|
| 1 | 8.9 | 0.52 |
| 2 | 7.9 | 0.44 |
| 3 | 8.4 | 0.49 |
| 4 | 7.9 | 0.45 |
| **Mean** | **8.3** | **0.48** |
| Std. Dev. | 0.5 | 0.04 |

The results for the FEA model are shown in Figures 56 and 57. Two cases were investigated for the effect of the cell size and thickness on the mechanical properties. For the first case, the cell size was varied by changing the side length of the hexagonal unit cell. The thickness used was the average thickness of the representative unit cell obtained from the scanning electron micrographs. The side lengths were varied above that obtained in the SEM graphs. For the second case considered, the wall thicknesses of the CNFs were varied and the side length of the hexagonal arrangement was kept constant, with a value of the average size of the unit cell obtained from the SEM micrographs. The maximum equivalent stresses, strains and the first normal stress and strain invariants were evaluated on a selection of the boundaries between the nanocellulose and the epoxy along the central strip of the model. The evaluated area is shown in Figure 55 marked in red.

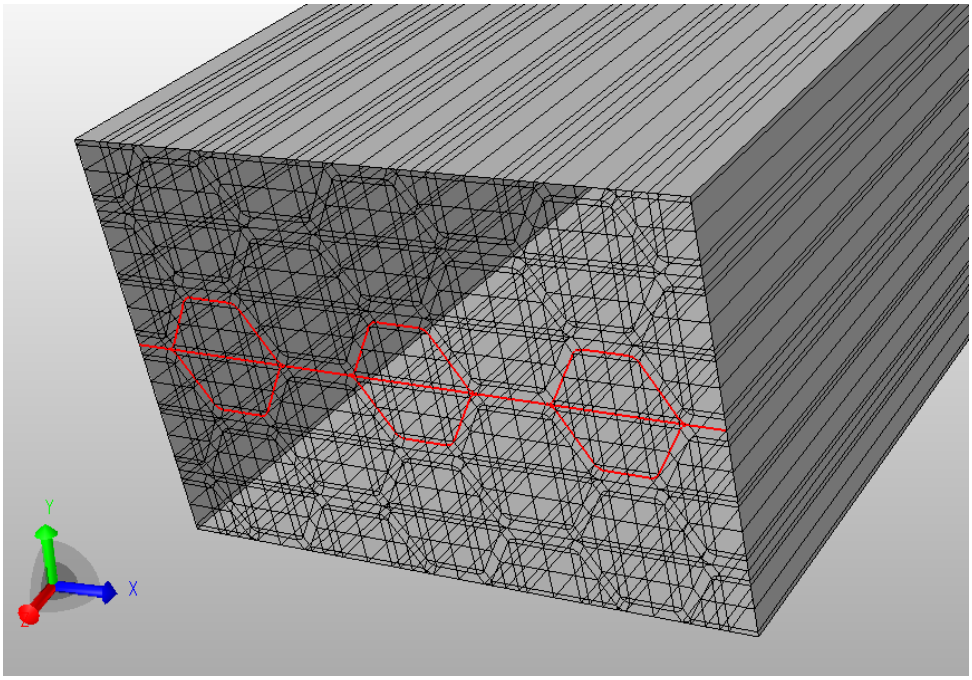


**Figure 55** P-FEA model showing the area of interest at which stresses are evaluated

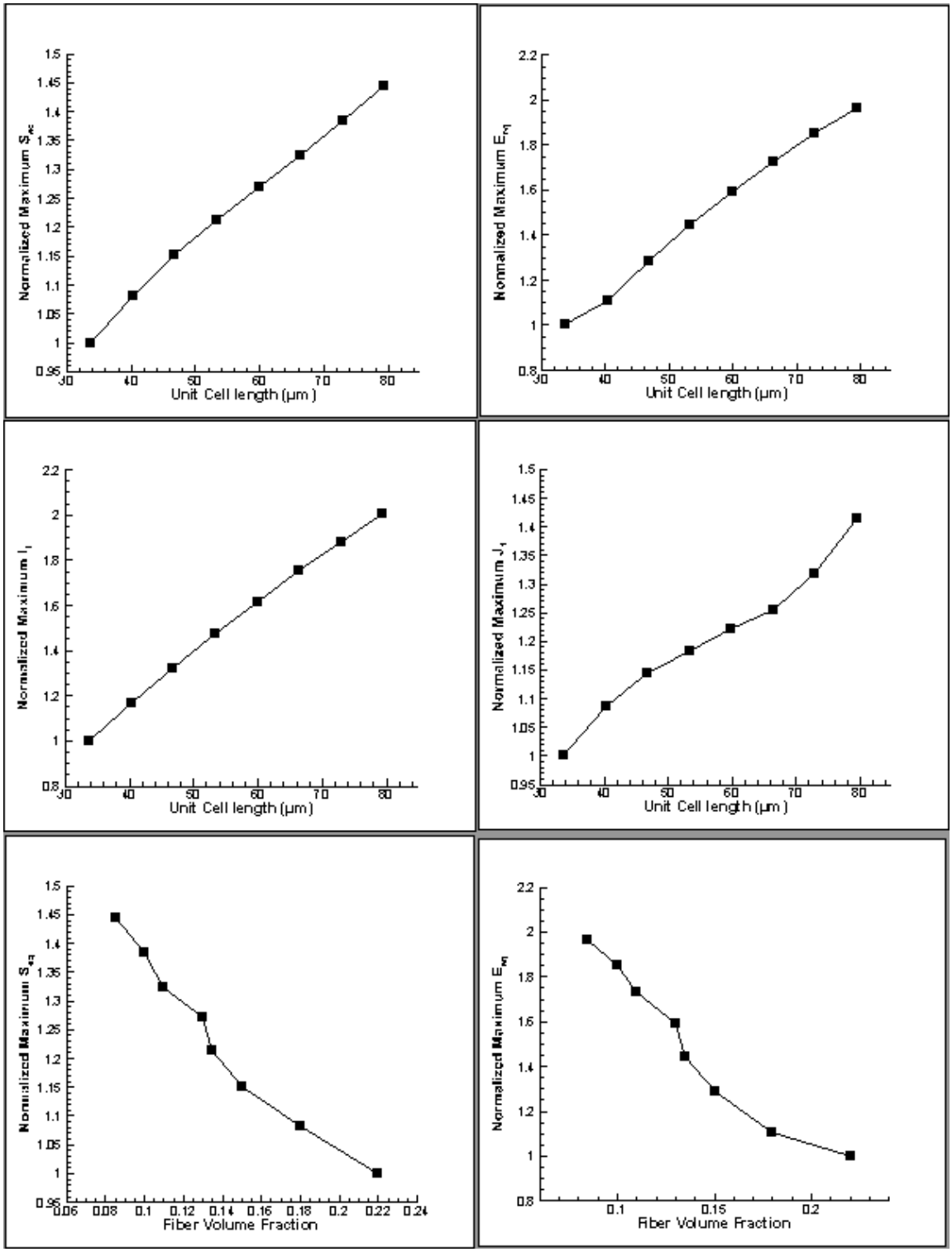


**Figure 56** Model results for varying unit cell length and a constant wall thickness (5.1 μm)

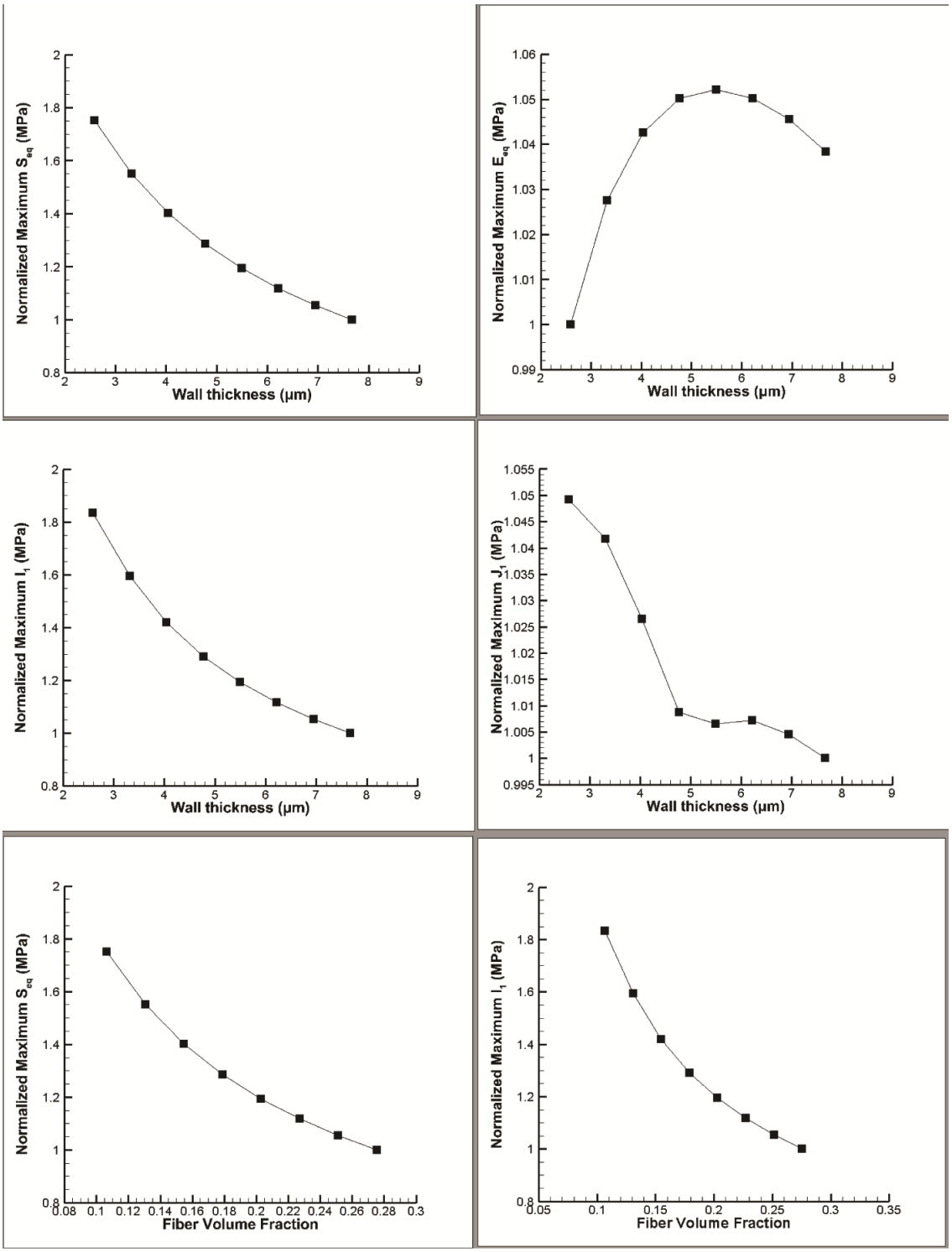


**Figure 57** Model results for varying wall thickness and a constant unit cell length (33.8 μm)

From the results shown above for varying the wall length (Figure 56), the maximum equivalent stresses and strains are seen to increase with increasing the side length of the hexagonal unit cell. The increase is nonlinear and shows an approximate bilinear behavior for cell size lengths ranging from 30 to 80 μm. Two reasons can be attributed to this increase in stresses and strains. The first is that increasing the cell size is lowering the fiber volume fraction, thus more stresses will be carried by the weaker epoxy resin as the stress is distributed on the distinct constituents. The second reason is the changes in the stresses and their distribution in the regions susceptible to stress concentrations between the two constituents. The stress concentration regions are shown in figures 58 and 59. The same trends are also seen for the effect of the unit cell size on the first stress and strain invariants, but the results are more nonlinear for the strain invariant. The results for the fiber volume fractions show an inverse relationship as explained above.

The results for varying the wall thickness (Figure 57), on the other hand, show an inverse relationship between maximum stress and strain invariants and maximum equivalent stress. The maximum equivalent strain shows an increase followed by a decrease as the wall thickness was varied from 2.5 to 8 μm, but the range of variation is small. The same discussion about the effect of fiber volume fraction and stress concentration also applies for this study. It is also worth noting that SEM micrographs for directionally oriented CNFs showed that a particular area of interest is at the corner boundaries between the unit cells, where the layers making the walls seem to delaminate (Figure 60), making it a critical area for failure and stress concentrations. The stress and strain concentration areas captured by the model are shown in figures 59 and 60.

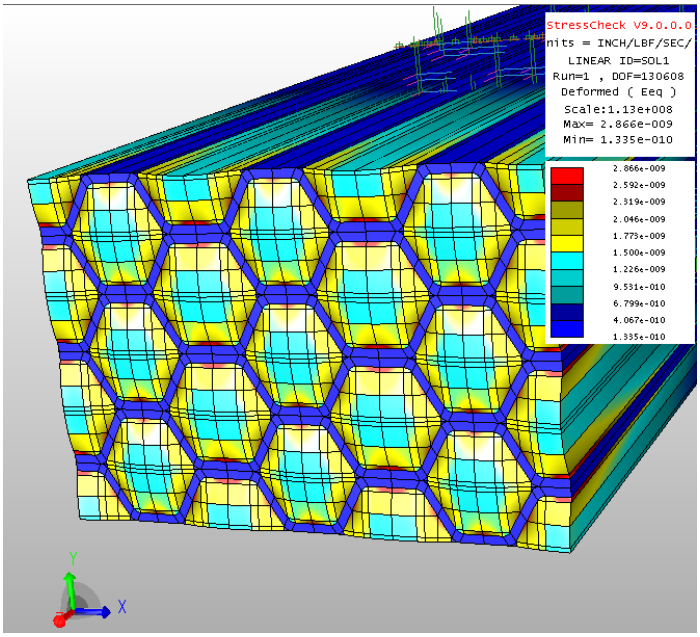


**Figure 58** Contour plot of the unit cell CNF model showing the equivalent strain distribution

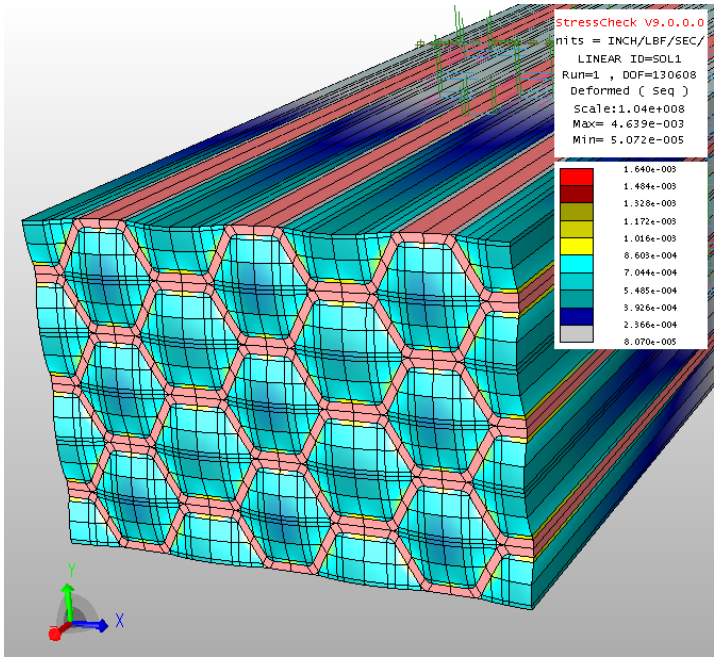


**Figure 59** Contour plot of the unit cell CNF model showing the equivalent stress distribution

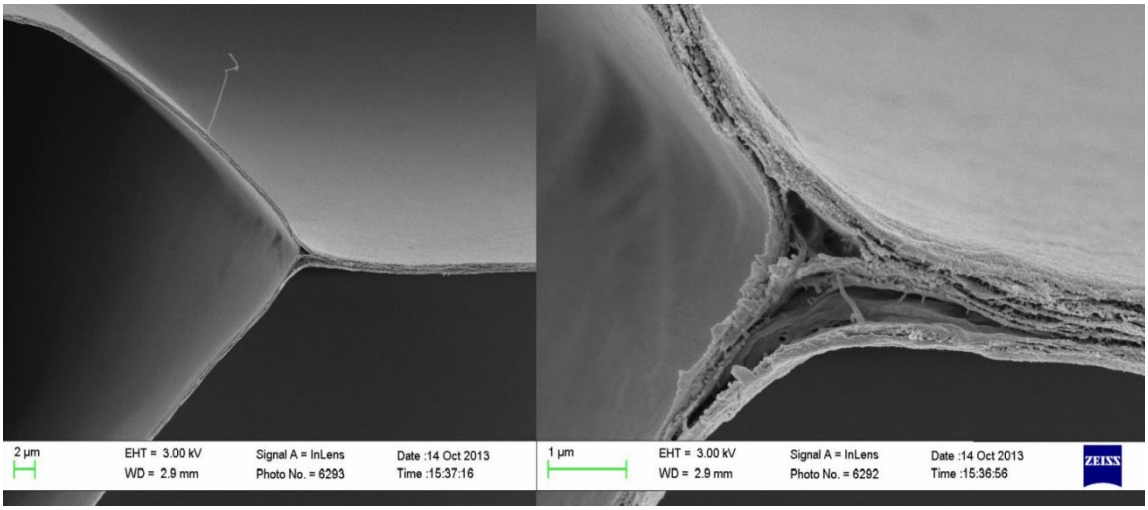


**Figure 60** SEM micrograph for directionally oriented CNFs for the junction of three pores showing the layered structure.

# 6. CONCLUSIONS

In this thesis, a combination of static and dynamic mechanical testing techniques and analytical and numerical solutions were used to analyze and characterize the behavior of cellulose-based thermosetting composites. A wide variety of advanced characterization tools for composite materials were used to fabricate and test these composites. The advanced characterization techniques that were used included DIC, DMA, DSC, and acoustic emission. Numerical and analytical solutions ranged from closed form numerical solutions to finite element analysis models. The research program was divided into three sections: unidirectional regenerated cellulose-based composites, triaxially braided regenerated cellulose-based composites, and microfibrillated scaffold-based cellulose composites. The conclusions drawn from each study and the suggested future research are summarized in the next sections.

## 6.1 Unidirectional Regenerated Cellulose Composites

- The mechanical properties of Lyocell tows are investigated under dry and wet conditions, showing bilinear and nonlinear elastic-plastic responses respectively.
- A multi-scale unit cell model incorporating a bilinear elastic-plastic stress-strain behavior can be approximated for the dry fibers. As the fibers absorb moisture, the knee of the stress-strain response shifts to the early stages of loading.
- The FE approach using p-FEA incorporating the bilinear constitutive response of Lyocell was proposed for possible modeling of these composites and predicting the composite behavioral response. The results show that the model was successfully used to predict the loading behavior of these composites under different fiber contents in dry conditions. The verification model shows a good

match to the experimental values with a little overestimation of strength and elasticity in the plastic region. The model can also be easily extended to determine the elastic-plastic orthotropic material constants.

- A nonlinear behavior and a drastic loss in modulus are observed for the wet fibers. In composite form, the behavior under wet conditions was less pronounced due to the barrier properties of the epoxy resin.
- Manufacturing composites from Lyocell fibers possesses unique challenges due to the hydrophilic and pilling nature of these fibers. The use of resin infusion produced higher FVF but some unwetted areas were seen even at high vacuum pressures. The use of wet layup followed by degasing overcomes that problem, but may be an issue when thicker parts or when more complex geometries are desired. The speed of preparation is also an issue since the resin takes around 35 minutes to harden and mold filling of large structures would need to account for this.

### 6.2 Triaxially Braided Regenerated Cellulose Composites

- The manufacturing of braided regenerated cellulose composites was found to be the most successful using a resin infusion technique.
- The initial elastic stiffness results are approximately 20% higher in the longitudinal direction when compared to the transverse direction. This may be due to the testing difficulties with the transverse specimens as there is no direct load transfer from the grips to all the bias yarns in the specimen.
- The acoustic emissions are measured and used to examine the damage initiation and propagation through the braided composite. The results show that damage

initiation start at lower stresses in the transverse direction compared to the longitudinal specimens. More energy is dissipated due damage in the longitudinal direction due to the breaking of fibers in the axial yarn. The acoustic emissions can be used to establish limiting failure stresses and strains corresponding to the onset of significant internal damage.

- The full field strain measurements using DIC show the limitations of the rectangular coupon in capturing the transverse deformation behavior due to the abnormal behavior at the specimen edges. This results in out-of-plane deformation creating areas of stress concentration at the edges from which failure can propagate. They also reduce the effective width of the specimen.
- The 3-layer discrete analytical model can be used to examine the effects of the braider angle, the aspect ratios, the crimp angle, and the yarn spacing on the elastic properties of the braided composite.
- The analytical model shows a reasonable prediction of the elastic properties within the range of the properties measured. The model was used to predict the effect of fiber volume fraction and aspect ratio (crimp angle) on the elastic modulus and Poisson ratio.
- For changes in the aspect ratio of the bias yarns, the sensitivity of the transverse properties was significantly higher. Longitudinal properties show a minimal variability with changes in the aspect ratio and crimp angle.
- The notched specimens appear to provide better estimates of the young's modulus for the triaxially braided regenerated cellulose composites.
- The addition of the regenerated cellulose was found to shift the glass transition to

higher temperatures. The peak in the *tan δ* curves for a constant loading frequency of 1Hz shifts from around 38ºC (100 ºF) to around 55 ºC (131 ºF) for the dry composites. The neat resin samples show higher damping which is characterized by the higher values of *tan δ*.

- When the composites are exposed to a humid environment such that the cellulose fibers are wetted, the glass transition temperature of the composite shifts to a lower temperature but this temperature is still higher than that of the neat resin. The mechanical properties also drop drastically, which appears in the DMA results as a drop in the elastic modulus.
- The wet specimens recover their storage modulus as temperature is increased approaching that of the dry specimens at high temperatures exceeding 70 ºC (158 ºF). When the water evaporates and the sample is reheated, part of the mechanical strength is recovered as indicated by an increased storage modulus. However, some of the elastic properties are permanently lost as the storage modulus doesn't recover back to the values of the storage modulus of the dry composite specimens.
- The DMA approach was able to capture the variation in the modulus in the axial and transverse directions of the triaxially braided composites. This difference is due to the undulations in the bias yarns that are braided above and below the main axial yarns leading to some loss in the quasi-isotropic properties in the transverse direction. The variation was also found in the previous study for the mechanical tensile loading of transverse and longitudinal coupons of the triaxially braided composite and is captured and confirmed by DMA results for the storage modulus.

### 6.3 Nanofibrillated Cellulose Scaffolds and Composites

- The reinforcement potential of novel nanocellulose-based reinforcements in the form of three-dimensional scaffolding is demonstrated. The success of the proposed *VAC-HP* in liquid molding processing is dependent on using a low viscosity epoxy that can be used in liquid forming processes.
- The DSC characterization showed that the incorporation of nanocellulose materials can result in an exothermic peak at 170 $^{o}$C (338 $^{o}$F) suggesting an alteration of the curing kinetics of the pure resin. This is confirmed with mechanical testing showing specimens with this exothermic peak corresponded to significantly lower mechanical properties. The exothermic peaks were eliminated when using the *VAC-HP* method.
- The results show that the nanocellulose scaffolds can be processed using the *VAC-HP* method and a low-viscosity epoxy resin resulting in improved modulus and lower strain to failure compared to the neat epoxy specimens.
- Results of the mechanical testing indicated a slight increase in the elastic modulus of the nanocellulose/epoxy composites with an average of 15% compared to the neat resin at reinforcement levels of 5.6-7.5% by volume.
- This increase is also seen by the analysis of the viscoelastic properties using DMA where a 14-18% increase in the storage modulus at room temperature is seen for these two reinforcement levels.
- The increase in the mechanical properties is only seen in the glassy state of the composites and the behavior is reversed at temperatures higher than the glass transition temperature.

- DMA results also revealed a decrease in the glass transition temperature with the addition of nanocellulose reinforcement and a drop in *tan* $\delta$ peaks proportional to the volume content of nanocellulose.
- The unit cell FEA model for the directionally oriented CNF composites was evaluated for the changes in the first stress and strain invariants and the equivalent strains and stresses for different cell wall lengths and thicknesses. The first invariants cover a normal stress failure criterion and the equivalent stresses cover the von Mises yield criterion. The results show the possibility to predict the properties of these composites from the distinct properties of the constituents.

### 6.4 Suggestions for Future Research

This research investigated the fabrication, mechanical, and thermal characterization for composites from natural cellulose-based fillers using epoxy resins. Exploration of methods to predict the mechanical properties were also investigated. Three different systems of cellulose composites were investigated: Unidirectional regenerated cellulose fibers, triaxially braided regenerated cellulose/epoxy composites, as well as micro-fibrillated cellulose scaffold-based composites. The research investigated optimal fabrication techniques to prepare these composites with the highest possible fiber content, least voids content and full cure and wetting of the resin. Following are some suggestions for future research to build on the effort done in this thesis:

1. Unidirectional regenerated cellulose composites

- Investigating the viscoelastic behavior of these composites using dynamic mechanical analysis. The effect on the frequency of loading in particular is required to understand how these composites will behave under different loading

frequencies. Before this is done, the potential uses for these composites in real life structure should be assessed for a more guided research into which temperature ranges and loading frequencies to target.

- More detailed environmental studies: future structural mechanics tools can use the proposed approach to incorporate the effects of moisture absorption in regenerated cellulose composites.

2. Triaxially braided regenerated cellulose composites

- The effects of swelling of the natural fibers due to the absorption of moisture need to be accounted for in any manufacturing approach through processing optimization studies.
- A more advanced fracture mechanics study and analytical solution that accounts for the properties of the constituents of the composite specimens, and the geometry properties of the triaxially braided fibers is required.
- The experimental investigation of the effect of notch sizes on the fracture properties and the strain energy release rate. This can be carried out using mechanical testing accompanied with advanced analysis techniques such as DIC and acoustic emission.

3. CNF/epoxy composites

- More investigation of the optimal fabrication and mechanical characterization techniques for directionally frozen micro-fibrillated cellulose scaffold systems and composites in which the nanocellulose fibers are oriented in one direction is required.

- The finite element analysis solution proposed in this thesis for the directionally oriented microfibrillated cellulose/epoxy composites can be expanded to cover various cell geometries and wall configurations.

## 7. REFERENCES


1. Cheng, Q., S. Wang, and D.P. Harper, *Effects of process and source on elastic modulus of single cellulose fibrils evaluated by atomic force microscopy.* Composites Part A: Applied Science and Manufacturing, 2009. **40**(5): p. 583-588.

2. Graupner, N. and J. Mussig, *A comparison of the mechanical characteristics of kenaf and lyocell fibre reinforced poly(lactic acid) (PLA) and poly(3-hydroxybutyrate) (PHB) composites.* Composites Part a-Applied Science and Manufacturing, 2011. **42**(12): p. 2010-2019.

3. Soykeabkaew, N., T. Nishino, and T. Peijs, *All-cellulose composites of regenerated cellulose fibres by surface selective dissolution.* Composites Part A: Applied Science and Manufacturing, 2009. **40**(4): p. 321-328.

4. Gindl, W. and J. Keckes, *Strain hardening in regenerated cellulose fibres.* Composites Science and Technology, 2006. **66**(13): p. 2049-2053.

5. Iwamoto, S., A.N. Nakagaito, and H. Yano, *Nano-fibrillation of pulp fibers for the processing of transparent nanocomposites.* Applied Physics a-Materials Science & Processing, 2007. **89**(2): p. 461-466.

6. Iwamoto, S., et al., *Optically transparent composites reinforced with plant fiber-based nanofibers.* Applied Physics a-Materials Science & Processing, 2005. **81**(6): p. 1109-1112.

7. Nogi, M., et al., *Optically transparent bionanofiber composites with low sensitivity to refractive index of the polymer matrix.* Applied Physics Letters, 2005. **87**(24).

8. Nogi, M., et al., *Fiber-content dependency of the optical transparency and thermal expansion of bacterial nanofiber reinforced composites.* Applied Physics Letters, 2006. **88**(13).

9. Nogi, M., et al., *Optically transparent nanofiber Papep.* Advanced Materials, 2009. **21**: p. 1595-1598.

10. Nogi, M. and H. Yano, *Transparent nanocomposites based on cellulose produced by bacteria offer potential innovation in the electronics device industry.* Advanced Materials, 2008. **20**: p. 1849-1852.

11. Nogi, M. and H. Yano, *Optically transparent nanofiber sheets by deposition of transparent materials: A concept for a roll-to-roll processing.* Applied Physics Letters, 2009. **94**.

12. Nogia, M., et al., *Property enhancement of optically transparent bionanofiber composites by acetylation.* Applied Physics Letters, 2006. **89**.

13. Sabo, R., J.-H. Seo, and Z. Ma. ***Cellulose Nanofiber Composite Substrates for Flexible Electronics***. in *2012 TAPPI International Conference on Nanotechnology for Renewable Materials*. 2012. Montreal, Quebec, Canada.

14. Okahisa, Y., et al., *Optically transparent wood–cellulose nanocomposite as a base substrate for flexible organic light-emitting diode displays.* Composites Science and Technology, 2009. **69**(11,Äì12): p. 1958-1961.

15. Azeredo, H.M.C.d., *Nanocomposites for food packaging applications.* Food Research International, 2009. **42**(9): p. 1240-1253.

16. Graupner, N. and J. Mussig, *A comparison of the mechanical characteristics of kenaf and lyocell fibre reinforced poly(lactic acid) (PLA) and poly(3-hydroxybutyrate) (PHB) composites.* Composites Part A: Applied Science and Manufacturing, 2011. **42**(12): p. 2010-2019.

17. Richard P. Wool, X.S.S., *Bio-Based Polymers and Composites*. 1 ed2005: Elsevier Science & Technology Books. 630.

18. Adusumali, R.-B., et al., *Mechanical Properties of Regenerated Cellulose Fibres for Composites.* Macromolecular Symposia, 2006. **244**(1): p. 119-125.

19. Cheng, Q. and S. Wang, *A method for testing the elastic modulus of single cellulose fibrils via atomic force microscopy.* Composites Part A: Applied Science and Manufacturing, 2008. **39**(12): p. 1838-1843.

20. Silva, M.C., et al., *Characterization of three non-product materials from a bleached eucalyptus kraft pulp mill, in view of valorising them as a source of cellulose fibres.* Industrial Crops and Products, 2008. **27**(3): p. 288-295.

21. Graupner, N., A.S. Herrmann, and J.r. Mussig, *Natural and man-made cellulose fibre-reinforced poly(lactic acid) (PLA) composites: An overview about mechanical characteristics and application areas.* Composites Part A: Applied Science and Manufacturing, 2009. **40**(6,7): p. 810-821.

22. Johnson, R.K., et al., *Mechanical properties of wetlaid lyocell and hybrid fiber-reinforced composites with polypropylene.* Composites Part A: Applied Science and Manufacturing, 2008. **39**(3): p. 470-477.

23. Mottershead, B. and S.J. Eichhorn, *Deformation micromechanics of model regenerated cellulose fibre-epoxy/polyester composites.* Composites Science and Technology, 2007. **67**(10): p. 2150-2159.

24. Wollerdorfer, M. and H. Bader, *Influence of natural fibres on the mechanical properties of biodegradable polymers.* Industrial Crops and Products, 1998. **8**(2): p. 105-112.

25. Miravete, A., R. Clemente, and L. Castejon., *3-D textile reinforcements in composite materials.* CRC Press LLC,2000 Corporate Blvd,NW,Boca Raton FL 33431,USA, 2000.

26. Poe, C., D.H. B., and I.S. Raju, *A Review of the NASA Textile Composites Research.* NASA Langley Technical Report, 1997.

27. Scholz, D.B., et al., *Advanced Technology Composite Fuselage - Materials and Processes*, 1997, Langley Research Center.

28. Byun, J.-H., *The analytical characterization of 2-D braided textile composites.* Composites Science and Technology, 2000. **60**(5): p. 705-716.

29. Yang, J.-M., C.-L. Ma, and T.-W. Chou, *Fiber Inclination Model of Three-Dimensional Textile Structural Composites.* journal of composite materials, 1986. **20**(5): p. 472-484.

30. Masters, J.E., et al., *Mechanical properties of triaxially braided composites: experimental and analytical results*. Vol. 15. 1993, Philadelphia, PA: American Society for Testing and Materials.

31. Naik, R.A., *Analysis of woven and braided fabric reinforced composites.* NASA CR-194930, 1994.

32. Quek, S.C., et al., *Analysis of 2D triaxial flat braided textile composites.* International Journal of Mechanical Sciences, 2003. **45**(6–7): p. 1077-1096.

33. Naik, R.A., P.G. Ifju, and J.E. Masters, *Effect of Fiber Architecture Parameters on Deformation Fields and Elastic Moduli of 2-D Braided Composites.* journal of composite materials, 1994. **28**(7): p. 656-681.

34. Ishikawa, T. and T.-W. Chou, *Elastic Behavior of Woven Hybrid Composites.* journal of composite materials, 1982. **16**(1): p. 2-19.

35. Ishikawa, T. and T.-W. Chou, *In-Plane Thermal Expansion and Thermal Bending Coefficients of Fabric Composites.* journal of composite materials, 1983. **17**(2): p. 92-104.

36. Ishikawa, T. and T.-W. Chou, *Stiffness and strength behaviour of woven fabric composites.* Journal of Materials Science, 1982. **17**(11): p. 3211-3220.

37. Whitney, T.J. and T.-W. Chou, *Modeling of 3-D Angle-Interlock Textile Structural Composites.* journal of composite materials, 1989. **23**(9): p. 890-911.

38. Challa, P. and K. Shivakumar, *mmTEXlam - a graphical user interfaced design code for laminated textile fabric composites.* AIAA-2001-1571 AIAA/ASME/ASCE/AHS/ASC Structures, Structural Dynamics, and Materials Conference and Exhibit, Apr. 16-19, 42nd, Seattle, WA, 2001.

39. Sankar, B.V. and R.V. Marrey, *Analytical method for micromechanics of textile composites.* Composites Science and Technology, 1997. **57**(6): p. 703-713.

40. Bowman, C.L., et al., *Mechanical Properties of Triaxial Braided Carbon/Epoxy Composites*, in *NASA Glenn Research Center*2003: Dayton, OH.

41. Zhang, P., L.-J. Gui, and Z.-J. Fan, *An Analytical Model for Predicting the Elastic Properties of Triaxially Braided Composites.* Journal of Reinforced Plastics and Composites, 2008.

42. Goldberg, R.K., B.J. Blinzler, and W.K. Binienda, *Investigation of a Macromechanical Approach to Analyzing Triaxially-Braided Polymer Composites.* AIAA Journal, 2011. **49**(1): p. 205-215.

43. Ayranci, C. and J.P. Carey, *Effect of Diameter in Predicting the Elastic Properties of 2D Braided Tubular Composites.* journal of composite materials, 2010. **44**(16): p. 2031-2044.

44. Hwang, J.T., A.M. Waas, and J.R.R.A. Martins, *Micromechanical Modeling and Design Optimization of 2-D Triaxial Braided Composites.* AIAA-2012-1257 50th AIAA Aerospace Sciences Meeting including the New Horizons Forum and Aerospace Exposition, Jan. 9-12, Nashville, Tennessee, 2012.

45. Shokrieh, M.M. and M.S. Mazloomi, *An analytical method for calculating stiffness of two-dimensional tri-axial braided composites.* Composite Structures, 2010. **92**(12): p. 2901-2905.

46. El-Hajjar, R.F., S.S. Shams, and D.J. Kehrl, *Closed form solutions for predicting the elastic behavior of quasi-isotropic triaxially braided composites.* Composite Structures, 2013. **101**(0): p. 1-8.

47. Moon, R.J., et al., *Cellulose nanomaterials review: structure, properties and nanocomposites.* Chemical Society reviews, 2011. **40**(7): p. 3941-94.

48. Sehaqui, H., et al., *Cellulose nanofiber orientation in nanopaper and nanocomposites by cold drawing.* ACS applied materials & interfaces, 2012. **4**(2): p. 1043-9.

49. Qing, Y., et al., *High-Performance Cellulose Nanofibril Composite Films.* BioResources, 2012. **7**(3): p. 3064-3075.

50. Ruiz, M.M., et al., *Processing and characterization of new thermoset nanocomposites based on cellulose whiskers.* Composite Interfaces, 2000. **7**(2): p. 117-131.

51. Nakagaito, A.N. and H. Yano, *The effect of fiber content on the mechanical and thermal expansion properties of biocomposites based on microfibrillated cellulose.* Cellulose, 2008. **15**(4): p. 555-559.

52. Siró, I. and D. Plackett, *Microfibrillated cellulose and new nanocomposite materials: a review.* Cellulose, 2010. **17**(3): p. 459-494.

53. Matos Ruiz, M., et al., *Processing and characterization of new thermoset nanocomposites based on cellulose whiskers.* Composite Interfaces, 2000. **7**(2): p. 117-131.

54. Lu, J., P. Askeland, and L.T. Drzal, *Surface modification of microfibrillated cellulose for epoxy composite applications.* Polymer, 2008. **49**(5): p. 1285-1296.

55. Sehaqui, H., et al., *Cellulose Nanofiber Orientation in Nanopaper and Nanocomposites by Cold Drawing.* ACS applied materials & interfaces, 2012. **4**(2): p. 1043-1049.

56. Gindl, W. and J. Keckes, *Drawing of self-reinforced cellulose films.* Journal of Applied Polymer Science, 2007. **103**(4): p. 2703-2708.

57. ASTM, *ASTM D638: Standard Test Method for Tensile Properties of Plastics*, in *ASTM International*2010.

58. ASTM, *ASTM D3822: Standard Test Method for Tensile Properties of Single Textile Fibers.* ASTM International, 2007.

59. ASTM, *D6866 Standard Test Methods for Determining the Biobased Content of Solid, Liquid, and Gaseous Samples Using Radiocarbon Analysis*, in *ASTM International*2007.

60. ASTM, *D3039 Standard test method for tensile properties of polymer matrix composite materials*, 2007, ASTM International: West Conshohocken, PA.

61. Morton, W.H., J, *Physical properties of textile fibres*. 4 ed2008: Woodhead Publishing. 796.

62. Composites_Technology, *New cellulose-based fiber*, in *Composites Technology*2012, Gardner Business Media: Cincinnati, Ohio, USA.

63. ASTM, *D2734 Standard Test Methods for Void Content of Reinforced Plastics*, 2009, ASTM International: West Conshohocken, PA.

64. El-Hajjar, R. and D.R. Petersen, *Adhesive Polyvinyl Chloride Coatings for Quantitative Strain Measurement in Composite Materials.* Composites Part B-Engineering, 2011. **42**(7): p. 1929-1936.

65. Schreier, H., J.-J. Orteu, and M.A. Sutton, *Image correlation for shape, motion and deformation measurements: basic concepts, theory and applications*2009, Verlag-US: Springer.

66. Littell, J.D., et al., *Characterization of Damage in Triaxial Braided Composites under Tensile Loading.* Journal of Aerospace Engineering, 2009. **22**(3): p. 270-279.

67. Roberts;, G.D., et al., *Characterization of Triaxial Braided Composite Material Properties for Impact Simulation*, 2009: Texas.

68. *StressCheck Master Guide*, 2009, Engineering Software Research & Development, Inc.

69. Bledzki, A.K., A. Jaszkiewicz, and D. Scherzer, *Mechanical properties of PLA composites with man-made cellulose and abaca fibres.* Composites Part A: Applied Science and Manufacturing, 2009. **40**(4): p. 404-412.

70. Tajvidi, M., R.H. Falk, and J.C. Hermanson, *Effect of natural fibers on thermal and mechanical properties of natural fiber polypropylene composites studied by dynamic mechanical analysis.* Journal of Applied Polymer Science, 2006. **101**(6): p. 4341-4349.

71. Jacob, M., et al., *Dynamical mechanical analysis of sisal/oil palm hybrid fiber-reinforced natural rubber composites.* Polymer Composites, 2006. **27**(6): p. 671-680.

72. Menard, K.P., *Dynamic Mechanical Analysis: A Practical Introduction*. Second Edition ed2008: CRC Press.

73. ASTM, *D4065 - 12 Standard Practice for Plastics: Dynamic Mechanical Properties: Determination and Report of Procedures.* 2012.

74. ASTM, *D5023 - 07 Standard Test Method for Plastics: Dynamic Mechanical Properties: In Flexure (Three-Point Bending).* 2007.

75. Margem, F.M., et al., *The dynamic-mechanical behavior of epoxy matrix composites reinforced with ramie fibers.* Revista Matéria, 2010. **15**: p. 164-171.

76. Guo, W. and M. Ashida, *Dynamic viscoelasticities for short fiber-thermoplastic elastomer composites.* Journal of Applied Polymer Science, 1993. **50**(8): p. 1435-1443.

77. Geethamma, V.G., et al., *Dynamic mechanical behavior of short coir fiber reinforced natural rubber composites.* Composites Part A: Applied Science and Manufacturing, 2005. **36**(11): p. 1499-1506.

78. Qamhia, I.I., R.C. Sabo, and R.F. Elhajjar, *Static and Dynamic Characterization of Cellulose Nanofibril Scaffold-Based Composites* BioResources, 2014. **9.1**.

79. Saito, T., et al., *Individualization of Nano-Sized Plant Cellulose Fibrils by Direct Surface Carboxylation Using TEMPO Catalyst under Neutral Conditions.* Biomacromolecules, 2009. **10**(7): p. 1992-1996.

80. ASTM, *D790 - 10 Standard Test Methods for Flexural Properties of Unreinforced and Reinforced Plastics and Electrical Insulating Materials.* 2010.

81. Masoodi, R., et al., *Mechanical characterization of cellulose nanofiber and bio-based epoxy composite.* Materials & Design, 2012. **36**(0): p. 570-576.

82. Jonoobi, M., et al., *Mechanical properties of cellulose nanofiber (CNF) reinforced polylactic acid (PLA) prepared by twin screw extrusion.* Composites Science and Technology, 2010. **70**(12): p. 1742-1747.

83. Bondeson, D., P. Syre, and K.O. Niska, *All Cellulose Nanocomposites Produced by Extrusion.* Journal of Biobased Materials and Bioenergy, 2007. **1**(3): p. 367-371.